Towards the Diagnosis of Madelung's Disease

Thesis Submitted in Partial Fulfilment of the Requirement For the Degree of

Master of Engineering
in
Electronics and Tele-Communication Engineering

Thesis Submitted By

SOHAM GHOSH

University Registration No.:154084 of 2020-2021
Class Roll No.: 002010702015
Exam Roll No.: M4ETC22015

UNDER THE GUIDANCE OF

PROFESSOR BHASKAR GUPTA

Department of Electronics and Tele-Communication Engineering

Faculty Council of Engineering and Technology

Jadavpur University, Kolkata – 700 032, India

2020 – 2022

JADAVPUR UNIVERSITY

KOLKATA – 700 032, INDIA

1. Title of the thesis: Towards the Diagnosis of Madelung's Disease

2. Name, Designation and Institution of the Supervisor:

Professor Bhaskar Gupta

Professor, Electronics and Telecommunication Engineering Department

Jadavpur University, Kolkata – 700 032, West Bengal, India

3. List of Presentations in National Conferences:

[1] **"Slot based Miniaturized Human Body Implantable Antenna at 2.45 GHz ISM Band,"** Soham Ghosh, Ardhendu Kundu and Bhaskar Gupta, *2022 Wireless, Antenna and Microwave Symposium (WAMS),* Rourkela, June 2022 (Presented in Conference).

[2] **"Design and Performance of a Slot Based Implantable Antenna in 2.45 GHz ISM Band,"** Soham Ghosh, Ardhendu Kundu and Bhaskar Gupta, *2021 IEEE Indian Conference on Antennas and Propagation (InCAP),* Rajasthan, December 2021.

CERTIFICATE OF RECOMMENDATION

This is to certify that the thesis entitled **"Towards the Diagnosis of Madelung's disease"** submitted by **Soham Ghosh** under my guidance and supervision and be accepted in partial fulfilment of the requirement for awarding the degree of **Master of Engineering** in **Electronics and Telecommunication Engineering** of Jadavpur University. The research results presented in this thesis have not been included in other paper submitted for the award of any degree to any other Institute or University.

Prof. Bhaskar Gupta
Professor
Dept. of E. & T.C. Engg.
Jadavpur University
Kolkata

Prof. Bhaskar Gupta
Thesis Supervisor
Dept. Electronics and Telecommunication Engineering
Jadavpur University
Kolkata 700 032, West Bengal, India

12/08/22

Head of the Department
Dept. Electronics and Telecommunication Engineering
Jadavpur University
Kolkata 700 032, West Bengal, India

MANOTOSH BISWAS
Professor and Head
Electronics and Telecommunication Engineering
Jadavpur University Kolkata - 32

17/8/22

Dean
Faculty of Engineering and Technology
Jadavpur University
Kolkata 700 032, West Bengal, India

DEAN
Faculty of Engineering & Technology
JADAVPUR UNIVERSITY
KOLKATA-700 032

CERTIFICATE OF APPROVAL#

The foregoing thesis is hereby approved as a credible study of an Engineering Subject carried out and presented in a manner of satisfactory to warrant its acceptance as a pre-requisite to the degree for which it has been submitted. It is to be understood that by this approval, the undersigned do not necessarily endorse or approve any statement made, opinion expressed or conclusion drawn therein but approve the thesis only for the purpose for which it has been submitted.

Committee on final examination
for the evaluation of the Thesis

_____

(Signature of the Supervisor)

_____

(Signature of the Examiner)

Only in case the thesis is approved

DECLARATION OF ORIGINALITY AND COMPLIANCE OF ACADEMIC ETHICS

I hereby declare that this thesis contains literature survey and original research work done by the undersigned candidate, as a part of his degree of **Master of Engineering** in **Electronics and Telecommunication Engineering** of Jadavpur University. All the information in this document has been obtained and presented in accordance with academic rules and ethical conduct. I also declare that as required by these rules and conduct, I have fully cited and referenced all materials and results that are not original to this work.

Date: 12·08·2022

Soham Ghosh

(Soham Ghosh)

University Reg. No. – 154084 of 2020-2021
Class Roll No. – 002010702015
Exam Roll No. – M4ETC22015

Acknowledgement

First of all, I wish to take opportunity to express gratitude to Prof. Bhaskar Gupta, my supervisor of Master degree thesis for cultivating interest and curiosity within me in the field of implantable antenna design and analysis and acknowledge him for holding my hand not only as a guide but also as a father in each step to enrich my knowledge as well as to complete my work successfully. Sometimes I felt like a caravan in search of an oasis in my journey when I cannot explain outcomes mathematically and physically. He always stays with me without getting tired. I would also like to thank everybody who came in touch during my work.

I am grateful to all the faculty members of the Electronics and Tele-Communication Engineering Department, Jadavpur University, for getting some valuable advices to gather knowledge in different subjects included in syllabus of Master of Engineering and get success in each semester exams. Suggestions from Prof. M. Biswas, Prof. S. Chatterjee, Prof. S. Ray, Prof. A. Konar and Prof. C. Bose have helped me in all the time. I am also thanking Prof. Somak Bhattacharyya, Indian Institute of Technology (BHU) for providing me an opportunity to explore my knowledge in research field and taste the flavour of research work in the time of my B. TECH degree.

This thesis would not have been completed without help and co - operation of all my seniors of JU Microwave Lab. I would like to thank Mr. Ardhendu Kundu, Mr. Joydeep Pal and Mr. Sayan Sarkar for their comments as well as helps to develop phantoms, perform experiments, acquire knowledges about different concepts from theoretical and practical perspectives of this domain and handle different instruments to carry out my work. I am also grateful to Dr. Kaushik Patra for sharing his many valuable thoughts and ideas and discussing concepts to expand

my knowledge and motivate me to perform this work successfully. I also take advantage to acknowledge Dr. Amartya Banerjee, Dr. Ayona Chakraborty and all other members of Microstrip Lab, Jadavpur University for their technical discussions which was really encouraging to enhance my interest in this topic. I would also like to acknowledge Dr. Cynthia Furse, Professor in Electrical and Computer Engineering Department at University of Utah, for clearing my doubt about the origin of electrical properties of human tissues and Prof. Erdem Topsakal, Professor and chair of Department of Electrical and Computer Engineering at Virginia Commonwealth University and Tutku Karacolak, Associate Professor at Washington State University, for enriching my interest in meander-line based implantable antenna design through e-mail. I want to thank Sanjana Chatterjee, student of M.Sc. Life Sciences in Central University of Jharkhand, for her cordial help to develop thoughts regarding biological concepts related to my work.

Lastly, but more importantly, I would like to thank all my family members and well-wishers who always encourage me to pursue my studies, stay with me and hold my hands in all ups and downs up to this journey in my life and motivate me to overcome all difficulties. I also like to acknowledge AICTE (All India Council for Technical Education) for providing me PG Scholarship to pursue my Post Graduate Degree course in duration of 2020-2022. Without their blessings, I could not complete this work successfully with little smile in my face.

Date: 12·08·2022

Soham Ghosh

(Soham Ghosh)

Contents

List of Figures

List of Tables

Chapter 1

Introduction

Contents	
	1.1 Preface
	1.2 Basic concept of Implantable Antenna
	1.3 Brief concept about Madelung's disease
	1.4 Analysis efforts
	1.5 Motivation of the Thesis
	1.6 Novel aspects
	1.7 Thesis outline

1.1 PREFACE

Field of bioelectromagnetics have been expanded with development of different implantable biomedical devices since innovation of implantable cardiac pacemaker over seventy years ago. Several such devices such as pacemakers, internal temperature sensors, deep brain stimulators, cardioverter defibrillators, functional electrical stimulators, implantable hormone therapy pumps, bone growth stimulators etc. make processes of medical treatments easy [1-3]. This development of bioelectromagnetics have been possible due to advancement of power source development, microelectronics and more importantly investment of valuable time and scientific views of scientists [4]. To understand interaction between electromagnetic energy and living biological objects along with possible applications in the field of medical diagnostic systems, researchers and scientists have devoted themselves to develop antennas and microwave technologies for different biomedical applications [5].

In early 1950s, stimulation of electric pulses was used to treat patients suffering from heart block. Innovation of the first external pacemaker by Dr. Paul Zoll [6] in 1952 diverted scientists' mind to develop low cost and small size pacemakers to ease painful treatment of heart block. A hand-held battery – operated device was developed by Earl Bakken and it was used by Dr. Lillehei and others [7].

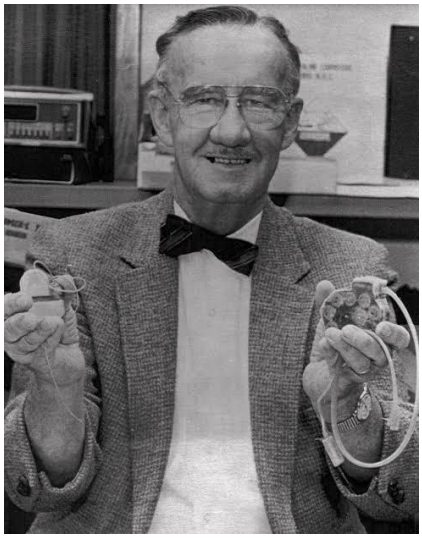

Fig. 1.1: Wilson Greatbatch, the inventor of implantable pacemaker

With the help of a surgeon named William Chardack, Wilson Greatbatch, an electrical engineer of Buffalo, was able to develop the first implantable pacemaker in 1958 [4]. In the year 1959, Dr. Senning attempted the first human use of pacemaker in Sweden but his work was clinically failure [8]. After trying heart and soul, Greatbatch and his group were successful to implant a pacemaker within human body in 1960 which was ground – breaking work and helped scientists to think about developing implantable devices [9]. In 1970s and 1980s, sort of revolution of implantable device development happened and different types of implantable devices such as implantable drug delivery systems, implantable defibrillator, implantable sensors etc. had been developed. However, the old-

generation devices had different limitations such as high capture thresholds, dislodgement, high fracture rates, electromagnetic interface and corrosion [10]. Therefore, advancement of the implantable devices had been performed gradually to solve those problems.

1.2 BASIC CONCEPT OF IMPLANTABLE ANTENNA

Implantable antenna refers to an antenna implanted inside body tissues to transfer information on different health parameters monitored by sensors connected with it. Implantable antenna is a key element of Wireless Body Area Network (WBAN) to communicate wirelessly between devices implantable in human body and external environment [11, 12].

With the advancement of communication and electronic technologies as well as requirement of technological supports in medical science, demand of body area network (BAN) is going up day by day. In BAN, wireless networks having some nodes are situated on human body or implanted inside the body. Assistance to some emergency services of police, fire fighters, applications in military field to track soldiers' location, image and video transmission, monitoring pulse rate and other health related parameters such as oxygen level, glucose level in blood etc., navigation support in car, identification of individuals etc. enhance the popularity of this field.

A number of frequency bands such as Medical Implant Communication System (MICS), Wireless Medical Telemetry Service (WMTS), and Industrial, Scientific and Medical (ISM) Band have been allotted to develop implantable antennas [1-3]. To design an implantable antenna in above mentioned allotted frequency bands, physical dimensions of the antenna come out to be significantly large. However, to implant an antenna within human body, the antenna size should be as small as possible. Therefore, different antenna miniaturization techniques can

be adopted to design and develop an implantable antenna. Meandering, spiralling, waffling or incorporating slots on patch of the antenna can help to reduce frequency of operation by increasing current-flow path length and thus maintaining compact dimensions of the implantable antenna [3].

There are some critical parameters such as high lossy nature of human tissues, size of antenna, impedance matching, low power constraint, Specific Absorption Rate (SAR) limit etc. which make design of an implantable antenna challenging [13, 14]. A superstrate can be placed on the top of patch because superstrate layer behaves as lower permittivity isolator from the human tissues [15, 16]. Most of the research on implantable antenna is grazing around production of hyperthermia for treatments and monitoring physiological parameters. Shapes and sizes of antennas depend on the location of implantation within body [17].

1.3 BRIEF CONCEPT ABOUT MADELUNG'S DISEASE

Madelung's disease, first described by Brodie in 1846, is a rare disorder occurring due to progressive, symmetrical and excessive deposition of adipose tissue in lowest skin layer or subcutaneous layer. This disease is also named as Benign or Multiple Symmetric Lipomatosis [18]. It occurs due to accumulation of fat in neck, arms, thighs, hips etc. Men who drink excessive alcohol are affected majorly in this disease. In spite of being painless, it can lead to develop other disorders such as liver disfunction, adrenal disfunction, diabetes, chronic obstructive pulmonary disease (COPD), neuropathy, gynecomastia, hyperuricemia etc. [18]. Fig. 1.3.1 shows how a patient is affected by Madelung's disease.

Madelung's disease can also be described as the presence of multiple lipomas or fatty tumours. In the disease, subcutaneous fat layer is grown at a high rate due to abnormal fat metabolism at the initial stage and after a certain time, the fat accumulation rate gets slow down for stabilizing fat mass [19].

Fig. 1.2: A patient affected by Madelung's disease [18]

1.4 ANALYSIS EFFORTS

For in-vitro testing of the performance of antenna performance inside human torso, it is required to use phantom model which can have symmetrical electrical behaviour with human body. The major parameters of human tissues are relative permittivity and conductivity at a particular frequency band. Due to non-magnetic nature of human tissues, relative permeability for all tissues can be taken as 1.

But development of multi-layered model of human body is very difficult. Therefore, it is required to estimate permittivity and conductivity of a single layer homogeneous phantom model so that implantable antenna can see equivalent environment like multi-layer human body when it radiates. For extracting complex permittivity of the equivalent homogeneous phantom, classical Nicolson-Ross-Wier method using S-band waveguide has been designed in CST Microwave Studio

2017. In this work, microstrip antenna technology has been used for ease of fabrication, low cost and simplicity in design.

1.5 MOTIVATION OF THE THESIS

Inclusion of wireless communication for medical diagnosis made a revolution in this field. Patient monitoring wirelessly has several benefits such as elimination of wires to increase patient mobility, comfort to paralysed patients for diagnosis from home, to monitor health parameters continuously, performing operation of serious patients remotely etc. Monitoring health parameters like blood sugar level, blood pressure, pulse rate etc., providing assist to heart by pacemakers, detection of growth of tumours etc. show benefits for patients for using implantable devices in patient diagnosis purposes.

One of the important considerations as discussed earlier is size of the implantable device. For proper placement of devices inside human torso, device size should be small. Therefore, microwave scientists are trying to design compact antennas for implantation purposes. But the gain of an antenna reduces with reduction of antenna size. Additionally, transmitted power of the implanted antenna has been attenuated by large amount due to high lossy nature of human tissues. Consequently, it is very challenging to communicate with the implanted antenna due to reduction of gain of the antenna. To establish proper communication links between implantable device and external devices, link budget should be computed to ensure proper power transfer and communication between them.

Yet, insertion of antenna inside human tissues can increase power of electromagnetic fields in human body which leads to augment specific absorption rate (SAR) of the tissue. So, an implantable antenna should be designed in such a way that SAR value should be within specific limits prescribed by different guidelines of International Commission on Non-Ionizing Radiation Protection

(ICNIRP), Federal Communications Commission (FCC), Department of Telecommunications (DOT) etc. [20-22].

In this context, designing of implantable antenna have become major candidate in bioelectromagnetics field and medical sciences. Many scientific works in this field have been grazed in the design of pacemakers, blood related parameters (blood sugar level, pressure etc.), tumour detection especially breast tumour detection etc. Now-a-days, many people are suffering from several diseases due to fat accumulation. However, there are a smaller number of reported research works to observing performance of implantable antenna with fat layer thickness variation. One of the important diseases related to this variation is Madelung's disease. Therefore, in our work, we are going to observe performance of the implantable antenna while it is radiating in such an environment where fat mass is changing. This analysis will be helpful to detect Madelung's disease using implantable antenna.

1.6 NOVEL ASPECTS

Following are the novel aspects focussed in this thesis.

- Development of miniaturized antenna using meander-lining technique having better radiation properties inside contiguous tissue model than reported implantable antenna.
- Analysis and observation of performance of implantable antenna with the variation of subcutaneous fat layer. Detection of Madelung's disease using implantable antenna and receiver at 2.45 GHz ISM band.
- Development of implantable antenna having higher gain compared to other reported antenna in spite of placing inside human skin and body equivalent phantoms to establish proper communication link.

1.7 THESIS OUTLINE

This thesis presents the performance analysis of implantable antenna within human body for detection of subcutaneous layer related diseases (e.g., Madelung's disease) at 2.45 GHz ISM band. A brief historical perspective and basic concepts related to implantable antenna and Madelung's disease have been discussed in Chapter 1.

Chapter 2 comprises of three sections. The first part of this chapter deals with previously reported implantable antennas and their performances. Effects of different parameters such as shape, length, feed point location, substrate and superstrate material and their thicknesses on antenna responses are discussed in next section. A survey on applications of implantable antennas in medical field has been discussed in third part of Chapter 2.

Chapter 3 presents a brief description of different frequency bands licensed for utilizing in medical purposes. Along with this, reason of using 2.45 GHz ISM band for this work has also been described from the size of microstrip antenna point of view. Different matching and radiation characteristics have been studied in this chapter.

Properties of different human tissues are discussed in Chapter 4. Dielectric constants and conductivities of skin, fat and muscle layers are tabulated in this chapter and attenuation constant, phase constant and intrinsic impedances of these three layers at different medical bands are calculated.

Chapter 5 presents behaviour of electric and magnetic fields in each layer of human body (skin, fat and muscle). Transfer matrices for the three-layer human body system for electric field are developed in this chapter.

Chapter 6 concentrates on the performance analysis of an implantable antenna in the skin layer using CST Microwave Studio 2017. Different parameters of antenna within a cubical skin phantom such as return loss, realized gain, SAR etc. are studied in Chapter 6.

For the thesis work, antenna should be implanted within muscle layer. But it is difficult to develop multi-layer phantom in our lab. Therefore, it is needed to design its homogeneous equivalent phantom model to test antenna characteristics. Chapter 7 deals with the development of homogeneous body phantom liquid based on FCC guideline. Dielectric properties of the liquid are also measured and plotted in this chapter.

In Chapter 8 and Chapter 9, two implantable antennas within homogeneous single-layer body phantom are designed and fabricated. Antenna in Chapter 8 has been designed based on meander-line slot and open slot in ground plane. In Chapter 9, a meander-lined body implantable antenna is designed.

Chapter 10 describes the performance of an implantable antenna while thickness of fat layer will increase. One of the most important fat-layer related disease is Madelung's disease. This is also explained in this chapter.

In the last chapter, conclusions and future scopes are discussed. Brief concept of electromagnetic behaviour of human body is explained in Appendix.

REFERENCES

[1] J. R. Nagel, C. M. Furse, D. A. Christensen and C. H. Durney, "Basic Introduction to Bioelectromagnetics," *CRC Press, Taylor & Francis*, 3rd Edition.

[2] W. G. Scanlon, N. E. Evans and Z. M. McCreesh, "RF Performance of a 418 MHz Radio Telemeter Packaged for Human Vaginal Placement," *IEEE Transactions on Biomedical Engineering*, vol. 44, no. 5, pp. 427 – 430, May 1997.

[3] A. Kiourti and K. S. Nikita, "A Review of Implantable Patch Antennas for Biomedical Telemetry: Challenges and Solutions [Wireless Corner]," *IEEE Antennas and Propagation Magazine*, vol. 54, no. 3, pp. 210 – 228, June 2012.

[4] W. Greatbatch and C. F. Homes, "History of Implantable devices," *IEEE Engineering in Medicine and Biology Magazine*, vol. 10. no. 3, pp. 38 – 41, September 1991.

[5] S. Ghosh, A. Kundu and B. Gupta, "Design and Performance of a Slot Based Implantable Antenna in 2.45 GHz ISM Band," *2021 IEEE Indian Conference on Antennas and Propagation (InCAP)*, Rajasthan, India, December 2021.

[6] P. M. Zoll, "Resuscitation of the heart in ventricular standstill by external electric stimulation," *The New England Journal of Medicine*, vol. 247, no. 20, pp. 768 – 771, November 1952.

[7] C. W. Lillehei, V. L. Gott, P. C. Hodges, D. M. Long and E. E. Bakken, "Transistor Pacemaker for Treatment of complete Atrioventricular Dissociation," *JAMA*, vol. 172, no. 18, pp. 2006 – 2010, April 1960.

[8] A. Senning, "Problems in the use of pacemakers," *The Journal of cardiovascular surgery*, vol. 5, pp. 651 – 656, 1964.

[9] W. Greatbatch and W. Chardack, "A transistorized, self – contained, implantable pacemaker for the long-term correction of complete heart block," *Surgery*, vol. 48, pp. 643 – 654, October 1960.

[10] H. Burri, H. Sunthorn and D. Shah, "Complications of pacemaker leads," *Heart*, vol. 89, no. 12, November 2003.

[11] A. Kiourti and K. S. Nikita, "Miniature scalp – implantable antennas for telemetry in the MICS and ISM bands: Design, safety considerations and link budget analysis," *IEEE Transactions on Antennas and Propagation*, vol. 60, no. 8, pp. 3568 – 3575, August 2012.

[12] R. Li and S. Xiao, "Compact slotted semi – circular antenna for implantable medical devices," *Electronics Letters*, vol. 50, no.23, pp. 1675 – 1677, November 2014.

[13] T. Karacolak, A. Z. Hood and E. Topsakal, "Design of a Dual – Band Implantable Antenna and Development of Skin Mimicking Gels for Continuous Glucose Monitoring," *IEEE Transactions on Microwave theory and Techniques*, vol. 56, no. 4, April 2008.

[14] T. Yilmaz, T. Karacolak and E. Topsakal, "Characterization and Testing of a Skin Mimicking Material for Implantable Antennas Operating at ISM Band (2.4 GHz – 2.48 GHz)," *IEEE Antennas and Wireless Propagation Letters*, vol. 7, pp. 418 – 420, June 2008.

[15] M. Zada and H. Yoo, "A Miniaturized Triple – Band Implantable Antenna System for Bio -Telemetry Applications," *IEEE Transactions on Antennas and Propagation,* vol. 66, no. 12, pp. 7378 – 7382, October 2018.

[16] Y. Rahmat–Samii and E. Topsakal, "Antenna and Sensor Technologies in Modern Medical Applications," *Wiley – IEEE Press,* 2021.

[17] C. H. Durney and M. F. Iskander, "Antennas for medical applications," in *Antenna Handbook,* Y. T. Lo and S. W. Lee (eds), Springer, Boston, pp. 596 – 654, 1993.

[18] M. Szewc, R. Sitarz, N. Moroz, R. Maciejewski and R. Wierzbicki, "Madelung's disease – progressive, excessive and symmetrical deposition of adipose tissue in the subcutaneous layer: case report and literature review," *Diabetes, Metabolic Syndrome and Obesity: Targets and Therapy*, vol. 11, pp. 819-825, November 2018.

[19] https://rarediseases.org/rare-diseases/madelungs-diseases.

[20] ICNIRP, "Guidelines for limiting exposure to electromagnetic fields (100 KHz to 300 GHz)," *Health Phys.,* vol. 118, no. 5, pp. 483-524, March 2020.

[21] R. F. Cleveland, Jr., D. M. Sylvar, and J. L. Ulcek, "Evaluating compliance with FCC guidelines for human exposure to radiofrequency electromagnetic fields," *FCC OET Bulletin,* vol. 65, Edition 97-01, Washington D.C., November 1997.

[22] https://dot.gov.in/journey-emf.

Chapter 2
Literature Review

Contents	
	2.1 Introduction
	2.2 Previously reported implantable antennas
	2.3 Effects of different parameters on antenna
	2.4 Application specific survey on implantable antenna
	2.5 Madelung's disease

2.1 INTRODUCTION

Implantable antennas are part and parcel of Wireless Body Area Network (WBAN) that are used for monitoring different human health parameters and transferring the collected or sensed data to external devices. However, some design considerations should be kept in mind before designing these types of antennas like high lossy nature of human tissues, miniaturization of antennas for implanting them properly, Specific Absorption Rate (SAR) etc.

2.2 PREVIOUSLY REPORTED IMPLANTABLE ANTENNAS

In the last few decades, utilization of wireless in-vitro and in-vivo communications in medical field have become popular with the advancement of communication and electronic technological world, development of compact intelligent devices and requirement of observing continuous record of different health parameters such as blood pressure, glucose level, temperature etc. [1-3]. To

sense these parameters and transfer them to the external devices, development of the implantable antennas had been studied in the last few years.

The word 'implant' means placement of any object inside any part of human body. Therefore, implantable antenna can be referred to as an antenna which can be placed inside the human body by surgery to perform in-vivo communication. Due to lossy nature of human tissues, design of implantable antennas is a very challenging task. Different types of antennas such as coaxial antenna, wire antenna, microstrip antenna etc. embedded within lossy environment have been examined earlier. Study of the embedded antennas have been performed for different therapeutical applications like pacemakers, deep brain stimulators, cardioverter defibrillators, internal temperature sensors, implantable hormone therapy pumps, functional electrical stimulators etc. [4-6].

Design of an implantable antenna is quite challenging due to some critical factors such as size of antenna, high absorbing nature and conductivity of tissues, low power constraint, impedance matching, Specific Absorption Rate (SAR) limit etc. [2, 8]. To design the implantable antenna in the specified frequency bands, physical dimensions of the conventional antenna will be comparatively large. However, the size of antenna should be as small as possible to implant it properly inside the human body. Thus, different miniaturization techniques such as meandering, waffling, spiralling or incorporating multiple number of slots on radiating patch, can be adopted for designing and developing an implantable antenna. These techniques can help reducing the frequency of operation by increasing the path length of current-flow, thereby ensuring the compactness of implantable antenna [6].

Another way to miniaturize an antenna is placement of a shorting wall from ground to patch. This process can reduce the size of antenna by 50 % [9-11]. Superstrate plays an important role in designing implantable antenna. The resonant

frequency can be reduced by placing thick superstrate on patch. Thicker superstrate reduces the effective permittivity by insulating the implantable antenna from highly lossy human body which has high permittivity. A superstrate having higher permittivity value reduce the phase velocity of the electromagnetic wave propagating through the material. This results in lowering the resonant frequency by shortening the effective wavelength [12].

In 2008, Karacolak, Hood and Topsakal designed a dual-band serpentine implantable antenna (refer to Fig. 2.1(a)) for continuous glucose monitoring [8]. They implanted the antenna within human skin equivalent phantom. Particle swarm optimization technique was used to optimize their antenna to tune at MICS and ISM bands. The return loss response of this antenna is shown in Fig. 2.1 (b). Karacolak and his group designed meander-line based implantable antennas in [2,13-14] and tested performances of their designed antennas in skin mimicking gels and implanting them within rat's body. In 2010, a CPW-fed ceramic implantable antenna was proposed in [15].

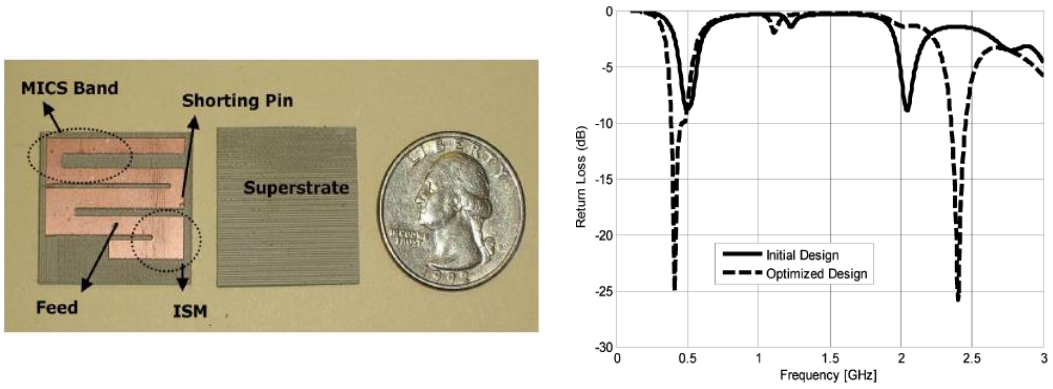

(a) **(b)**

Fig. 2.1: (a) Fabricated implantable antenna and (b) return loss vs frequency plot designed by Karacolak et. al. [8] © IEEE

To improve bandwidth and reduce tissue erosion, generally superstrate is placed on antennas. However, the authors in their literature [15] did not load any superstrate on antenna radiator due to use of biocompatible Ag/Pd paste and biocompatible ceramic substrate. The proposed antenna had three parts – central monopole section, two inductive inverted L-shaped sections and two back-to-back short L sections as shown in Fig. 2.2(a). From its S_{11} vs frequency plot (Fig. 2.2 (b)), it is observed that their proposed antenna was tuned at MICS band and it provided 33.5% fractional bandwidth and 25 dB return loss at resonant frequency.

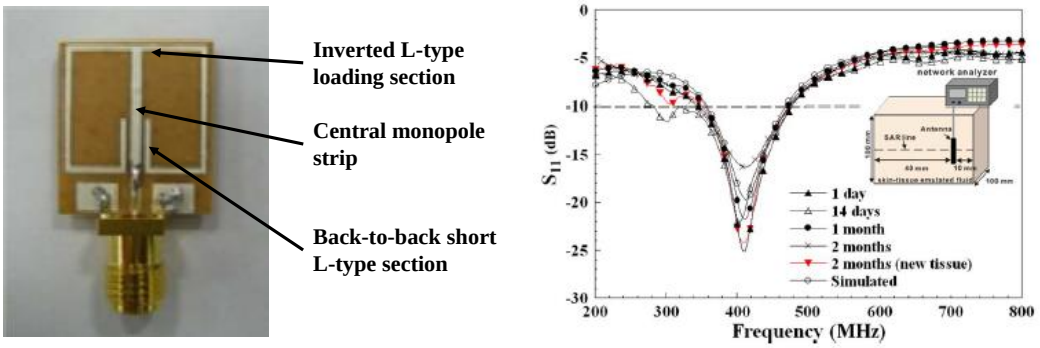

(a) **(b)**

Fig. 2.2: (a) Proposed antenna in Chien et. al. [15] (b) S_{11} vs frequency of this antenna [15] © IEEE

According to [16-17], miniaturization and bandwidth enhancement are adopted by utilising planar inverted-F- antenna (PIFA) and stacked multilayers. A multi-layered triple band miniaturized implantable antenna was designed in Huang et. al. [18]. That antenna was tuned at 402 MHz, 433 MHz and 2.45 GHz ISM band. Frequency band around 433 MHz could provide that antenna facility to be used in rectenna application. Meander-line slot was used in the upper layer of the antenna conducting part and different slots were also incorporated for tuning properly. That 4-layer triple band antenna is shown in Fig. 2.3 (a). Kiourti and Nikita also designed

multi-layered implantable PIFA tuned at MICS and ISM band in the article [19]. That antenna geometry is shown in Fig. 2.3 (b). They used Rogers RO 3210 substrate and a 0.6 mm thick biocompatible superstrate for their work.

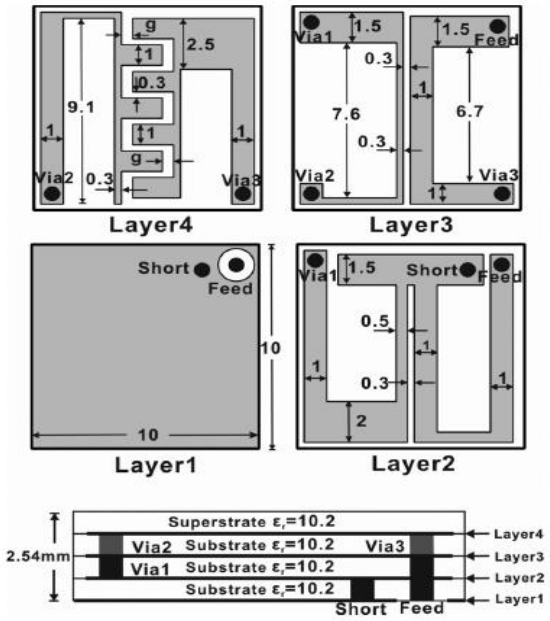

(a)

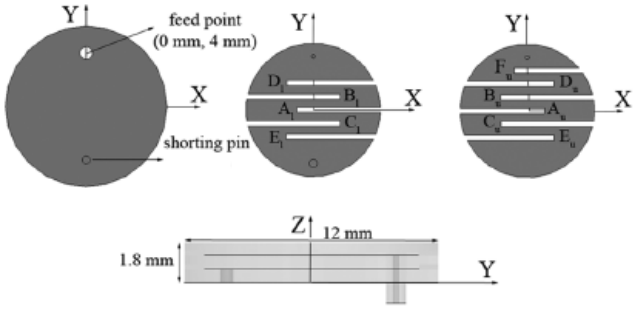

(b)

Fig. 2.3: (a) 4-layer implantable antenna [18] © IEEE (b) 3-layer implantable antenna [19] © IEEE

Differentially fed dual band antenna for implantation was proposed in 2012 by Duan and his research group in [20]. Rectangular spiral type antenna (shown in Fig. 2.4) was designed for biomedical applications in MICS band and sub-GHz wideband communication. The electrical current path of that antenna is also added in Fig 2.4. A characteristic study was also shown by placing the same antenna in muscle, fat and skin layer in simulation.

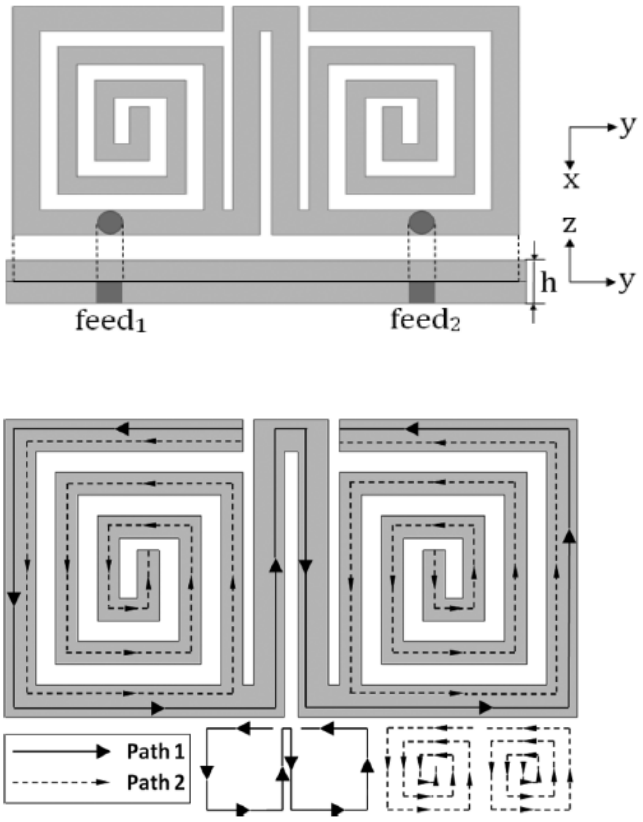

Fig. 2.4: Rectangular spiral type skin implantable antenna and its electrical current paths [20] © IEEE

In some other published reports [21-22] also, spiral or planar inverted-F antennas (PIFA) were used for designing miniaturized implantable antenna. Cavity slot antennas were also tested in the same perspective in articles [23-24]. But, those

types of antennas provide narrow bandwidth and they are highly sensitive to environment. A compact slot based dual band PIFA with broad bandwidth (52.6% around MICS and 4.4 % around 2.45 GHz ISM) was developed in [25]. The antenna geometry is shown in Fig. 2.5. Open slot was placed at the ground plane as shown in this figure.

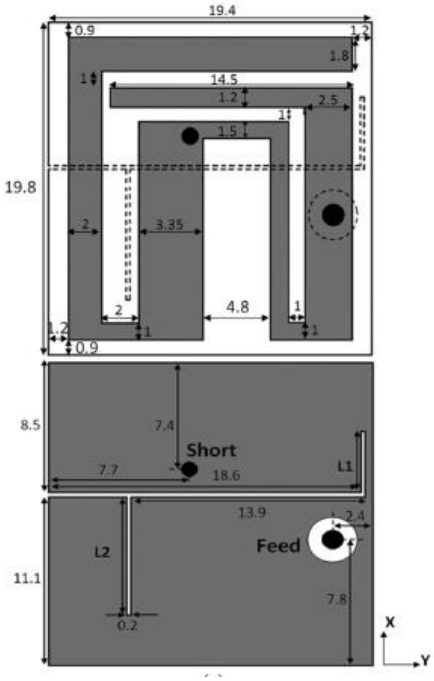

Fig. 2.5: Top and bottom view of antenna proposed in [25] © IEEE

A printed meandered folded dipole antenna (PMFD) was proposed by Magill, Conway and Scanlon [26] in 2017. A scalp implantable biotelemetry device was proposed in [27] which used an ultra-miniaturized dual band (915 MHz and 2.45 GHz) implantable antenna. For validation, the authors immersed the antenna within a 3D head phantom (saline solution). The proposed antenna system was employed in scalp implantation, especially for intracranial pressure monitoring [27].

[28] shows the realization of Reactive Impedance Surface (RIS) in an implantable environment for designing a compact wideband antenna for biotelemetry applications. The antenna was designed to operate at 2.45 GHz ISM band within skin model. The circular RIS could improve the gain, impedance matching and bandwidth of the antenna.

Biocompatibility is another factor for ascertaining patient safety. Human body is conductive in nature. Therefore, it may short circuit the antenna in case of direct contact with metal parts of antenna. Different biocompatible materials were used in different literature. Teflon, MACOR, ceramic alumina etc. are most often used biocompatible superstrates. For encapsulation purposes, some other proposed materials are used zirconium, PEEK, Silastic MDX-4210 Biomedical-Grade base Elastomer etc. [6].

2.3 EFFECTS OF DIFFERENT PARAMETERS ON ANTENNA

In Section 2.2, different types of implantable antennas along with miniaturization techniques were studied. In this section, different factors influencing the performances of implantable antenna have been studied.

In [22], authors discussed about the effects of shape, length, feed point location, substrate and superstrate material and their thicknesses on antenna responses. From their study it is observed that in case of spiral antenna, electric field has strong coupling at its center whereas for serpentine antenna, electric field has strong coupling to its adjacent arms. Serpentine radiator is electrically shorted than spiral antenna. However, serpentine radiator radiates as good as spiral antenna.

From the same article, it is also concluded that length of antenna can influence resonant frequency and matching as shown in Fig. 2.6 (a). Proper choice of feed location is very important for impedance matching. Substrate and

superstrate materials also have impact on determining resonant frequency of the antenna. Due to shorter wavelength, dielectric materials with high permittivity reduce resonant frequency (refer to Fig. 2.6(b)). Effective permittivity can be increased with the increment of substrate thickness which can make antenna electrically larger. As discussed in [22], if the thickness of superstrate increases, resonant frequency gets reduced due to lowering effective permittivity by insulating implantable antenna from body with high permittivity. Effects of substrate and superstrate thickness on resonant frequency and return loss are shown in Fig. 2.6 (c) and (d) respectively.

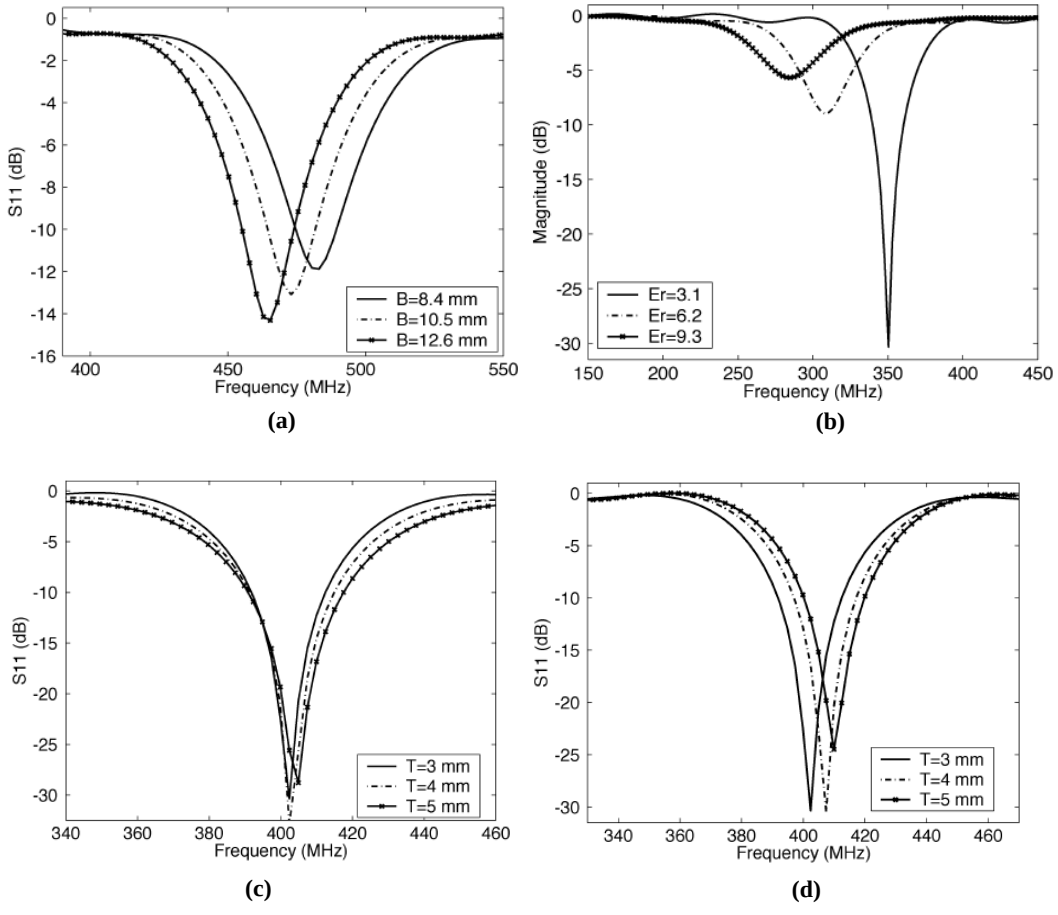

Fig. 2.6: Effects of (a) length of radiator, (b) permittivity of superstrate, (c) substrate thickness, (d) superstrate thickness on S_{11} vs frequency [22] © IEEE

2.4 APPLICATION SPECIFIC SURVEY ON IMPLANTABLE ANTENNA

Implantable antennas were investigated for different medical applications which are discussed below. Antenna plays an important role as a communication carrier for wireless electronic medical equipment.

2.4.1. *Wireless pacemaker system*

The wireless cardiac pacemaker provides the patients with good medical services through antennas. When the wireless pacemaker satisfies the normal process of pacemaker, the real-time monitoring and protection become more significant. Therefore, the design and research of implantable antennas used in wireless cardiac pacemaker systems is an important research area [29].

A compact meander-line based implantable antenna tuned at 2.45 GHz ISM band for wireless cardiac pacemaker systems was designed by authors in [29]. The size of the antenna was 3 mm × 3 mm × 0.5 mm as shown in Fig. 2.7 (a, b, c). The antenna shows good impedance matching in the ISM frequency band while placed it in heart phantom which is shown in Fig. 2.7 (d). In the reports [30-31], two compact antennas were designed by two group of scientists for leadless cardiac pacemaker system.

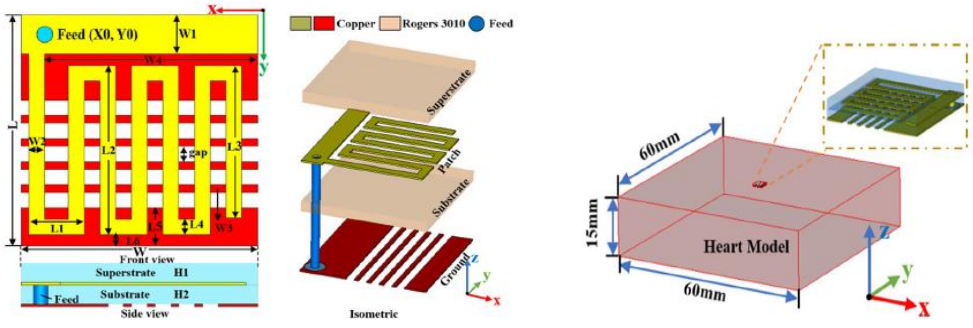

(a) **(b)**

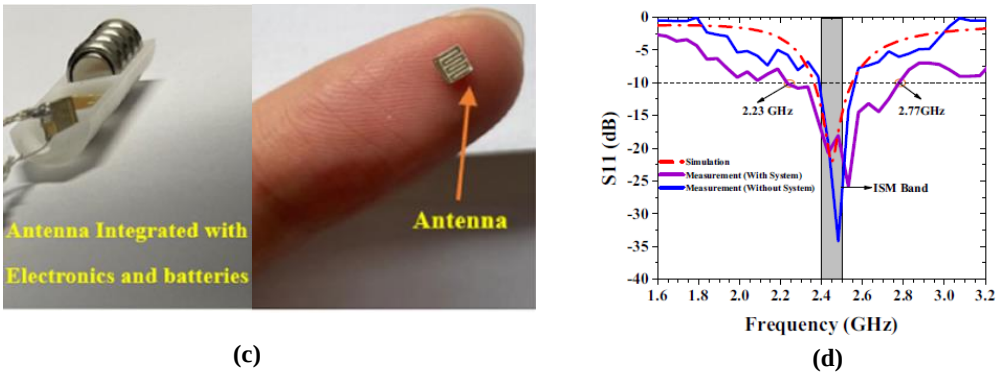

Fig. 2.7: Wireless cardiac pacemaker [29] (a) Schematic diagram of antenna part, (b) Antenna within heart muscle, (c) Fabricated antenna and system and (d) S_{11} vs Frequency plot of antenna within phantom (Simulated and measured)

2.4.2. *Blood glucose level monitoring*

Diabetes mellitus is now one of the most serious chronic diseases. According to the report of the International Diabetes Federation (IDF) [32], annually around 4 million deaths are caused by diabetes. The number of people suffering from the diabetes is rising rapidly [33]. Insufficiency of glucose may be the cause of some serious diseases, such as kidney failure, cardiac diseases, retinal damage, slow wound healing etc. [34-35].

Different studies were reported on implantable sensor design for continuous glucose monitoring to reduce the pain by enzyme-based finger-pricking [36]. An enzymatic electrochemical technique [37] was reported for sensing glucose concentration using a biosensor. The main problem of this system is the requirement of a transponder chip along with an electrochemical biosensor for powering. Some optical biosensors based on fluorescent chemicals were discussed in [38-39] for observing the change in glucose level. But those biosensors were inconvenient for patients for use in daytime because of the ambient light intensity.

In [40], the authors proposed another approach as shown in Fig. 2.8 (a). They designed a biosensor composed of an LC tank resonator (shown in Fig. 2.8 (b)) implanted under the human skin, where the interstitial dermal fluid environs the LC tank resonator. Variations in glucose concentration can change relative permittivity of the fluid. This variation will change the capacitance of the LC tank resonator and resonant frequency. The change in the resonant frequency was observed by the inductively coupled reader antenna located outside the tissue.

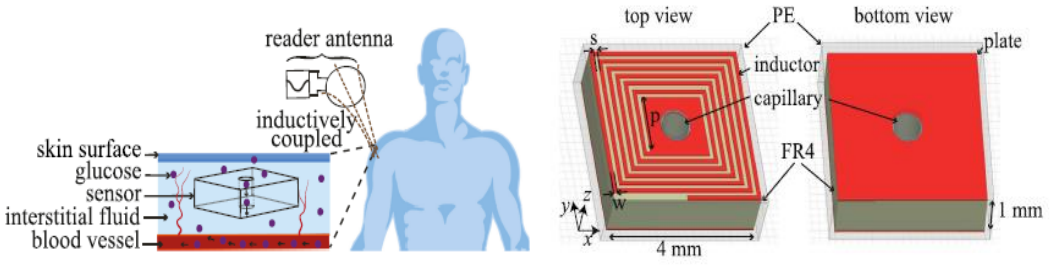

Fig. 2.8: (a) Glucose sensor within interstitial fluid, (b) LC glucose sensor [40]

2.4.3. *Other applications*

Besides them, many researchers designed implantable antennas in wireless medical purposes like blood pressure monitoring [41], intracranial pressure monitoring [42], tumour detection etc.

The major problem related to these systems are powering of implanted devices. Number of surgeries should be performed to replace the batteries of them. To overcome this problem, scientists designed their system in such a way that power could be transfer to implanted system wirelessly in [1, 43-45].

From the above discussions, it is observed that the researchers designed implantable antennas to monitor mostly blood related parameters and detect blood related diseases. They also focused on heart and brain or head implantation. But there is a knowledge gap in studying fat related disease (e.g., Madelung's disease). Therefore, this thesis work will be on study of antenna performance with the growth of fat layer and based on this, we will try to detect Madelung's disease using implantable antenna.

2.5 MADELUNG'S DISEASE

Madelung's disease or Multiple Symmetric Lipomatosis (MSL) is a rare disease of fat metabolism. It is characterized by subcutaneous painless non-encapsulated and symmetric fatty deposits in the torso, neck, mammary, abdominal areas and in the upper and lower limbs. The aetiology of this disease is still unknown. MSL typically presents between the third and the fifth decade of life and is more prevalent in males especially who consume alcohol at a large amount [46].

A case report published in [46] is mentioned here.

"A 45-year-old male patient sought medical attention because of a growing mass. The lesion was in the anterior cervical region initially, but over the last 2 years it also appeared in the occipital and dorsal regions. At the time of medical evaluation, the lesions caused him aesthetic embarrassment. He also had type 2 diabetes mellitus and asymptomatic chronic pancreatitis. He had a history of alcoholic abuse of 1 liter/day for 10 years. He denied other comorbidities. He had worked as a bricklayer; however, due to the deformation caused by the masses, he was unemployed. The physical evaluation revealed bulging masses of soft consistency in the anterior cervical region, in the pre- and post-auricular regions bilaterally, and on the back (refer to Fig. 2.9.1).

Fig. 2.9.1 Pre-operative examination shown in [46]

Fig. 2.9.2 Post-operative examination shown in [46]

A two-step surgical treatment was scheduled. In the first procedure, the anterior cervical mass was resected followed by closed vacuum system drainage. The occipital mass was resected with similar drainage after 1 month in a second surgery. In both surgeries, no dissection plan was identified between the adipose mass and the surrounding structures. The anatomopathological study of the masses showed a mature adipocyte proliferation, which was compatible with lipomatosis. Both procedures had a favourable outcome (Fig. 2.9.2) and after 1 year of follow-up the final aesthetic result was satisfactory. After 1 year, the patient was able to look for employment." [46]

REFERENCES

[1] T. Shaw and D. Mitra, "Wireless Power Transfer System Design for Biomedical Implants at 2.45 GHz," *2019 IEEE Asia – Pacific Microwave Conference (APMC)*, March 2020.

[2] T. Yilmaz, T. Karacolak and E. Topsakal, "Characterization and Testing of a Skin Mimicking Material for Implantable Antennas Operating at ISM Band (2.4 GHz – 2.48 GHz)," *IEEE Antennas and Wireless Propagation Letters*, vol. 7, pp. 418 – 420, June 2008.

[3] Y. Hao, A. Alomainy and W. F. F. Pasveer, "Antennas for Wearable Devices," *Wiley Telecom*, pp. 197-229, March 2007.

[4] J. R. Nagel, C. M. Furse, D. A. Christensen and C. A. Durney, "Basic Introduction to Bioelectromagnetics," *CRC Press, Taylor & Francis Group*, 2019.

[5] W. G. Scanlon, N. E. Evans and Z. M. McCreesh, "RF Performance of a 418 MHz Radio Telemeter Packaged for Human Vaginal Placement," *IEEE Transaction on Biomedical Engineering*, vol. 44, no. 5, pp. 427-430, May 1997.

[6] A. Kiourti and K. S. Nikita, "A Review of Implantable Patch Antennas for Biomedical Telemetry: Challenges and Solutions [Wireless Corner]," *IEEE Antennas and Propagation Magazine*, vol. 54, no. 3, pp. 210 – 228, June 2012.

[7] S. A. Kumar and T. Shanmuganantham, "Implantable CPW fed Dual Folded Dipole Antenna for Biomedical Applications," *2012 Third International Conference on Computing, Communication and Networking Technology (ICCCNT'12)*, December 2012.

[8] T. Karacolak, A. Z. Hood and E. Topsakal, "Design of a Dual – Band Implantable Antenna and Development of Skin Mimicking Gels for Continuous Glucose Monitoring," *IEEE Transactions on Microwave Theory and Techniques*, vol. 56, no. 4, April 2008.

[9] Z. Qi, F. Kan and L. Tie – Zhu, "Analysis of planar inverted – F antenna using equivalent models," *2005 IEEE Antennas and Propagation Society International Symposium*, December 2005.

[10] M. C. Huynh and W. Stutzman, "Ground plane effects on planer inverted – F antenna (PIFA) performance," *IEEE Proceedings – Microwaves, Antennas and Propagation*, vol. 150, no. 4, August 2003.

[11] V. Antonchik and R. Vaughan, "Far field pattern for rectangular PIFA antenna from the cavity model," *2005 IEEE Antennas and Propagation Society International Symposium*, December 2005.

[12] R. B. Green, M. V. Smith and E. Topsakal, "In Vitro and In Vivo Testing of Implantable Antennas," *Antenna and Sensor Technologies in Modern Medical Applications*, Wiley – IEEE Press, pp. 145 – 189, 2021.

[13] T. Karacolak, R. Cooper and E. Topsakal, "Electrical Properties of Rat skin and design of Implantable antennas for Medical Wireless Telemetry," *IEEE Transactions on Antennas and Propagation*, vol. 57, no. 9, pp. 2806-2812, September 2009.

[14] T. Karacolak, R. Cooper, J. Butler and E. Topsakal, "In Vivo Verification of Implantable Antennas Using Rats as Model Animals," *IEEE Antennas and Wireless Propagation Letters*, vol. 9, pp. 334-337, 2010.

[15] T. F. Chien, C. M. Cheng, H. C. Yang, J. W. Jiang and C. H. Luo, "Development of Non superstrate Implantable Low-Profile CPW-Fed Ceramic Antennas," *IEEE Antennas and Wireless Propagation Letters*, vol. 9, pp. 599-602, 2010.

[16] W. C. Liu, S. H. Chen, and C. M. Wu, "Implantable broadband circular stacked PIFA Antenna for biotelemetry communication," *Journal of Electromagnetic Waves and Applications*, vol. 22, pp. 1791–1800, Apr. 2008.

[17] C. M. Lee, T. C. Yo, F. J. Huang, and C. H. Luo, "Bandwidth enhancement of planar inverted F antenna for implantable biotelemetry," *Microwave and Optical Technology Letters*, vol. 51, pp. 749-751, 2009.

[18] F. J. Huang, C. M. Lee, C. L. Chang, L. K. Chen, T. C. Yo and C. H. Luo, "Rectenna Application of Miniaturized Implantable Antenna Deign for Triple-Band Biotelemetry Communication," *IEEE Transactions on Antennas and Propagation*, vol. 59, no. 7, pp. 2646-2653, July 2011.

[19] A. Kiourti and K. S. Nikita, "Miniature Scalp-Implantable Antennas for Telemetry in the MICS and ISM Bands: Design, Safety Considerations and Link Budget Analysis," *IEEE Transactions on Antennas and Propagation*, vol. 60, no. 8, pp. 3568-3575, August 2012.

[20] Z. Duan, Y. X. Guo, R. F. Xue, M. Je and D. L. Kwong, "Differentially Fed Dual-Band Implantable Antenna for Biomedical Applications," *IEEE Transactions on Antennas and Propagation*, vol. 60, no. 12, pp. 5587-5593, December 2012.

[21] J. Kimand, Y. Rahmat-Samii, "Implanted antennas inside a human body: Simulations, designs, characterizations," *IEEE Transactions on Microwave Theory and Techniques*, vol.52, no.8, pp.1934-1943, August 2004.

[22] P. Soontornpipit, C.M. Furse, and Y.C. Chung, "Design of implantable microstrip antenna for communication with medical implants," *IEEE Transactions on Microwave Theory and Techniques*, vol. 52, no. 8, pp. 1944-1951, August 2004.

[23] H. Usui, M. Takahashi and K. Ito, "Radiation characteristics of an implanted cavity slot antenna into the human body," *IEEE Antennas and Propagation Society International Symposium*, Albuquerque, NM, July 2006.

[24] W. Xia, K. Saito, M. Takahashi and K. Ito, "Performances of an implanted cavity slot antenna embedded in the human arm," *IEEE Transactions on Antennas and Propagation,* vol.57, no.4, pp. 894-899, April 2009.

[25] L. J. Xu, Y. X. Guo and W. Wu, "Dual-Band Implantable Antenna with Open-end slots on Ground," *IEEE Antennas and Wireless Propagation Letters*, vol. 11, October 2012.

[26] M. K. Magill, G. A. Conway and W. G. Scanlon, "Tissue-independent Implantable antenna for in-body communications at 2.36-2.5 GHz," *IEEE Transactions on Antennas and Propagation*, vol. 65, no. 9, pp. 4406-4417, May 2017.

[27] S. A. A. Shah and H. Yoo, "Scalp-implantable antenna systems for intracranial pressure monitoring," *IEEE Transactions of Antennas Propagations.* vol. 66, no. 4, pp. 2170-2173, 2018.

[28] G. Samanta and D. Mitra, "Miniaturised and radiation efficient implantable antenna using reactive impedance surface for biotelemetry," *IET Microwaves, Antennas and Propagation*, vol.14, no. 2, pp. 177-184, 2020.

[29] Y. Feng, Z. Li, L. Qi, W. Shen and G. Li, "A compact and miniaturized implantable antenna for ISM band in wireless cardiac pacemaker system," *Scientific reports*, vol. 12, no. 1, January 2022.

[30] M. Zada, I. A. Shah, A. Basir and H. Yoo, "Ultra-Compact Implantable Antenna with enhanced performance for Leadless Cardiac Pacemaker System," *IEEE Transactions on Antennas and Propagation*, vol. 69, no. 2, February 2021.

[31] D. Sharma, B. K. Kanaujia, V. Kaim, R. Mittra, R. K. Arya and L. Matekovits, "Design and implementation of compact dual-band conformal antenna for leadless cardiac pacemaker system," *Scientific Reports*, vol. 12, no. 1, February 2022.

[32] International Diabetes Federation, "IDF Diabetes Atlas Eighth Edition," 2017. [Online]. Available: http://diabetesatlas.org/

[33] X. Xiao and Q. Li, "A non-invasive measurement of blood glucose concentration by UWB microwave spectrum," *IEEE Antennas and Wireless Propagation Letters*, vol. 16, pp. 1040–1043, 2017.

[34] T. Yilmaz, R. Foster, and Y. Hao, "Broadband tissue mimicking phantoms and a patch resonator for evaluating non-invasive monitoring of blood glucose

levels," *IEEE Transactions on Antennas and Propagation*, vol. 62, no. 6, pp. 3064–3075, Jun. 2014.

[35] X. Y. Liu, Z. T. Wu, Y. Fan, and E. M. Tentzeris, "A miniaturized CSRR loaded wide-beamwidth circularly polarized implantable antenna for subcutaneous real-time glucose monitoring," *IEEE Antennas and Wireless Propagation Letters*, vol. 16, pp. 577–580, 2017.

[36] D. Bruen, C. Delaney, L. Florea, and D. Diamond, "Glucose sensing for diabetes monitoring: Recent developments," *Sensors*, vol. 17, no. 8, p. 1866, 2017.

[37] M. M. Ahmadi and G. A. Jullien, "A wireless-implantable microsystem for continuous blood glucose monitoring," *IEEE Transactions on Biomedical Circuits and Systems*, vol. 3, no. 3, pp. 169–180, Jun. 2009.

[38] H. Shibata, Y. J. Heo, T. Okitsu, Y. Matsunaga, T. Kawanishi, and S. Takeuchi, "Injectable hydrogel microbeads for fluorescence-based in vivo continuous glucose monitoring," *Proceedings of the National Academy of Sciences*, vol. 107, no. 42, pp. 17 894–17 898, 2010.

[39] Y. J. Heo, H. Shibata, T. Okitsu, T. Kawanishi, and S. Takeuchi, "Long-term in vivo glucose monitoring using fluorescent hydrogel fibres," *Proceedings of the National Academy of Sciences*, vol. 108, no. 33, pp. 13399–13403, 2011.

[40] R. S. Hassan, J. Lee and S. Kim, "A Minimally Invasive Implantable Sensor for Continuous Wireless Glucose Monitoring Based on a Passive sensor,"

IEEE Antennas and Wireless Propagation Letters, vol. 19, no. 1, pp. 124-128, January 2022.

[41] O. H. Murphy, M. R. Behmanyar, A. Borgi, C. Mcleod, M. Navaratnarajah, M. Yacoub and C. Toumazou, "Continuous in vivo blood pressure measurements using a fully implantable wireless SAW sensor," *Biomedical Microdevices*, vol. 15, no. 5, April 2013.

[42] M. W. A. Khan, E. Moradi, L. Sydanheimo, T. Bjorninen, Y. R. Samii and L. Ukkonen, "Miniature Coplanar Implantable Antenna on Thin and Flexible Platform for Fully Wireless Intracranial Pressure Monitoring System," *International Journal of Antennas and Propagation*, vol. 2017, January 2017.

[43] T. Shaw, B. Mondal, D. Mitra and R. Augustine, "Wireless Power Transfer System Design in Reactive Near-field for Implantable Devices," *European Conference on Antennas and Propagation (EuCAP)*, Denmark, July 2020.

[44] Z. Chen, H. Sun and W. Geyi, "Maximum Wireless Power Transfer to the Implantable Device in the Radiative Near-field," *IEEE Antennas and Wireless Propagation Letters*, March 2017.

[45] R. A. Bercich, D. R. Duffy and P. P. Irazoqui, "Far – Field RF Powering of Implantable Devices: Safety Considerations," *IEEE Transactions on Biomedical Engineering*, vol. 60, no. 8, August 2013.

[46] L. F. Maximiano, M. T. Gaspar and E. S. Nakahira, "Madelung disease (multiple symmetric lipomatosis)," *Autops Case Reports*, vol. 8, no. 3, 2018.

Chapter 3

Choice of Frequency Range

Contents	
	3.1 Introduction
	3.2 Brief concept of medical frequency bands
	3.3 Reason of using microstrip patch antenna for implantation
	3.4 Brief concept of microstrip patch antenna
	3.5 Method of calculation of the patch size
	3.6 Selection of frequency band for this work
	3.7 Simple patch in MICS Band
	3.8 Simple patch in WMTS Band
	3.9 Simple patch in 2.45 GHz ISM Band
	3.10 Conclusion

3.1 INTRODUCTION

Inductive links between monitoring equipment and implantable devices to establish wireless communication path dates back to 1980 [1]. Selection of frequency band before designing an antenna to operate in particular application is very important task for an engineer. Several frequency bands were allocated for utilizing in medical purposes by FCC (Federal Communication Commission) [2].

MICS (Medical Implant Communication System) band and 2.45 GHz ISM (Industrial, Scientific and Medical) band have been used majorly for designing implantable antenna. WMTS (Wireless Medical Telemetry Service) and MedRadio

(Medical Device Radiocommunication Service) bands are also used for the same purposes. In this chapter, brief concept about them is discussed as well as performance of simple patch antennas in those bands has been studied.

3.2 BRIEF CONCEPT OF MEDICAL FREQUENCY BANDS

In this section, three medical bands such as MICS, WMTS and ISM band, have been discussed.

3.2.1 *MICS band:*

MICS is basically a technology which supports short range communication for transmitting data from implantable device to external environment and vice versa. The operating frequency for this communication system is 402-405 MHz. Therefore, wavelength is ranging from 74.63 cm to 74.07 cm. The U.S. FCC proposed this frequency band for MICS in July 1999 [1].

3.2.2 *WMTS band:*

WMTS is generally used for monitoring pulse and respiration of patients. Major advantage of using this band for patients' health monitoring is that patients are allowed to move and there is no restriction to lie on bed or stay in one place to monitor the parameters [3]. There are three frequency bands defined as WMTS bands by FCC. They are 608 - 614 MHz, 1395-1400 MHz and 1427-1432 MHz. The 1427-1432 MHz band of WMTS was majorly focused by scientists for implantable device design purposes [4-5].

3.2.3 *ISM band:*

The ISM band refers to parts of radio frequency spectrum which is reserved for use of radio frequencies for industrial, scientific and medical usage rather than communications. For commercial uses 2.45 GHz ISM band (2.4-2.48 GHz) is majorly used especially for WiFi, Bluetooth, implantable devices, wearable devices etc. The 5.8 GHz ISM band (5.725-5.875 GHz) is used in commercial WiFi applications. 5.8 GHz ISM band is used for 802.11ac which can provide up to 1.3 Gbps but 2.45 GHz ISM band is used for 802.11n which can provide up to 300 Mbps. In spite of having high data rate in 5.8 GHz ISM band, 2.45 GHz is majorly used in medical purposes due to less power loss. Other ISM frequency bands are 6.765-6.795 MHz, 13.553-13.567 MHz, 40.66-40.7 MHz, 902-928 MHz, 24 GHz – 24.25 GHz, 61-61.5 GHz, 122-123 GHz, 244-246 GHz [6-7].

3.3 REASON OF USING MICROSTRIP PATCH ANTENNA FOR IMPLANTATION

Basic requirements for designing an implantable antenna are –

(i) antenna size should be small to implant antenna within human body properly,

(ii) antenna with light weight and conformal characteristic is preferable for implantation purposes

(iii) a superstrate should be used to protect human tissues from the direct contact with conducting patch

(iv) SAR[1] (Specific Absorption Rate) should be within prescribed limit as mentioned in Chapter 1 and

(v) cost should be low so that it can be bought easily.

[1] Concept of SAR is described in Appendix.

All these requirements can be fulfilled if microstrip patch antenna will be used due to having some interesting characteristics like low volume, light weight, thin and easy to conform, low fabrication cost, easily integrable in microwave circuits and chips etc [8].

3.4 BRIEF CONCEPT OF A MICROSTRIP PATCH ANTENNA

Microstrip patch antenna (Fig. 3.1) consist of two conducting plates (upper conductor part is called patch and lower conductor part is called ground surface) and a very thin substrate with height h ($0.003\,\lambda_0 \leq h \leq 0.05\,\lambda_0$, where λ_0 is free space wavelength). The relative permittivity (ϵ_r) of substrate should be in the range of [2.2, 12]. The patch geometry can be rectangular, circular, square, triangular, elliptical etc. [9]. A simple patch structure is illustrated in Fig. 3.1.

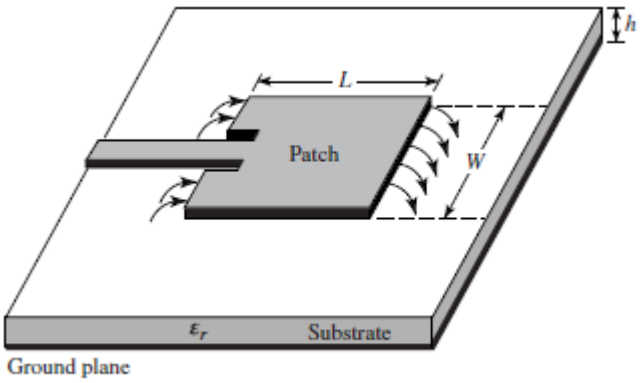

Fig. 3.1: Microstrip Patch antenna with microstrip line feed [9]

There are many techniques to feed such antennas. Majorly used feeds are coaxial probe, microstrip line, proximity coupling and aperture coupling. The microstrip feed is small-width conducting strip to match the patch element with source by insetting it in patch. This is very easy to fabricate. However, surface

waves and feed radiation can be increased in this case with the increment of substrate thickness [9].

A coaxial line feed has two cylindrical shaped conductors named as inner and outer conductor respectively separated by a cylindrical shaped dielectric material (usually Teflon is used as dielectric material here) in such a way that it can provide an impedance. This coaxial cable should be designed in such a way that the outer conductor should be connected with ground plane and inner conductor with patch.

Due to asymmetries, both coaxial probe and microstrip line generate higher order modes to produce cross-polarized radiation [9]. To overcome these problems, aperture-coupled feed can be utilized. Here, two substrates of different relative permittivities and thicknesses are used and they are separated by ground plane. Patch is placed at the top surface of the top substrate layer and microstrip feed is on the bottom surface of bottom substrate. A coupling slot is incorporated here in the ground plane to transfer energy to patch from feed. But this is very difficult to fabricate and it has narrow bandwidth compared to that of microstrip feed and probe feed.

In proximity coupled feeding techniques also, two different substrates with different permittivities and thicknesses are used. Instead of using coupling slot, here a microstrip line is placed between two dielectric materials and ground is placed at the bottom surface of bottom substrate. For these two coupling techniques, major disadvantages are the fabrication complexity, enhancement of size and cost.

Therefore, aperture-coupled and proximity-coupled feeding techniques are not satisfying requirements of this work. Coaxial feeding technique has been used in this work. The inner and outer conductor diameters are 4.22 mm and 1.26 mm respectively. Fig. 3.2 shows that the used coaxial feed can achieve 50 Ω impedance

matching which is calculated using 'impedance calculator' in CST Microwave Studio 2017.

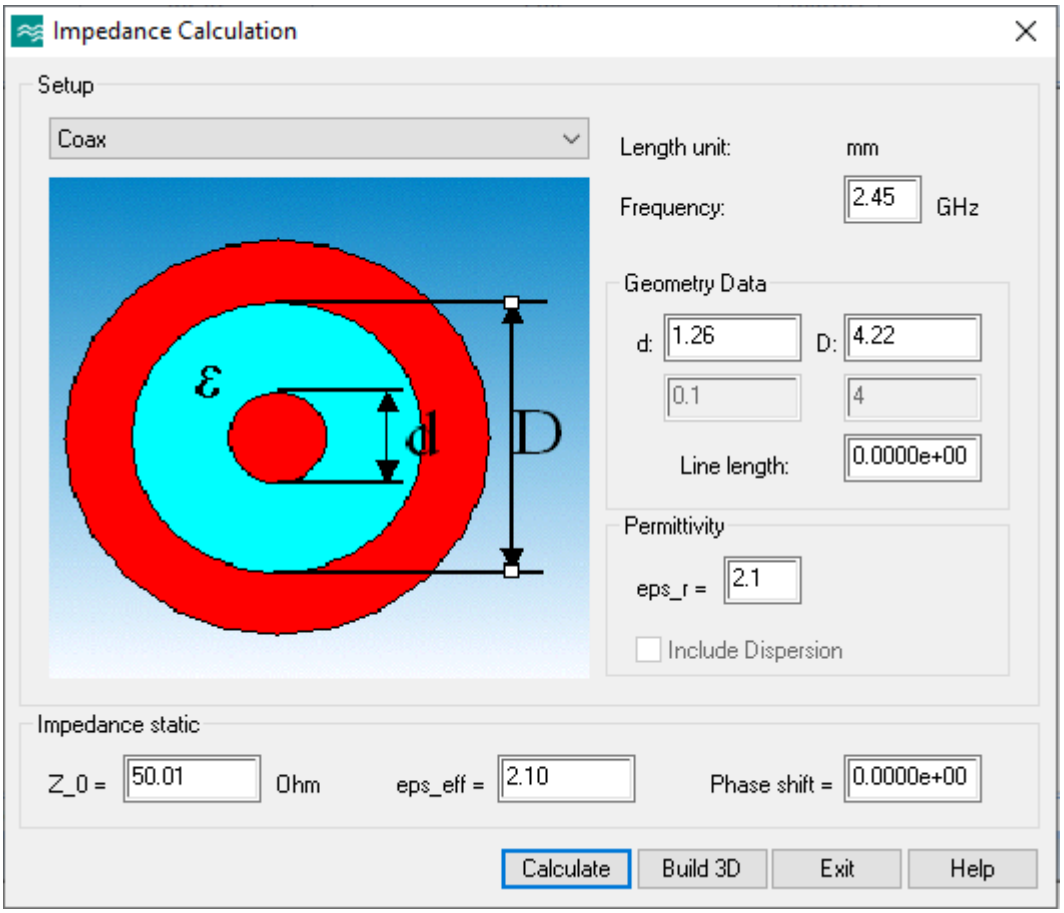

Fig. 3.2: Selection of coaxial probe dimensions to provide 50 Ω

3.5 METHOD OF CALCULATION OF THE PATCH SIZE

There are several methods to analyse microstrip antennas such as transmission-line model, cavity model and full wave techniques. Transmission line is the easiest one. In transmission-line model, microstrip antenna is considered as two radiating apertures or slots of width W separated by the length of patch L. Due to finite length and width of patch, fringing fields present along both length and

width. This fringing is a function of ratio between length or width and height of substrate and dielectric constant of substrate. As (L/h) is much greater than 1, fringing is reduced. However, it should be considered because it impacts the resonant frequency of antenna [9].

The fringing fields from patch experience a nonhomogeneous two-dielectric environment (typically air and substrate). For that reason, the effective dielectric constant is introduced to account for wave propagation and fringing. The value of effective permittivity (ϵ_{eff}) is $1 < \epsilon_{eff} < \epsilon_r$, where relative permittivity of substrate should be much greater than 1. The ϵ_{eff} value depends on frequency of operation. As W/h is much greater than unity, the effective permittivity can be written as [9],

$$\epsilon_{eff} = \frac{\epsilon_r + 1}{2} + \frac{\epsilon_r + 1}{2}\left[1 + 12\frac{h}{W}\right]^{-\frac{1}{2}} \qquad (3.5.1)$$

Due to presence of fringing fields, electrical dimensions of microstrip patch antenna greater than physical size. The extended length ΔL can be expressed as [9],

$$\frac{\Delta L}{h} = 0.412\,\frac{\left(\epsilon_{eff} + 0.3\right)\left(\frac{W}{h} + 0.264\right)}{\left(\epsilon_{eff} - 0.258\right)\left(\frac{W}{h} + 0.8\right)} \qquad (3.5.2)$$

For dominant mode (TM_{10}), physical length L is taken as $\frac{\lambda}{2}$. The effective length of patch will be, $L_{eff} = L + 2\Delta L$ and resonant frequency at dominant mode is given by [9],

$$(f_r)_{10} = \frac{c}{2L_{eff}\sqrt{\epsilon_{eff}}}$$

$$L_{eff} = \frac{c}{2(f_r)_{10}\sqrt{\epsilon_{eff}}}$$

The term 'c' refers to the speed of light in free space and its value is 3×10^8 m/s. Putting the value of L_{eff},

$$L + 2\Delta L = \frac{c}{2(f_r)_{10}\sqrt{\epsilon_{eff}}}$$

Therefore, the physical length (L) of the patch is given by,

$$L = \frac{c}{2(f_r)_{10}\sqrt{\epsilon_{eff}}} - 2\Delta L$$

The width of an efficient radiator is given by [9],

$$W = \frac{c}{2f_r}\sqrt{\left(\frac{2}{\epsilon_r + 1}\right)}$$

From the above discussion, it is clear that the size of patch can be estimated based on relative permittivity and height of substrate, environment of antenna and resonant frequency of antenna.

3.6 SELECTION OF FREQUENCY BAND FOR THIS WORK

From the Section 3.5, it is clear that the area of patch i.e., L × W, is inversely proportional to square of the frequency of operation. So, the area of patch reduces with increase in frequency.

Before starting the work, we need to choose the frequency of operations in between 402-405 MHz, 1427-1432 MHz and 2400-2448 MHz. According to our previous discussion, the antenna size should be miniaturized to implant it properly within human body. Dimensions of patch antenna are calculated within frequency range of 300 MHz (0.3 GHz) to 3000 MHz (3 GHz) by using 'Microstrip patch

antenna calculator (https://www.emtalk.com/mpacalc.php)' as it follows the expressions described in above section (Section 3.5) to estimate length and width of patch. Patch area with frequency is shown in Fig. 3.3.

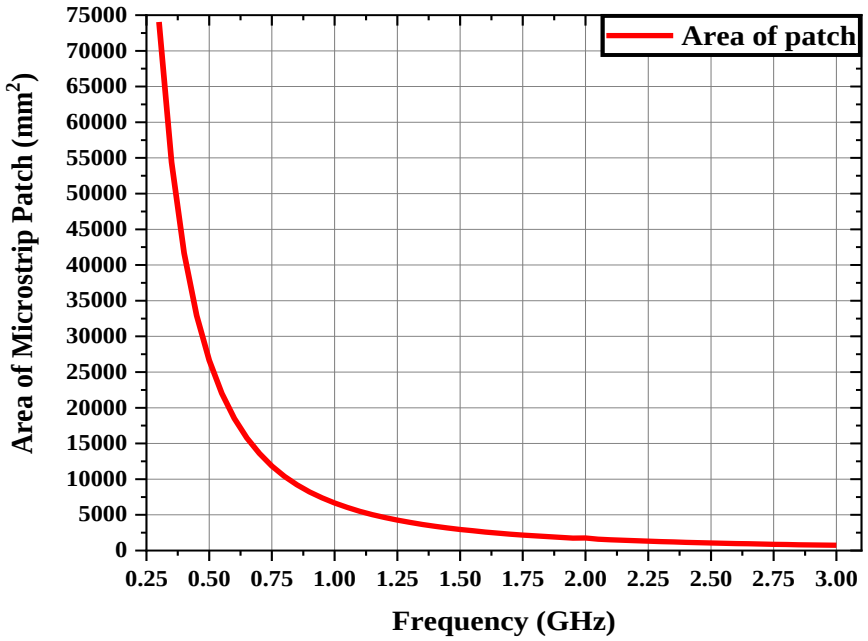

Fig. 3.3: Area of microstrip patch vs frequency

From this plot, it is very clear that the antenna size at 2.45 GHz ISM band is much smaller than those of MICS and WMTS bands. From the literature survey, typical area of implantable antenna is reported around 160mm^2 [10-14]. One of the popular miniaturization techniques is cutting of slots on patch. It can increase wavelength by increasing current path length and reduce resonant frequency. However, it can reduce gain of the antenna. Therefore, to reduce size keeping the resonant frequency fixed in MICS and WMTS bands, a greater number of slots should be added which leads to reduction of gain in both cases. However, less amount of size reduction is required while the antenna is operating in 2.45 GHz ISM band. Reduction of gain can hamper the communication between implantable

antenna and external world due to high lossy nature of human body. Therefore, reduction of antenna gain cannot be entertained for this purpose. So, 2.45 GHz ISM band has been chosen for designing implantable antenna. In Section 3.7, 3.8 and 3.9, antenna performances in MICS, WMTS and 2.45 GHz ISM band have discussed.

3.7 SIMPLE PATCH IN MICS BAND

A simple microstrip patch antenna is designed in CST Microwave Studio 2017 and presented in Fig. 3.4. A coaxial probe is connected to feed this antenna. Copper is used here as conducting parts and Arlon AD 430 is utilized as substrate material. The relative permittivity of Arlon AD 430 is 4.3 and loss tangent ($\tan \delta$) is 0.003. The dimensions of this antenna are tabulated in Table 3.1.

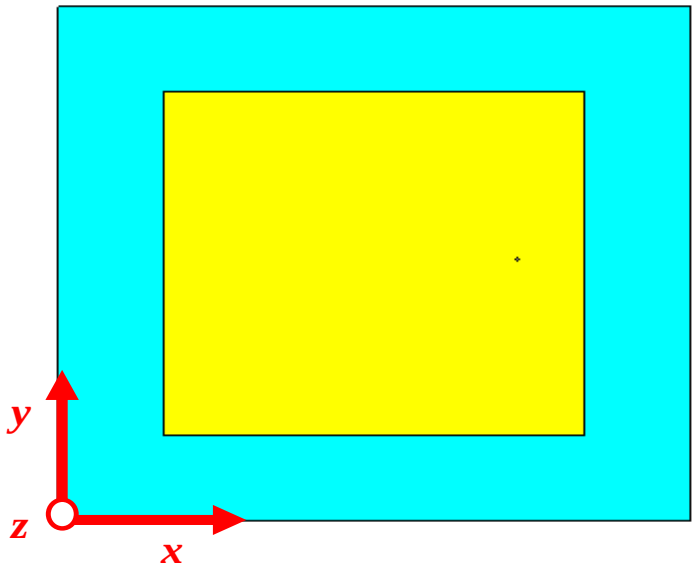

Fig. 3.4: Top view of patch of antenna operating in MICS band

TABLE 3.1: Dimensions of the antenna structure operating in MICS Band

Parameters	Values (mm)	Parameters	Values (mm)
Length of ground	354	Width of ground	320
Length of substrate	354	Width of substrate	320
Length of patch	177	Width of patch	160
Thickness of substrate	0.762	Thickness of copper	0.01

The simulation is performed in CST Microwave Studio 2017. Simulated reflection coefficient (S_{11}), real and imaginary parts of input impedance (Zin) are shown in Fig. 3.5. From this figure, it is observed that this antenna is tuned at 403.6 MHz. Maximum realized gain with frequency is shown in Fig. 3.6. Radiated far fields for H-plane ($\varphi = 0^0$) and E-plane ($\varphi = 90^0$) at resonant frequency are plotted in Fig. 3.7.

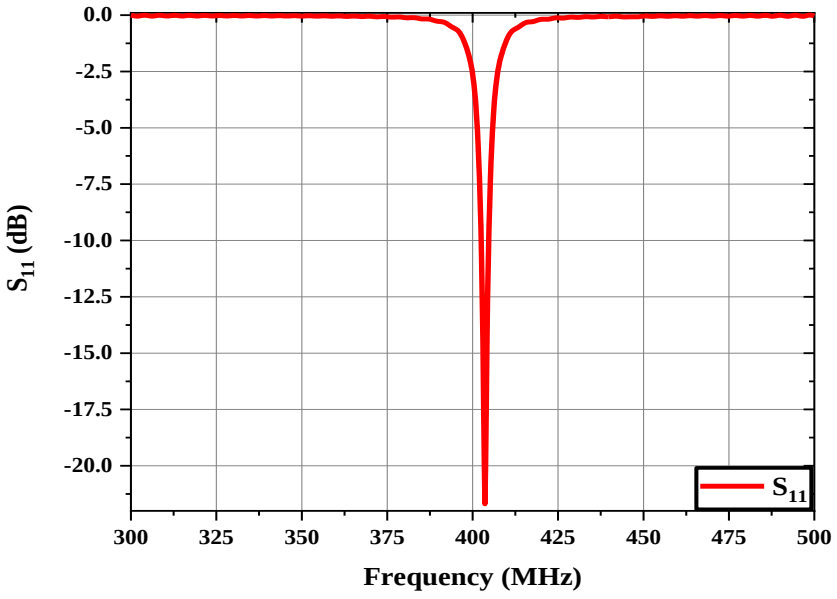

(a)

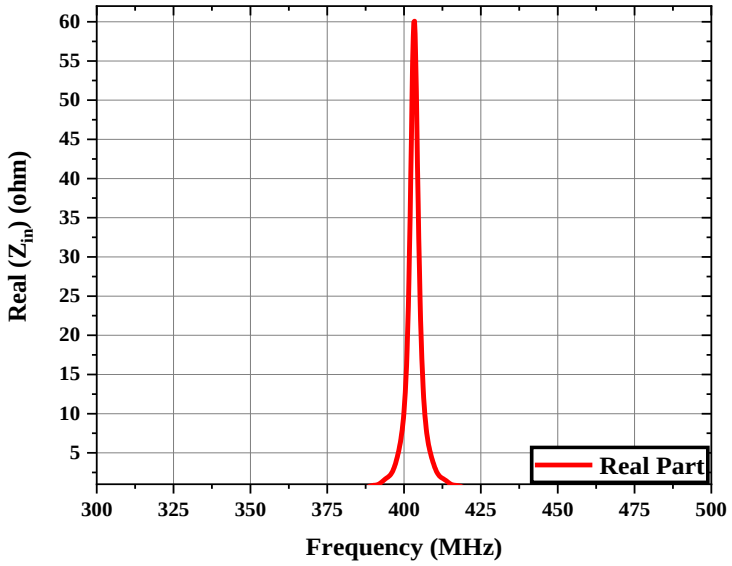

(b)

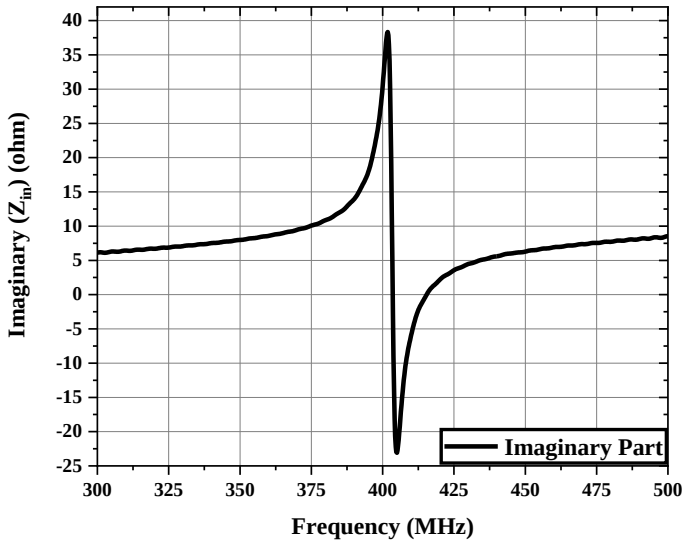

(c)

Fig. 3.5: (a) S_{11} vs Frequency, (b) real part and (c) imaginary part of input impedance with frequency of antenna tuned at MICS band

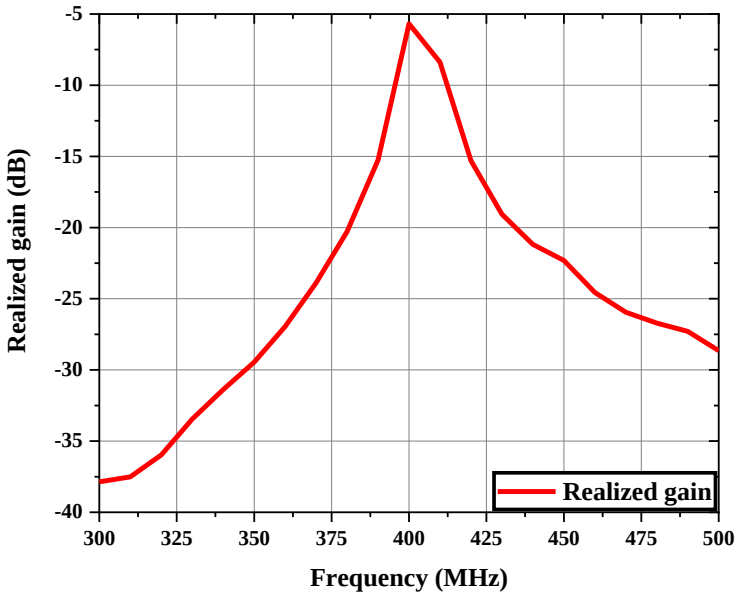

Fig. 3.6: Realized gain vs frequency plot of antenna tuned at 403.6 MHz

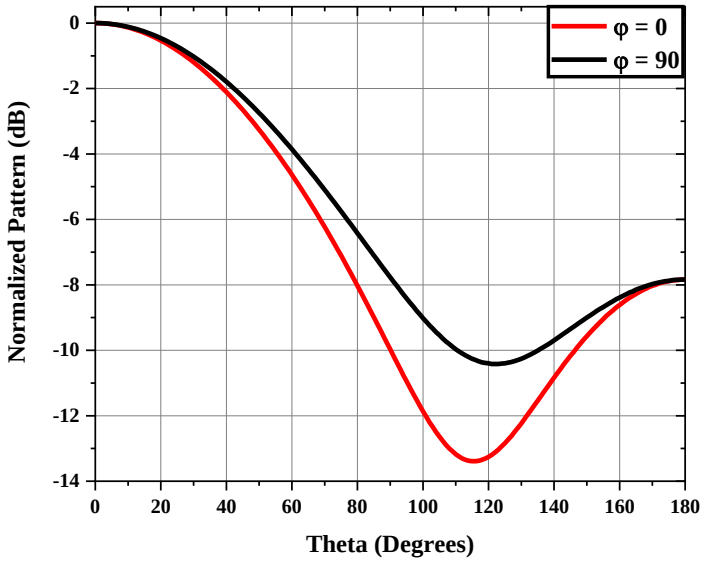

Fig. 3.7: Normalized radiated power pattern in $\varphi = 0^0$ and $\varphi = 90^0$ plane at 403.6 MHz

3.8 SIMPLE PATCH IN WMTS BAND

A microstrip patch antenna tuned at WMTS band (1427-1432 MHz) is designed in CST Microwave Studio 2017 and presented in Fig. 3.8. Here also, copper is used here as conducting parts and Arlon AD 430 is utilized as substrate material. The dimensions of this antenna are tabulated in Table 3.2.

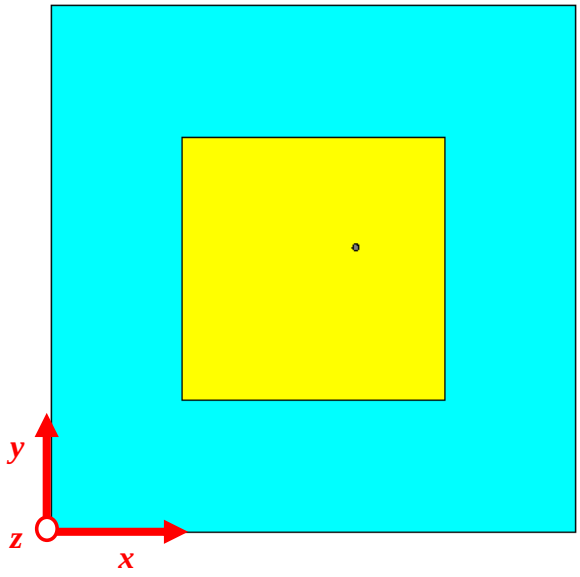

Fig. 3.8: Top view of patch of antenna operating in WMTS band

TABLE 3.2: Dimensions of the antenna structure operating in WMTS Band

Parameters	Values (mm)	Parameters	Values (mm)
Length of ground	100	Width of ground	99.5
Length of substrate	100	Width of substrate	99.5
Length of patch	50	Width of patch	49.75
Thickness of substrate	0.762	Thickness of copper	0.01

Simulated reflection coefficient (S_{11}), real and imaginary parts of input impedance (Zin) are shown in Fig. 3.9. From this figure, it is observed that this antenna is tuned at 1429.4 MHz. Maximum realized gain with frequency is shown in Fig. 3.10. Radiated far fields for H-plane ($\varphi = 0^0$) and E-plane ($\varphi = 90^0$) at resonant frequency are plotted in Fig. 3.11.

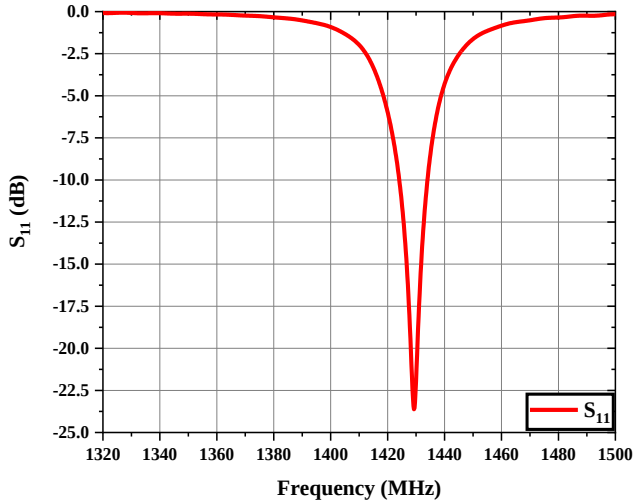

(a)

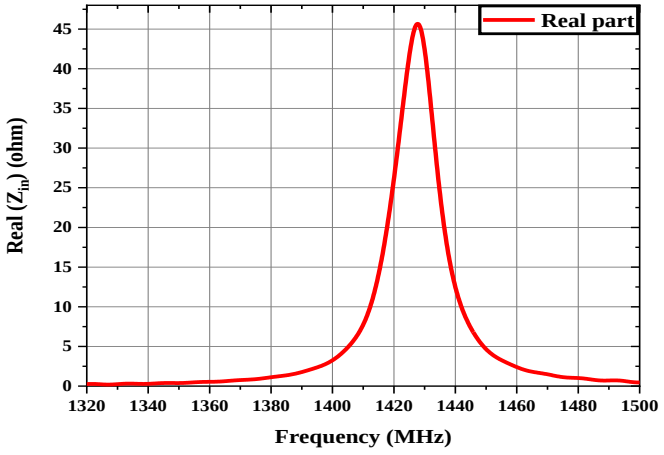

(b)

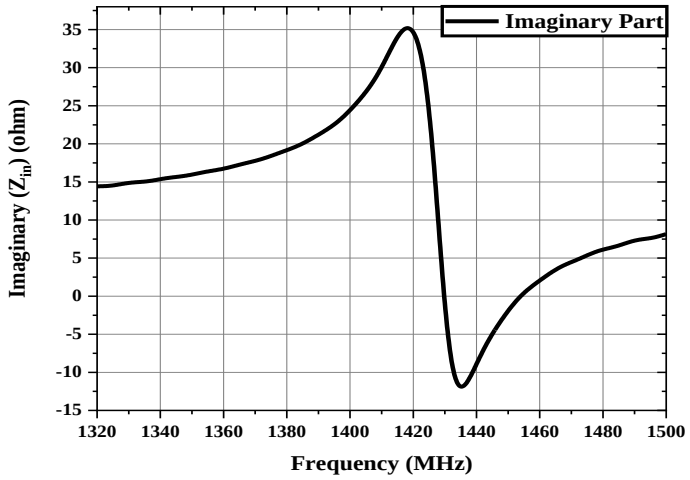

(c)

Fig. 3.9: (a) S_{11} vs Frequency, (b) real part and (c) imaginary part of input impedance with frequency of antenna tuned at WMTS band

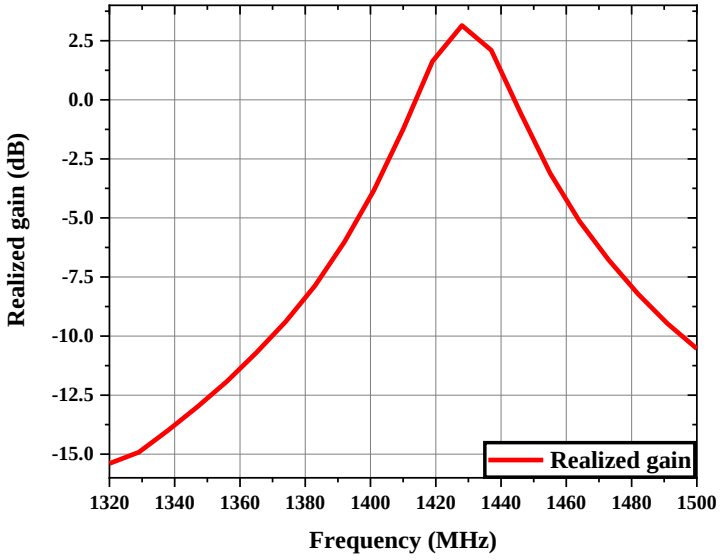

Fig. 3.10: Realized gain vs frequency plot of antenna tuned at 1429.4 MHz

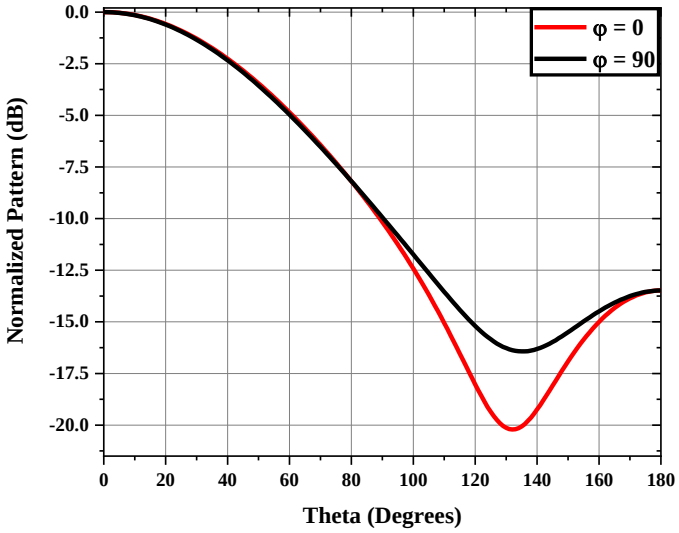

Fig. 3.11: Normalized radiated power pattern in $\varphi = 0^0$ and $\varphi = 90^0$ plane at 1429.4 MHz

3.9 SIMPLE PATCH IN 2.45 GHz ISM BAND

Fig. 3.12 presents a patch antenna tuned at 2.45 GHz ISM band and the materials of this antenna is same as pervious designs. Dimensions of this antenna are tabulated in Table 3.3.

TABLE 3.3: Dimensions of the antenna structure operating in ISM Band

Parameters	Values (mm)	Parameters	Values (mm)
Length of ground	100	Width of ground	99.5
Length of substrate	100	Width of substrate	99.5
Length of patch	50	Width of patch	49.75
Thickness of substrate	0.762	Thickness of copper	0.01

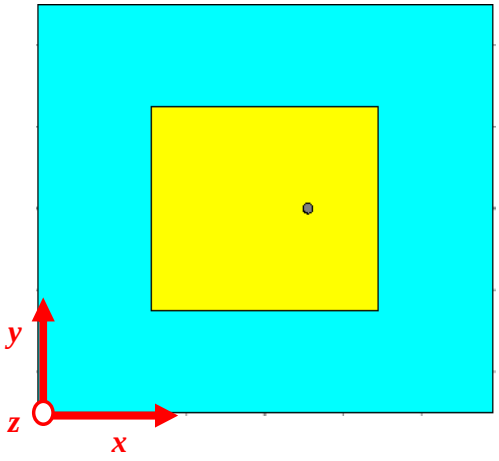

Fig. 3.12: Top view of patch of antenna operating in 2.45 GHz ISM band

Simulated reflection coefficient (S_{11}), real and imaginary parts of input impedance are shown in Fig. 3.13. From this figure, it is observed that this antenna is tuned at 2443.1 MHz. Maximum realized gain with frequency is shown in Fig. 3.14. Radiated far fields for H-plane ($\varphi = 0^0$) and E-plane ($\varphi = 90^0$) at resonant frequency are plotted in Fig. 3.15.

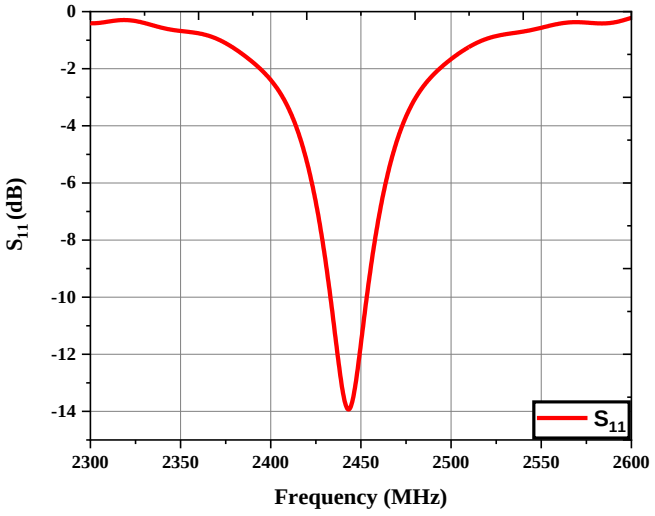

(a)

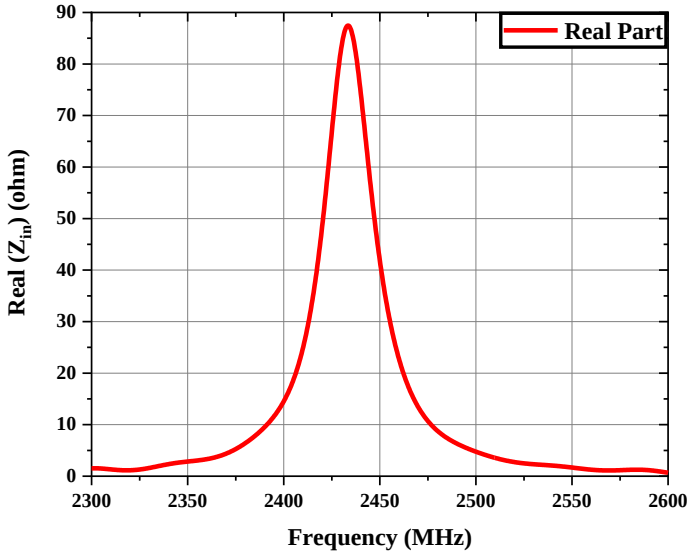

(b)

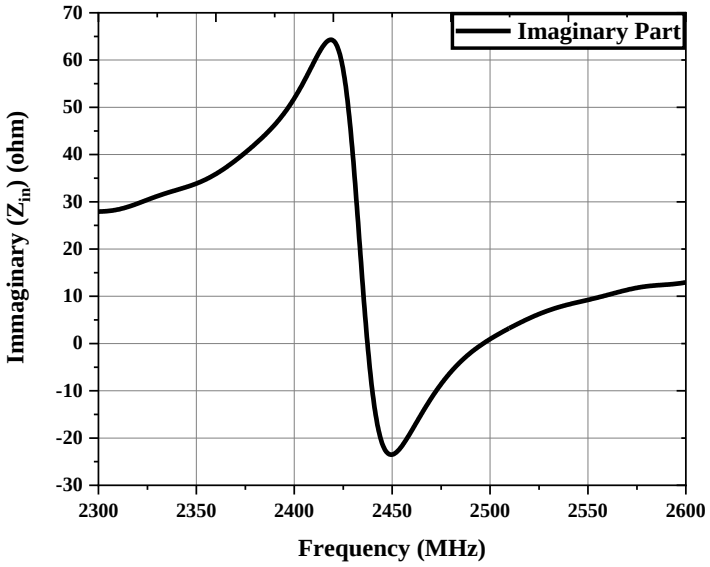

(c)

Fig. 3.13: (a) S_{11} vs Frequency, (b) real part and (c) imaginary part of input impedance with frequency of antenna tuned at 2.45 GHz ISM band

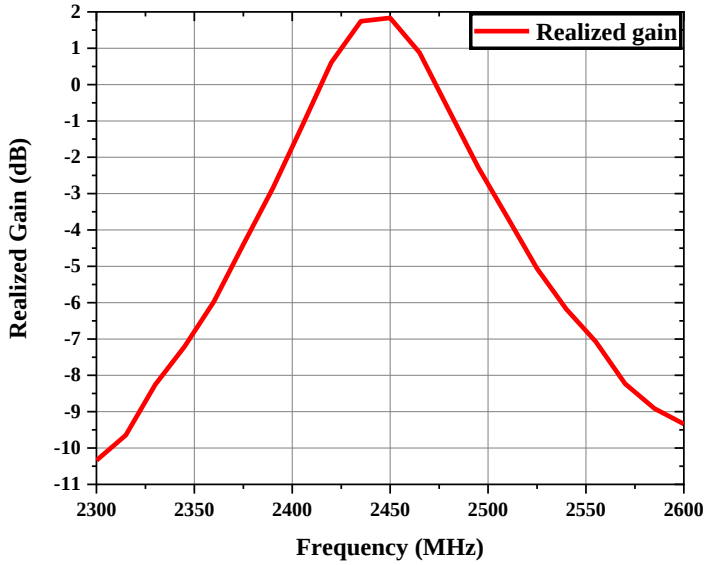

Fig. 3.14: Realized gain vs frequency plot of antenna tuned at 2443.1 MHz

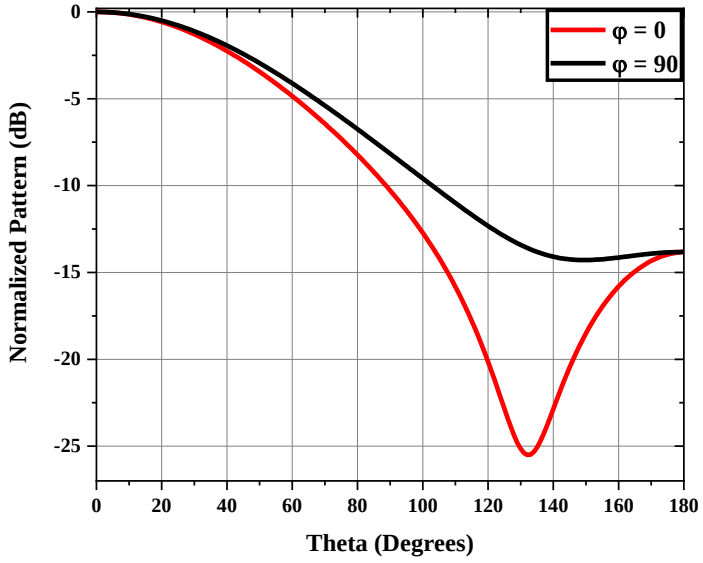

Fig. 3.15: Normalized radiated power pattern in $\varphi = 0^0$ and $\varphi = 90^0$ plane at 2443.1 MHz

3.10 CONCLUSION

In this chapter, brief concept about electromagnetic frequency bands dedicated for medical applications is discussed. Along with it, design procedure of a microstrip antenna and relation of patch area with operating frequency has also been studied. It is clear that the patch size can be reduced with the increment of frequency. 2.45 GHz ISM band has been chosen for designing implantable antenna due to smaller size of antenna than size in 403 MHz and 1429.4 MHz. Coaxial feeding in microstrip patch antenna is used here because this feeding technique can satisfy many design requirements.

REFERENCES

[1] M. N. Islam and M. R. Yuce, "Review of Medical Implant Communication System (MICS) band and network," *ICT Express,* vol. 2, vo. 4, September 2016.

[2] https://transition.fcc.gov.in (Revised in 1st July, 2022).

[3] https://www.fda.gov/medical-devices/wireless-medical-devices/wireless-medical - telemetry-systems.

[4] C. K. Wu, T. F. Chien, C. L. Yang and C. H. Luo, "Design of Novel S- Shaped Quad-Band Antenna for MedRadio/WMTS/ISM Implantable Biotelemetry Applications," *International Journal of Antennas and Propagation,* July 2012.

[5] M. N. Shakib, M. Moghavvemi, W. N. L. Mahadi and M. R. Ahmed, "Design of a Broadband implantable antenna in the rat for biotelemetry applications," *2015 IEEE MTT-S 2015 International Microwave Workshop Series on RF and Wireless Technologies for Biomedical and Healthcare Applications (IMWS-BIO),* October 2015.

[6] https://resources.altium.com/p/ism-bands-around-world.

[7] N. Ganesamoorthy, M. Malathi, A. K. Srinivasan and T. Shanmuganantham, "Performance of implantable antenna at ISM band characteristics for biomedical base," *ICT Express,* vol. 8, no. 2, May 2021.

[8] R. Garg, P. Bhartia, I. Bahl and A. Ittipiboon, "*Microstrip Antenna Design Handbook*," Artech House, London.

[9] C. A. Balanis, "*Antenna theory: Analysis and Design*," Wiley, 4th Edition.

[10] F-J. Huang, C-M. Lee, C-L. Chang, L-K. Chen, T-C. Yo and C-H. Luo, "Rectenna Application of Miniaturized Implantable Antenna Design for Triple-Band Biotelemetry Communication," *IEEE Transactions on Antennas and Propagation,* vol. 59, no. 7, pp. 2646 – 2653, July 2011.

[11] C. Liu, Y-X. Guo and S. Xiao, "A Hybrid Patch/Slot Implantable Antenna for Biotelemetry Devices," *IEEE Antennas and Wireless Propagation Letters,* vol. 11, pp. 1646 – 1649, 2012.

[12] L-J. Xu, Y-X. Guo and W. Wu, "Miniaturised slot antenna for biomedical applications," *Electronics Letters,* vol. 49, no. 17, pp. 1060 – 1061, August 2013.

[13] S. Das and D. Mitra, "A Compact Wideband Flexible Implantable Slot Antenna Design with Enhanced Gain," *IEEE Transactions an Antennas and Propagation*, vol. 66, no. 8, pp. 4309 – 4314, August 2018.

[14] C. Liu, Y. X. Guo and S. Xiao, "Circularly Polarized Helical Antenna for ISM-Band Ingestible Capsule Endoscope Systems," *IEEE Transactions an Antennas and Propagation*, vol. 62, no. 12, pp. 6027 – 6039, December 2014.

Chapter 4

Properties of Human tissues

Contents	
	4.1 Introduction
	4.2 Properties of lossy dielectric medium
	4.3 Properties of skin layer
	4.4 Properties of fat layer
	4.5 Properties of muscle layer
	4.6 Comparison between skin, fat and muscle properties
	4.7 Conclusion

4.1 INTRODUCTION

The behaviour of electromagnetic waves within a medium depends on properties of that medium. When an electromagnetic wave travels through a perfect dielectric no attenuation takes place as the medium contains no charges whereas the wave is reflected back completely due to incidence on a perfect conductor which has very high conductivity. However, the wave is attenuated and partially reflected while it propagates through a lossy dielectric medium. Therefore, it is required to know the medium properties to study wave propagation through that medium. In this chapter, properties of different human tissues like permittivity, permeability, conductivity, attenuation and phase shift constant etc. have been studied.

4.2 PROPERTIES OF LOSSY DIELECTRIC MEDIUM

Objective of this thesis work is basically implantation of antenna within human body to detect Madelung's disease. Therefore, it is very important to understand the behaviour of electromagnetic waves propagating through different layers of human body such as skin, fat, muscle. Their electrical properties i.e., relative permittivity and conductivity depend on their water, oil and salt contents. Different tissues have different shapes of cells or molecules. Due to these factors, all layers of human body have different properties. However, all types of tissues are non-magnetic in nature and that means relative permeability of human tissues can be considered as unity [1-2]. Human body layers are considered as lossy dielectric materials. In this section 4.2, different properties of a general lossy dielectric material are discussed very briefly.

4.2.1. Permittivity and loss tangent

Electric permittivity or simply *permittivity* of a material is a measure of its electrical polarizability. In electromagnetics, permittivity can be defined as the ratio of electric flux density ($\vec{D}$) and electric field intensity ($\vec{E}$). For a lossy dielectric, permittivity is complex in nature and it can be written as [3-4],

$$\epsilon_r{}^* = \epsilon_r' - j\epsilon_r'' \qquad (4.2.1)$$

where, ϵ_r' and $\epsilon_r{}''$ are frequency dependent real and imaginary parts of the complex dielectric constant $\epsilon_r{}^*$. The real part (ϵ_r') decreases from maximum value to 1 for low frequency to high frequency. The imaginary part is there due to dielectric loss [3]. This part is discussed in Appendix thoroughly.

The *loss tangent* can be determined as [3],

$$\tan\delta = \frac{\epsilon_r''}{\epsilon_r'} \qquad (4.2.2)$$

In lossy medium, loss tangent can be defined also in another way. It is the ratio of conduction current density ($\overrightarrow{J_c}$) and displacement current density ($\overrightarrow{J_d}$). Therefore,

$$\tan\delta = \frac{|\overrightarrow{J_c}|}{|\overrightarrow{J_d}|} = \frac{|\sigma E|}{|j\omega\epsilon E|} = \frac{\sigma}{\omega\epsilon_0\epsilon_r'} \tag{4.2.3}$$

where σ, ϵ_0 and ϵ_r' are conductivity, permittivity of free space and relative permittivity of the lossy medium respectively. Sometimes the term $\left(\frac{\sigma}{\omega\epsilon_0\epsilon_r'}\right)$ is also called *dissipation factor* [5].

4.2.2. Propagation constant

Helmholtz's wave equation for electric field can be written as,

$$\nabla^2\vec{E} + \omega^2\mu\epsilon\left(1 - j\frac{\sigma}{\omega\epsilon}\right)\vec{E} = 0 \tag{4.2.4}$$

$$\nabla^2\vec{E} + \gamma^2\vec{E} = 0$$

where the term γ is called *propagation constant* of the lossy medium. The propagation constant can be written as [4],

$$\gamma = \sqrt{\omega^2\mu\epsilon\left(1 - j\frac{\sigma}{\omega\epsilon}\right)} = \alpha + j\beta \tag{4.2.5}$$

The terms α and β are called attenuation constant and phase constant respectively. When an electromagnetic wave propagates through a lossy medium, it is attenuated by some amount which is characterized by attenuation constant (α) whose unit is Np/m. Along with attenuation, some phase shift occurs in electromagnetic wave. The phase constant (β) is the measure of phase shift (in

radians) per unit length while wave is propagating through the medium and its unit is rad/m. The expressions of attenuation and phase constant are shown below [4].

$$\alpha = \omega \sqrt{\frac{\mu\epsilon}{2}\left[\sqrt{1+\left(\frac{\sigma}{\omega\epsilon}\right)^2}-1\right]} \tag{4.2.6}$$

$$\beta = \omega \sqrt{\frac{\mu\epsilon}{2}\left[\sqrt{1+\left(\frac{\sigma}{\omega\epsilon}\right)^2}+1\right]} \tag{4.2.7}$$

For a lossy medium, $\left(\frac{\sigma}{\omega\epsilon}\right)$ is finite. Therefore, propagation constant for this type of medium is *complex* in nature [4].

4.2.3. Intrinsic impedance

Intrinsic impedance or *characteristic impedance* of a medium is defined by the ratio between amplitudes of electric and magnetic field and its unit is ohm [5]. Intrinsic impedance for free space is $120\,\pi \approx 377\,\Omega$ ($\because \frac{E}{H} = \sqrt{\frac{\mu_0}{\epsilon_0}} = 120\pi$). But it is complex for lossy dielectric medium and it can be expressed as,

$$\eta = \frac{j\omega\mu}{\gamma} \tag{4.2.8}$$

4.2.4. Phase velocity

Phase velocity is a rate at which an electromagnetic wave propagates through a medium. The phase of any one frequency-component of wave travels at this velocity. This velocity can be written as,

$$v_p = \frac{\omega}{\beta} \tag{4.2.9}$$

4.3 PROPERTIES OF SKIN LAYER

According to experiment on dielectric properties of different parts of human body by Gabriel and others in [6-9], relative permittivity and conductivity of human body layers change with frequency. Therefore, all the properties related to these two parameters can be varied with frequency of operation. Permittivities and conductivities of human skin layer for different frequency values ranging from 300 MHz to 3000 MHz are enlisted in Table 4.1 by using references [10-11]. Attenuation and phase constant at each frequency is also included in the table.

Table 4.1. Properties of Skin in different frequencies

Frequency (MHz)	ϵ_r	σ **(S/m)**	α **(Np/mm)**	β **(rad/mm)**
300	49.80	0.64	0.0161	0.0472
354	48.00	0.67	0.0172	0.0542
408	46.60	0.69	0.0182	0.0611
462	45.50	0.71	0.0191	0.0680
516	44.70	0.73	0.0199	0.0750
570	44.00	0.75	0.0207	0.0819
624	43.40	0.77	0.0215	0.0888
678	42.90	0.79	0.0222	0.0956
732	42.40	0.81	0.0229	0.1025
786	42.10	0.83	0.0235	0.1094

Frequency (MHz)	ϵ_r	σ **(S/m)**	α **(Np/mm)**	β **(rad/mm)**
840	41.70	0.85	0.0242	0.1162
894	41.40	0.87	0.0248	0.1230
948	41.20	0.88	0.0254	0.1300
1002	40.90	0.90	0.0260	0.1368
1056	40.70	0.92	0.0266	0.1436
1110	40.50	0.94	0.0273	0.1505
1164	40.30	0.95	0.0279	0.1573
1218	40.20	0.97	0.0285	0.1643
1272	40.00	0.99	0.0291	0.1711
1326	39.80	1.01	0.0297	0.1778
1380	39.70	1.03	0.0304	0.1847
1434	39.60	1.05	0.0310	0.1916
1488	39.50	1.07	0.0317	0.1985
1542	39.30	1.09	0.0323	0.2051
1596	39.20	1.11	0.0330	0.2120
1650	39.10	1.13	0.0336	0.2188
1704	39.00	1.15	0.0343	0.2256

Frequency (MHz)	ϵ_r	σ **(S/m)**	α **(Np/mm)**	β **(rad/mm)**
1758	38.90	1.17	0.0349	0.2324
1812	38.90	1.19	0.0355	0.2394
1866	38.80	1.21	0.0362	0.2462
1920	38.70	1.23	0.0369	0.2530
1974	38.60	1.25	0.0375	0.2597
2028	38.50	1.28	0.0385	0.2664
2082	38.50	1.30	0.0391	0.2735
2136	38.40	1.32	0.0397	0.2802
2190	38.30	1.35	0.0407	0.2869
2244	38.20	1.37	0.0413	0.2935
2298	38.20	1.39	0.0420	0.3005
2352	38.10	1.42	0.0429	0.3072
2406	38.10	1.44	0.0435	0.3142
2460	38.00	1.47	0.0445	0.3208
2514	37.90	1.49	0.0452	0.3274
2568	37.90	1.52	0.0461	0.3344
2622	37.80	1.55	0.0470	0.3410

Frequency (MHz)	ϵ_r	σ **(S/m)**	α **(Np/mm)**	β **(rad/mm)**
2676	37.80	1.57	0.0477	0.3480
2730	37.70	1.60	0.0486	0.3546
2784	37.70	1.63	0.0495	0.3616
2838	37.60	1.66	0.0505	0.3681
2892	37.60	1.68	0.0511	0.3751
2946	37.50	1.71	0.0521	0.3816
3000	37.50	1.74	0.0530	0.3886

The relative permittivity and conductivity with frequency plot for skin are shown in Fig. 4.1 and 4.2 respectively.

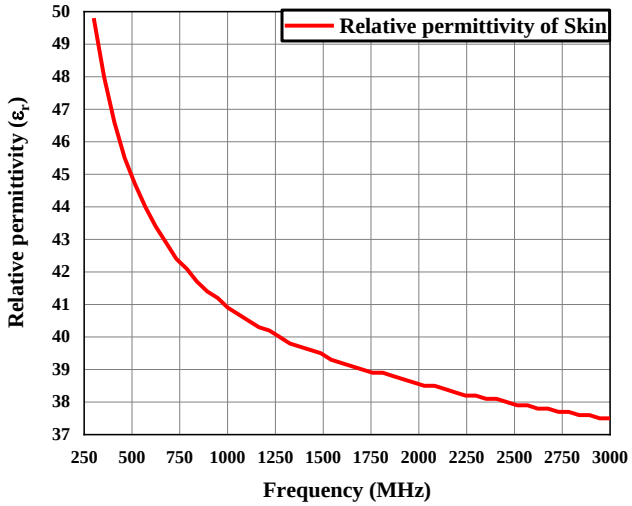

Fig. 4.1: Relative permittivity vs. frequency for skin

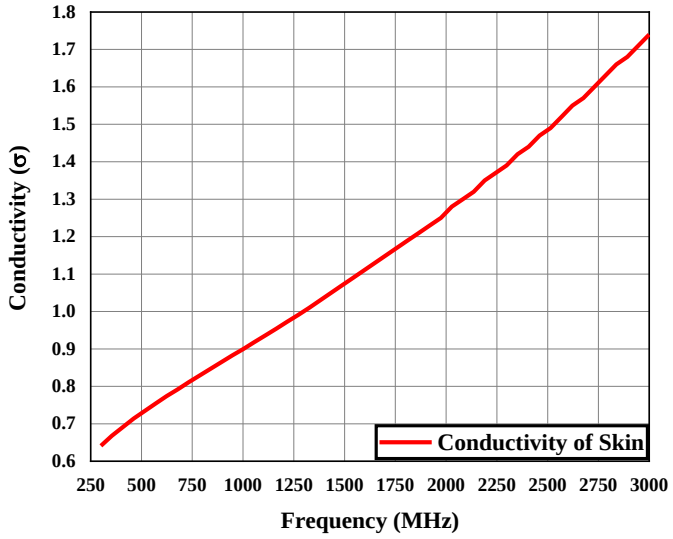

Fig. 4.2: Conductivity vs. frequency for skin

The calculated values of attenuation and phase constant by using formulas in Section 4.2 are plotted with frequency for skin as illustrated in Fig. 4.3 and 4.4 respectively.

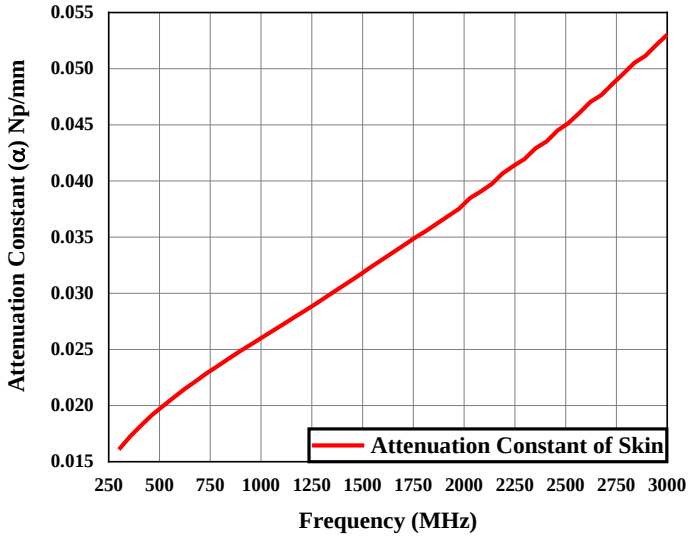

Fig. 4.3: Attenuation constant vs. frequency for skin

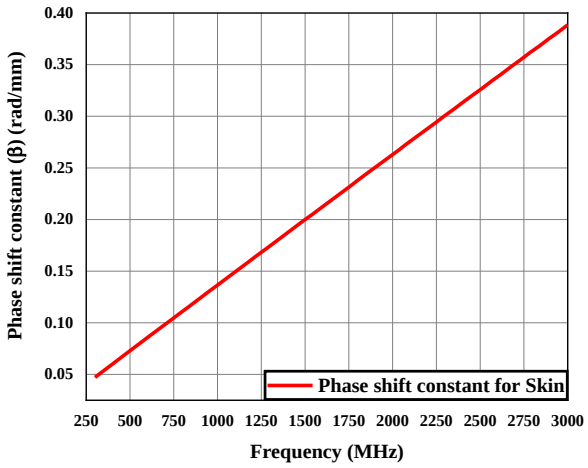

Fig. 4.4: Phase constant vs. frequency for skin

As discussed in Chapter 3, 2.45 GHz ISM band is used for this thesis work. It is required to know properties of skin at 2.45 GHz before starting the design of implantable antenna.

At 2.45 GHz, respective values of relative permittivity (ϵ_r) and conductivity (σ) are 38 and 1.46 S/m. Putting those values in equations 4.2.6 and 4.2.7, the values of attenuation and phase constant are obtained as 0.0442 Np/mm and 0.32 rad/mm respectively. Propagation constant (γ) will be (0.0442 + j 0.32). Characteristic impedance (η) of skin is $60.03 < 7.882^0$.

4.4 PROPERTIES OF FAT LAYER

Tabulation of permittivities and conductivities of human fat layer for different frequency values ranging from 300 MHz to 3000 MHz are shown in Table 4.2 from [10-11]. Along with them, the values of α and β for each frequency are enlisted.

Table 4.2. Properties of fat in different frequencies

Frequency (MHz)	ϵ_r	σ **(S/m)**	α **(Np/mm)**	β **(rad/mm)**
300	11.7	0.0765	0.00413764	0.021894964
354	11.7	0.0787	0.004274492	0.025728101
408	11.6	0.081	0.004429635	0.029450421
462	11.6	0.0835	0.004575058	0.033284816
516	11.5	0.0861	0.004743838	0.036968965
570	11.5	0.0889	0.004903139	0.040795918
624	11.5	0.0919	0.005072519	0.044626285
678	11.4	0.0949	0.005263748	0.048251979
732	11.4	0.0982	0.005449398	0.052070093
786	11.4	0.102	0.005662243	0.055891849
840	11.4	0.105	0.005830919	0.059709829
894	11.3	0.109	0.006080685	0.063259507
948	11.3	0.113	0.006305106	0.067066969
1002	11.3	0.117	0.006529451	0.070874693
1056	11.3	0.121	0.006753733	0.07468264
1110	11.3	0.125	0.006977963	0.078490777

Frequency (MHz)	ϵ_r	σ **(S/m)**	α **(Np/mm)**	β **(rad/mm)**
1164	11.2	0.129	0.007233735	0.081939697
1218	11.2	0.134	0.007514535	0.085736204
1272	11.2	0.138	0.007739662	0.089527913
1326	11.2	0.143	0.008020439	0.093324507
1380	11.2	0.148	0.00830121	0.097121122
1434	11.1	0.153	0.008619986	0.100472748
1488	11.1	0.158	0.008901997	0.104252595
1542	11.1	0.163	0.009184003	0.108032458
1596	11.1	0.169	0.009521946	0.111817085
1650	11.1	0.174	0.00980395	0.115596956
1704	11.1	0.18	0.010141894	0.119381579
1758	11	0.186	0.010526674	0.122618194
1812	11	0.191	0.010809943	0.126381189
1866	11	0.197	0.011149395	0.130148997
1920	11	0.203	0.011488847	0.133916807
1974	11	0.21	0.011884476	0.137689456
2028	11	0.216	0.012223925	0.141457276

Frequency (MHz)	ϵ_r	σ **(S/m)**	α **(Np/mm)**	β **(rad/mm)**
2082	10.9	0.222	0.012620009	0.144573371
2136	10.9	0.229	0.013017399	0.148329245
2190	10.9	0.235	0.013358375	0.152080186
2244	10.9	0.242	0.013755755	0.155836095
2298	10.9	0.248	0.014096729	0.159587041
2352	10.9	0.255	0.014494102	0.163342981
2406	10.8	0.262	0.014959154	0.166342861
2460	10.8	0.269	0.01535831	0.170081956
2514	10.8	0.276	0.01575746	0.173821074
2568	10.8	0.284	0.016213223	0.177565372
2622	10.8	0.291	0.016612357	0.181304547
2676	10.8	0.298	0.017011486	0.185043739
2730	10.7	0.306	0.017547245	0.187927097
2784	10.7	0.313	0.017948181	0.191649372
2838	10.7	0.321	0.018405951	0.195377007
2892	10.7	0.329	0.018863703	0.199104699
2946	10.7	0.336	0.01926462	0.20282704
3000	10.7	0.344	0.01972235	0.20655481

The relative permittivity and conductivity with frequency plot for fat are shown in Fig. 4.5 and 4.6 respectively.

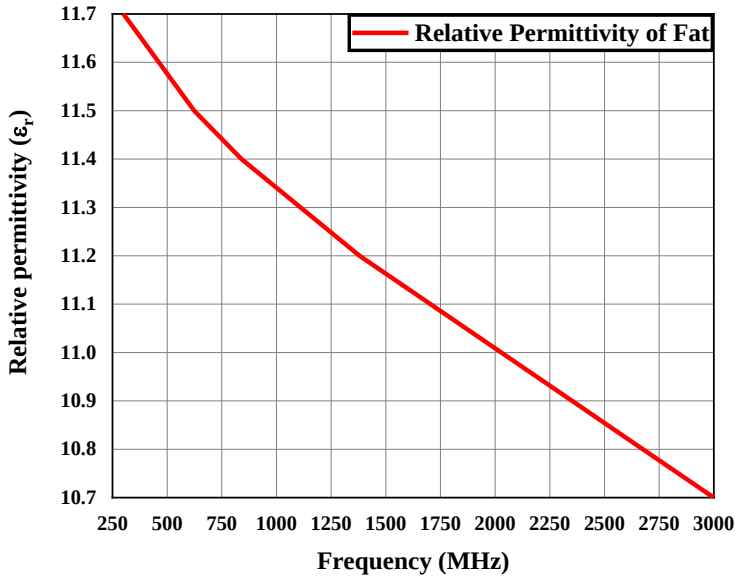

Fig. 4.5: Relative permittivity vs. frequency for fat

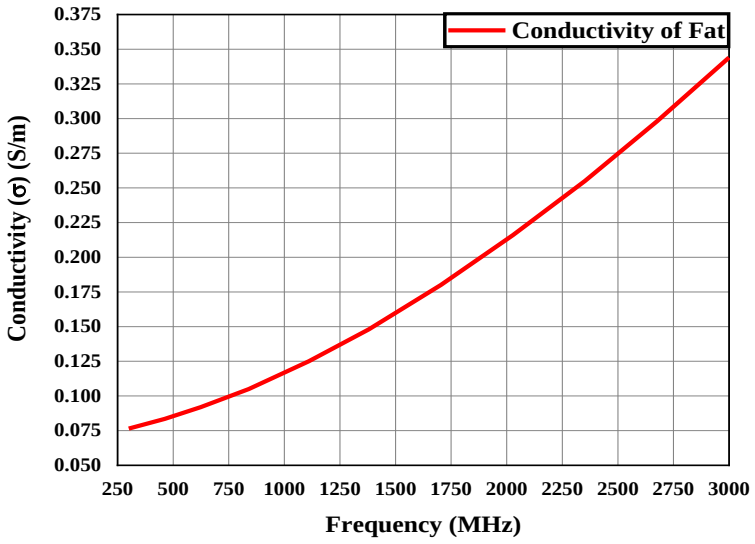

Fig. 4.6: Conductivity vs. frequency for fat

The calculated values of attenuation and phase constant are plotted with frequency for fat are illustrated in Fig. 4.7 and 4.8 respectively.

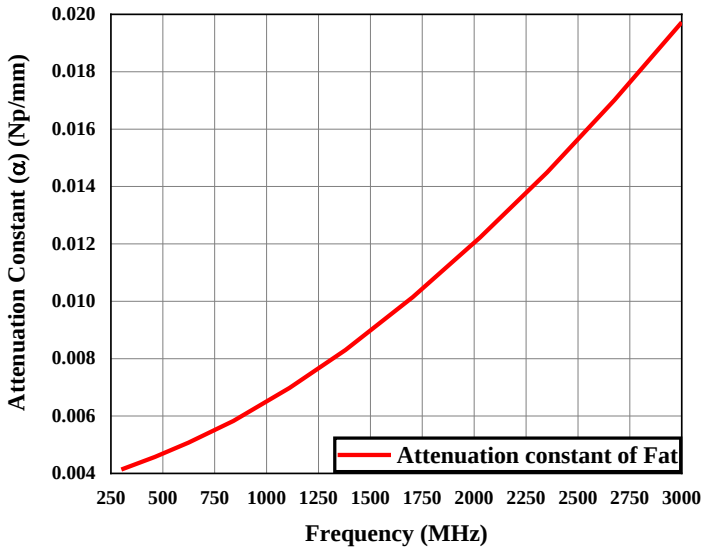

Fig. 4.7: Attenuation constant vs. frequency for fat

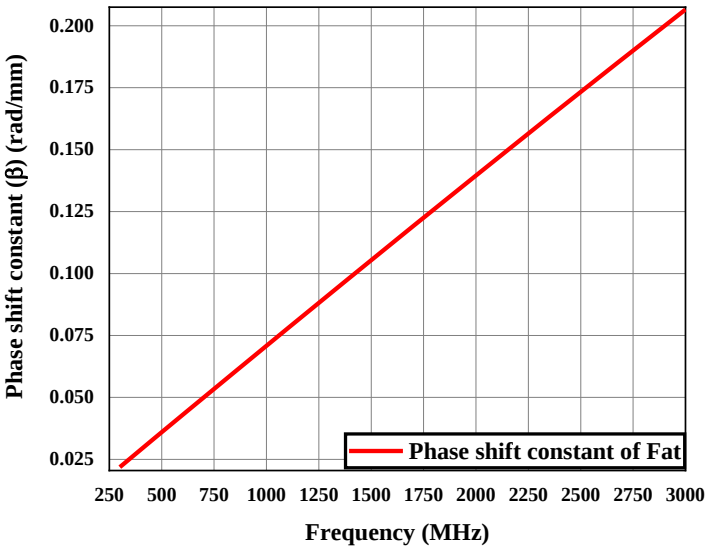

Fig. 4.8: Phase constant vs. frequency for fat

At 2.45 GHz, respective values of relative permittivity (ϵ_r) and conductivity (σ) are 10.8 and 0.268 S/m. The values of attenuation and phase constant are obtained from equations 4.2.6 and 4.2.7, as 0.0153 Np/mm and 0.17 rad/mm respectively. Propagation constant (γ) will be (0.0153 + j 0.17). Characteristic impedance (η) of fat is $113.84 < 5.17^0$.

4.5 PROPERTIES OF MUSCLE LAYER

Relative permittivities and conductivities of human mascle layer for different frequency values ranging from 300 MHz to 3000 MHz are shown in Table 4.3 from [10-11]. The calculated values of attenuation and phase constant at each frequency are mentioned in below table.

Table 4.3. Properties of muscle in different frequencies

Frequency (MHz)	ϵ_r	σ **(S/m)**	α **(Np/mm)**	β **(rad/mm)**
300	58.2	0.771	0.017844769	0.051165708
354	57.6	0.784	0.018490025	0.059251058
408	57.1	0.798	0.019080974	0.06735608
462	56.7	0.812	0.01961818	0.075483767
516	56.4	0.827	0.020136565	0.083653496
570	56.1	0.841	0.020613869	0.091796392
624	55.9	0.857	0.021108585	0.100004738

Frequency (MHz)	ϵ_r	σ **(S/m)**	α **(Np/mm)**	β **(rad/mm)**
678	55.7	0.872	0.021570596	0.10819279
732	55.5	0.889	0.022073905	0.116371855
786	55.3	0.905	0.022549003	0.124525432
840	55.2	0.923	0.023049872	0.132778193
894	55	0.941	0.023568237	0.140901081
948	54.9	0.96	0.024089338	0.149131362
1002	54.8	0.979	0.024609108	0.157350748
1056	54.7	0.999	0.025152558	0.165562329
1110	54.6	1.02	0.025720202	0.173765299
1164	54.5	1.04	0.026262987	0.181951851
1218	54.4	1.06	0.026805713	0.190125369
1272	54.3	1.09	0.027596973	0.198319967
1326	54.2	1.11	0.02814054	0.206465914
1380	54.1	1.13	0.028658866	0.214789379
1434	54.1	1.16	0.029452171	0.222948272
1488	54	1.18	0.029969989	0.231266449
1542	53.9	1.21	0.03076476	0.239403498

Frequency (MHz)	ϵ_r	σ **(S/m)**	α **(Np/mm)**	β **(rad/mm)**
1596	53.8	1.23	0.031310365	0.247493697
1650	53.8	1.26	0.032107504	0.255600809
1704	53.7	1.29	0.032876361	0.263930659
1758	53.6	1.32	0.033675482	0.272015252
1812	53.5	1.35	0.034476009	0.280084616
1866	53.5	1.38	0.035277955	0.28813871
1920	53.4	1.41	0.03604858	0.29644659
1974	53.3	1.44	0.036852599	0.304477918
2028	53.3	1.47	0.037658069	0.312493882
2082	53.2	1.5	0.038429924	0.320786984
2136	53.1	1.54	0.039490336	0.328810308
2190	53.1	1.57	0.040299684	0.336787841
2244	53	1.6	0.041072874	0.345065883
2298	52.9	1.64	0.042137742	0.35305055
2352	52.8	1.67	0.042951023	0.360989493
2406	52.8	1.71	0.044019654	0.368943099
2460	52.7	1.75	0.045048767	0.377228528

Frequency (MHz)	ϵ_r	σ **(S/m)**	α **(Np/mm)**	β **(rad/mm)**
2514	52.7	1.78	0.045866298	0.385128684
2568	52.6	1.82	0.04693967	0.393043534
2622	52.5	1.86	0.048015058	0.40094283
2676	52.5	1.9	0.049047021	0.409205397
2730	52.4	1.94	0.050125387	0.417081491
2784	52.3	1.98	0.051205789	0.424941983
2838	52.3	2.02	0.052239658	0.433189292
2892	52.2	2.06	0.053323063	0.441026519
2946	52.1	2.1	0.054408522	0.448848094
3000	52.1	2.14	0.055444309	0.457080118

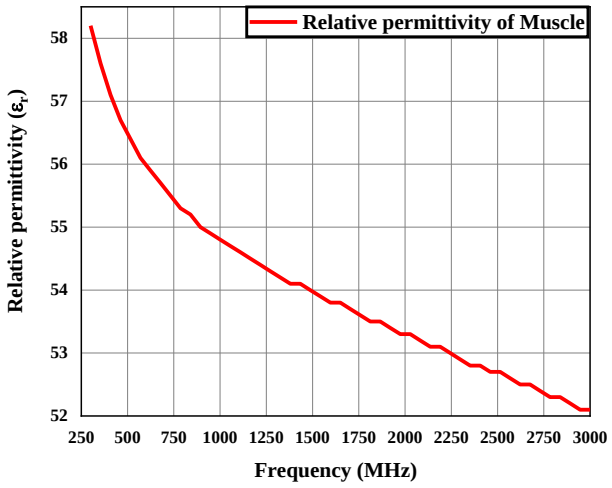

Fig. 4.9: Relative permittivity vs. frequency for muscle

The relative permittivity and conductivity with frequency plot for muscle are shown in Fig. 4.9 and 4.10 respectively.

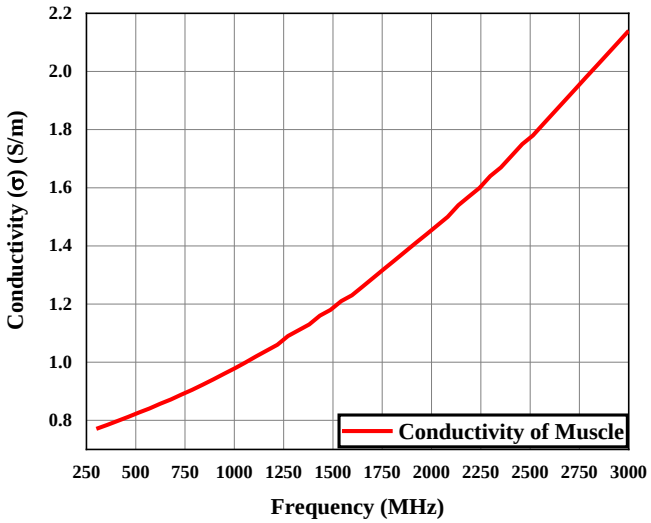

Fig. 4.10: Conductivity vs. frequency for muscle

Plots of Attenuation and phase constant with frequency for muscle are shown in Fig. 4.11 and 4.12 respectively.

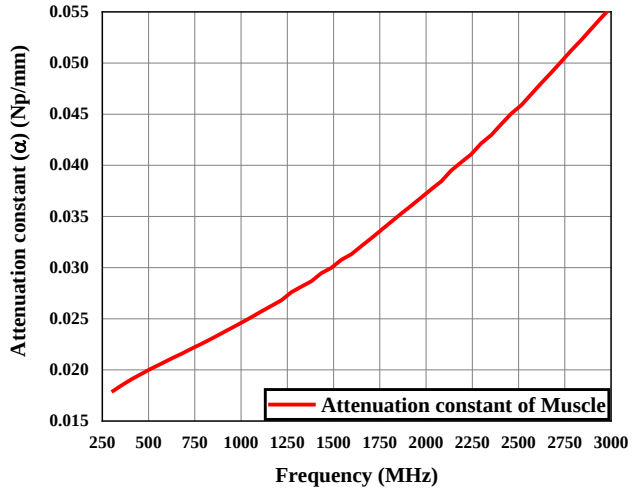

Fig. 4.11: Attenuation constant vs. frequency for muscle

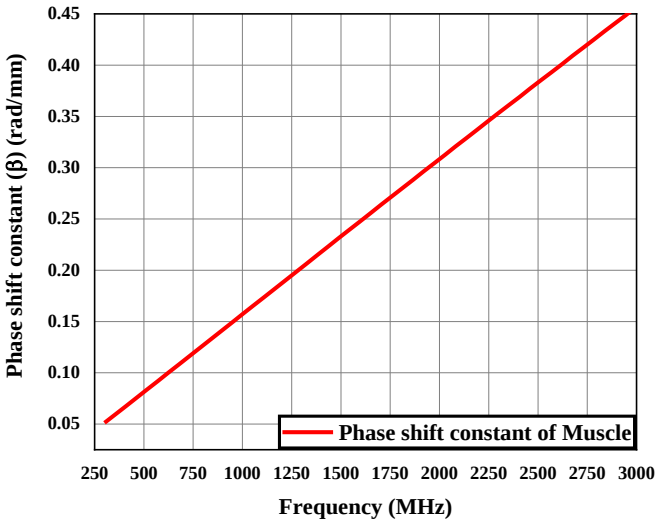

Fig. 4.12: Phase constant vs. frequency for muscle

At 2.45 GHz, respective values of relative permittivity (ϵ_r) and conductivity (σ) are 52.7 and 1.74 S/m. The attenuation and phase constant for muscle are 0.0448 Np/mm and 0.38 rad/mm respectively. Propagation constant (γ) value will be (0.0448 + j 0.38). Characteristic impedance (η) of skin is $51.22 < 6.82^0$.

4.6 COMPARISON BETWEEN SKIN, FAT AND MUSCLE PROPERTIES

In this section, a comparative study between skin, fat and muscle layers in terms of relative permittivity, conductivity, attenuation constant, phase constant and intrinsic impedance at 2.45 GHz is discussed and tabulated in Table 4.4. From this table, order of permittivity and conductivity is Muscle > Skin > Fat.

Table 4.4. Comparative study of skin, fat and muscle at 2.45 GHz

Layer	ϵ_r	σ **(S/m)**	α **(Np/mm)**	β **(rad/mm)**	η **(Ω)**
Skin	38	1.46	0.0442	0.32	$60.03 < 7.882^0$
Fat	10.8	0.268	0.0153	0.17	$113.43 < 5.17^0$
Muscle	52.7	1.74	0.0448	0.38	$51.22 < 6.82^0$

When an electromagnetic wave propagates through skin, fat and muscle layers, wave is more attenuated and phase shifted in muscle due to high conductivity and permittivity than skin and fat. From the above table, intrinsic impedance of fat is higher than other layers.

4.7 CONCLUSION

The study of medium properties is very important to predict the behaviour of electromagnetic wave passing through it. In case of implantable antenna, electromagnetic waves should pass through different layers of human body. If attenuation and phase shift occurred due to medium are known to the engineers and scientists, they can design antenna property to establish communication path with external world. In this chapter, different properties like permittivity, permeability, conductivity, attenuation and phase constant, intrinsic impedance and their variation with frequency of skin, fat and muscle at 2.45 GHz are studied which will be helpful for next discussion.

REFERENCES

[1] J. R. Nagel, C. M. Furse, D. A. Christensen and C. A. Durney, "*Basic Introduction to Bioelectromagnnetics,*" *CRC Press, Taylor & Francis Group*, 2019.

[2] M. F. Iskander, "*Electromagnetic Fields and Waves*," Waveland Press, 2nd edition.

[3] S. O. Kasap, "*Principles of Electronic Materials and Devices*," Mc-Graw Hill, 3rd edition.

[4] D. M. Pozar, "*Microwave Engineering*," Wiley, 4th edition

[5] E. C. Jordan and K. G. Balmain, "*Electromagnetic Waves and Radiating Systems*," PHI Learning Private Limited, India, 2nd Edition, 2013.

[6] C. Gabriel and S. Gabriel, "Compilation of the Dielectric Properties of Body tissues at RF and Microwave Frequencies," *Physics*, 1996.

[7] C. Gabriel, S. Gabriel and E. Corthout, "The dielectric properties of biological tissues: I. Literature survey," *Physics in Medicine and Biology*, vol. 41, no. 11, pp. 2231-2249, December 1996.

[8] S. Gabriel, R. W. Lau and C. Gabriel, "The dielectric properties of biological tissue II: Measurements in the frequency range 10 Hz to 20 GHz," *Physics in Medicine and Biology*, vol. 41, no. 11, pp. 2251-2269, December 1996.

[9] S. Gabriel, R. W. Lau and C. Gabriel, "The dielectric properties of biological tissue III: Parametric models for the dielectric spectrum of tissues," *Physics in Medicine and Biology*, vol. 41, no. 11, pp. 2271-2293, December 1996.

[10] http://niremf.ifac.cnr.it/tissprop/htmlclie/htmlclie.php.

[11] https://itis.swiss/virtual-population/tissueproperties/database/dielectric properties

Chapter 5

Transfer matrix of body model

Contents	
	5.1 Introduction
	5.2 Transfer matrix for a multilayer model
	5.3 Problem statement
	5.4 Transfer matrix for the problem
	5.5 Conclusion

5.1 INTRODUCTION

Human body consists of several layers such as skin, fat, muscle etc. For analysing reflection, transmission, absorption, field distributions within human body, three-layer body model is used widely. Instead of three layers (i.e., skin, fat and muscle), many layers can be considered to get more precise result. However, the 3-layer model is taken to reduce complexity. According to several research works, it was observed that, layers other than skin, fat and muscle such as blood, bone, individual skin layers (epidermis, dermis etc. instead of a homogeneous skin layer) do not contribute major effects on performance of implantable antenna. Therefore, in this work, a three-layer human body model is considered.

It is very important to understand how electric field variation occurs while it is transferred through a multilayer human body. In this chapter, electric field variations at each interface of the body layers are calculated and a transfer matrix is calculated for the multilayer- human body model. To calculate the transfer matrix

of a system, whole structure of a multilayer system is decomposed into some small elements and the matrix is obtained by using properties of ABCD matrices. This technique is applicable equally for both transverse-electric (TE) and transverse-magnetic (TM) incident waves. [1-2].

5.2 TRANSFER MATRIX FOR A MULTILAYER MODEL

An isotropic and homogeneous N-layer (let) system is considered where the boundaries are at z = $Z_1, Z_2, \ldots, Z_N$ as shown in Fig. 5.1. Each layer is assumed to be constant in terms of electric and magnetic properties like permittivity, permeability and conductivity. Let for a layer l, permittivity, permeability and conductivity are ϵ_l, μ_l and σ_l respectively. An electric field ($\overrightarrow{E_i}$) is incident from air to the surface of layer-1.

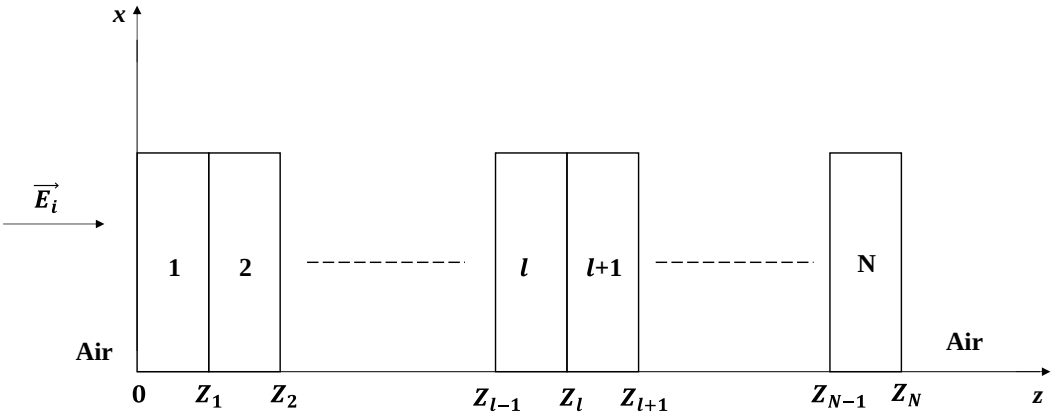

Fig. 5.1: N-layer dielectric system

The electric field variation is in x direction and electromagnetic wave is assumed to propagate along +z direction. The expression of incident electric field can be written as,

$$\overrightarrow{E_i} = E_0^+ e^{-jk_0 z} \hat{a}_x$$

where k_0 is the wave vector through free space and its value is $\omega\sqrt{\mu_0 \epsilon_0}$. Here ω, μ_0 and ϵ_0 are operating angular frequency, permeability and permittivity of free space. One part of incident electric field gets reflected back to air from the first medium. Therefore, in the region of z < 0, reflected wave exists in form of

$$\overrightarrow{E_r} = \Gamma E_0^+ e^{+jk_0 z} \hat{a}_x$$

The term Γ is reflection coefficient of this reflected electric field. Another part of incident wave is transmitted to the first medium. If T is transmission coefficient of transmitted field, the transmitted wave in first layer (z > 0) can be written as,

$$\overrightarrow{E_t} = \mathrm{T} E_0^+ e^{-\gamma_1 z} \hat{a}_x$$

The term γ_1 is intrinsic impedance of the first layer. This wave is again reflected back to first medium from the interface between first and second layer and transmitted to second medium. Each medium has different propagation constants $(\gamma_1, \gamma_2, \dots, \gamma_l, \gamma_{l+1}, \dots, \gamma_N)$ and intrinsic impedances $(\eta_1, \eta_2, \dots, \eta_l, \eta_{l+1}, \dots, \eta_N)$. For interface between two layers (say 1 and 2), relation between reflection and transmission coefficients are,

$$\Gamma_{21} = 1 + T_{12}$$

Transfer matrix can be obtained by multiplying two types of matrices. They are – amplitude transmission matrix and discontinuity transfer matrix. Amplitude transmission matrix $[A]_{2X2}$ is related to the change in amplitude of electric field within a layer and discontinuity transfer matrix $[D]_{2X2}$ describes the amount of reflection and transmission in interface between two layers.

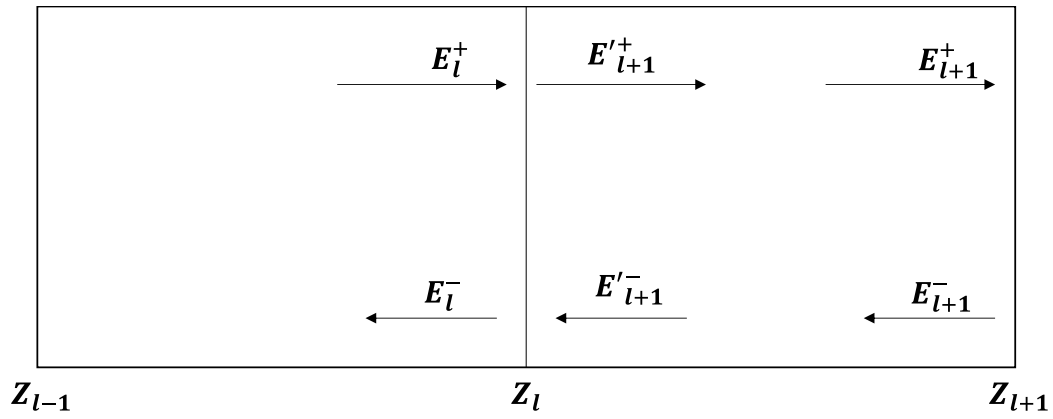

Fig. 5.2: Reflecting and transmitting electric field inside l^{th} and $(l+1)^{th}$ layers

From Fig. 5.2, amplitude transmission matrix of $(l+1)^{th}$ layer can be defined as [1],

$$\begin{bmatrix} E_{l+1}^+ \\ E_{l+1}^- \end{bmatrix} = [A]_{l+1} \begin{bmatrix} E'^+_{l+1} \\ E'^-_{l+1} \end{bmatrix}$$

The discontinuity transfer matrix of the interface between l^{th} and $(l+1)^{th}$ layer can be written [1] from Fig. 5.2 as

$$\begin{bmatrix} E'^+_{l+1} \\ E'^-_{l+1} \end{bmatrix} = [D]_{(l+1)l} \begin{bmatrix} E_l^+ \\ E_l^- \end{bmatrix}$$

Then the transfer matrix will be,

$$[T]_{(l+1)l} = [A]_{l+1}\,[D]_{(l+1)l}$$

Now, for $(l+1)^{th}$ layer, the amplitude transmission matrix from [1] will be,

$$[A]_{(l+1)} = \begin{bmatrix} e^{-\gamma_{l+1}(Z_{l+1} - Z_l)} & 0 \\ 0 & e^{\gamma_{l+1}(Z_{l+1} - Z_l)} \end{bmatrix}$$

and discontinuity transfer matrix $[D]_{(l+1)l}$ is obtained from [1] as,

$$[D]_{(l+1)l} = \frac{1}{1-\Gamma_{(l+1)l}}\begin{bmatrix} 1 & -\Gamma_{(l+1)l} \\ -\Gamma_{(l+1)l} & 1 \end{bmatrix}$$

The transfer matrix can be defined from Fig. 5.2 as,

$$\begin{bmatrix} E_{l+1}^{+} \\ E_{l+1}^{-} \end{bmatrix} = [T]_{(l+1)l}\begin{bmatrix} E_{l}^{+} \\ E_{l}^{-} \end{bmatrix}$$

5.3 PROBLEM STATEMENT

As mentioned in the previous chapter, human body has high absorbing nature. Therefore, it is very crucial to know how much attenuation and phase shift of electric field have occurred while it is propagating through different layers of human body. Communication with external devices is one of the main concerns for implantable antenna designers. In this thesis work, an antenna is going to be placed at muscle layer. Let us suppose an antenna is placed in free space and three- layer human body model consisting of skin, fat and muscle, is placed at the far field of it as shown in Fig. 5.3 to investigate the change in incident electric field characteristics for each layer. For 2.45 GHz, the propagation constants and intrinsic impedances of skin, fat and muscle layers are enlisted in Table 5.1.

Table 5.1. Properties of human body layers at 2.45 GHz

Layer	$\boldsymbol{\gamma = \alpha + j\beta}$	$\boldsymbol{\eta}$ **(Ω)**
Skin	0.0442+j0.32	$60.03 < 7.882^0$
Fat	0.0153+j0.17	$113.43 < 5.17^0$
Muscle	0.0448+j0.38	$51.22 < 6.82^0$

The thickness of skin, fat and muscle layers are 6 mm, 2 mm and 20 mm respectively. Thickness of muscle layer is set based on implantation depth of antenna within muscle layer. Variables assigned for skin, fat and muscle thicknesses are h_s, h_f and h_m respectively. Therefore, h_s = 6mm, h_f = 2mm and h_m = 20mm. A superstrate should be placed on the antenna to protect tissues from direct contact with conducting patch. Therefore, a superstrate is placed at the right side of muscle layer.

Fig. 5.3: Electric field incident on a three-layer human body model

5.4 TRANSFER MATRIX FOR THE PROBLEM

The transmission line equivalent model for the problem is shown in Fig. 5.4. The whole problem is divided into 3 parts to calculate the overall transfer matrix as described below.

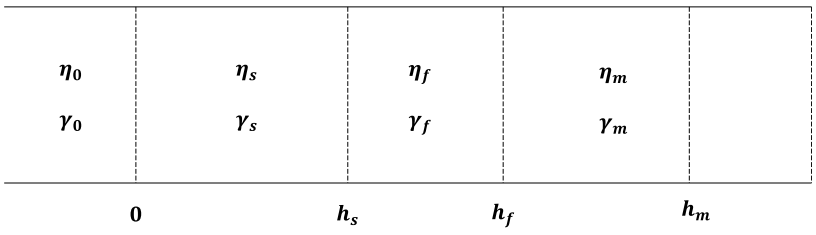

Fig. 5.4: Transmission line equivalent model of the problem

5.4.1. Interface between air and skin

The reflection coefficient at the interface between air and skin can be calculated as,

$$\Gamma_{10} = \frac{\eta_1 - \eta_0}{\eta_1 + \eta_0}$$

$$= \frac{(60.03 < 7.882°) - 120\pi}{(60.03 < 7.882°) + 120\pi}$$

$$= \frac{(59.46 + j8.23) - 120\pi}{(59.46 + j8.23) + 120\pi}$$

$$= \frac{-317.65 + j8.23}{436.46 + j8.23}$$

$$= 0.728 < 177.48°$$

$$= -0.728 + j0.033$$

Therefore,

$$\frac{1}{1 - \Gamma_{10}} = 0.58 + j0.01 = 0.58 < 1.09°.$$

Propagation constant of skin is $\gamma_s = 0.0442 + j0.32 = 0.323 < 82.14°$.

Therefore, $\gamma_s h_s = (0.0442 + j0.32) \times 6 = 0.265 + j1.92$.

So, $e^{\gamma_s h_s} = e^{0.265}.e^{j1.92} = 1.303\ (\cos 1.92 + j \sin 1.92)$

$$= 1.303\ (-0.34 + j0.94)$$

$$= -0.45 + j1.22$$

and, $e^{-\gamma_s h_s} = e^{-0.265}.e^{-j1.92} = 0.77\ (\cos 1.92 - j \sin 1.92)$

$$= 0.77\ (-0.34 - j0.94)$$

$$= -0.26 - j0.72$$

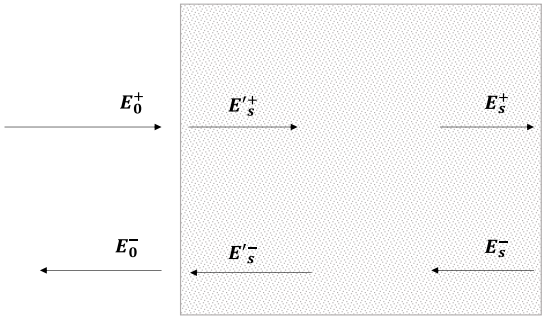

Fig. 5.5: Reflecting and transmitting electric fields from air to skin layer

Amplitude transmission matrix for skin layer,

$$[A]_{skin} = \begin{bmatrix} -0.26 - j0.72 & 0 \\ 0 & -0.45 + j1.22 \end{bmatrix}$$

Discontinuity transfer matrix for the interface between air and skin layer is,

$$[D]_{skin,air} = \begin{bmatrix} 1 & 0.73 - j0.033 \\ 0.73 - j0.033 & 1 \end{bmatrix} \times\ 0.58 < 1.09°$$

Therefore, transfer matrix for air and skin will be,

$$[T]_{skin,air} = [A]_{skin} \times [D]_{skin,air}$$

$$= \begin{bmatrix} -0.26 - j0.72 & 0 \\ 0 & -0.45 + j1.22 \end{bmatrix} \times \begin{bmatrix} 1 & 0.73 - j0.033 \\ 0.73 - j0.033 & 1 \end{bmatrix}$$

$$\times\ 0.58 < 1.09°$$

$$[T]_{skin,air} = \begin{bmatrix} -0.14 - j0.42 & -0.12 - j0.3 \\ -0.18 + j0.52 & -0.27 + j0.70 \end{bmatrix}$$

From Fig. 5.5, it can be written as,

$$\begin{bmatrix} E_s^+ \\ E_s^- \end{bmatrix} = \begin{bmatrix} -0.14 - j0.42 & -0.12 - j0.3 \\ -0.18 + j0.52 & -0.27 + j0.70 \end{bmatrix} \begin{bmatrix} E_0^+ \\ E_0^- \end{bmatrix}$$

where E_0^+, E_0^-, E_s^+ and E_s^- are respective peak values of transmitting electric field in air, reflecting electric field from air and skin interface, transmitting electric field in skin and the reflecting electric field from skin and fat interface.

5.4.2. Interface between skin and fat

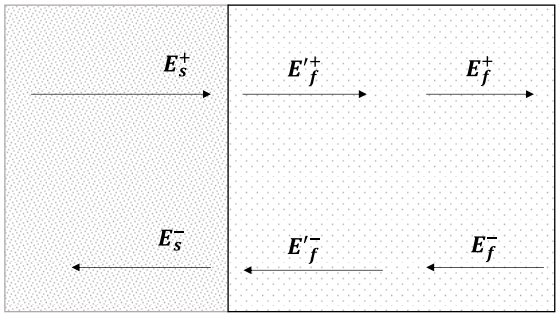

Fig. 5.6: Reflecting and transmitting electric fields from skin to fat layer

The reflection coefficient at the interface between skin and fat can be calculated as,

$$\Gamma_{21} = \frac{\eta_2 - \eta_1}{\eta_2 + \eta_1}$$

$$= \frac{(113.84 < 5.17°) - (60.03 < 7.882°)}{(113.84 < 5.17°) + (60.03 < 7.882°)}$$

$$= \frac{(113.38 + j10.26) - (59.46 + j8.23)}{(113.38 + j10.26) + (59.46 + j8.23)}$$

$$= \frac{53.92 + j2.03}{172.82 + j18.49}$$

$$= 0.31 - j0.02$$

$$\frac{1}{1 - \Gamma_{21}} = 1.45 - j0.04$$

Propagation constant of fat is $\gamma_f = 0.0153 + j0.17$.

Therefore, $\gamma_f h_f = (0.0153 + j0.17) \times 2 = 0.03 + j0.34$.

So, $e^{\gamma_f h_f} = e^{0.03}.e^{j0.34} = 1.03\ (\cos 0.34 + j \sin 0.34)$

$$= 0.97 + j0.34$$

and, $e^{-\gamma_f h_f} = e^{-0.03}.e^{-j0.34} = 0.97\ (\cos 0.34 - j \sin 0.34)$

$$= 0.91 - j0.32$$

Amplitude transmission matrix for fat layer,

$$[A]_{fat} = \begin{bmatrix} 0.91 - j0.32 & 0 \\ 0 & 0.97 + j0.34 \end{bmatrix}$$

Discontinuity transfer matrix for the interface between skin and fat layer is,

$$[D]_{fat,skin} = \begin{bmatrix} 1 & -0.31 + j0.02 \\ -0.31 + j0.02 & 1 \end{bmatrix} \times (1.45 - j0.04)$$

Therefore, transfer matrix for air and skin will be,

$$[T]_{fat,skin} = [A]_{fat} \times [D]_{fat,skin}$$

$$= \begin{bmatrix} 0.91 - j0.32 & 0 \\ 0 & 0.97 + j0.34 \end{bmatrix} \times \begin{bmatrix} 1 & -0.31 + j0.02 \\ -0.31 + j0.02 & 1 \end{bmatrix}$$

$$\times (1.45 - j0.04)$$

$$[T]_{fat,skin} = \begin{bmatrix} 1.31 - j0.5 & -0.40 + j0.17 \\ -0.45 - j0.12 & 1.42 + j0.45 \end{bmatrix}$$

From Fig. 5.6, it can be written as,

$$\begin{bmatrix} E_f^+ \\ E_f^- \end{bmatrix} = \begin{bmatrix} 1.31 - j0.5 & -0.40 + j0.17 \\ -0.45 - j0.12 & 1.42 + j0.45 \end{bmatrix} \begin{bmatrix} E_s^+ \\ E_s^- \end{bmatrix}$$

where E_s^+, E_s^-, E_f^+ and E_f^- are respective peak values of transmitting electric field in skin, reflecting electric field from fat and skin interface, transmitting electric field in fat and the reflecting electric field from muscle and fat interface.

5.4.3. Interface between fat and muscle

The reflection coefficient at the interface between fat and muscle can be calculated as,

$$\Gamma_{32} = \frac{\eta_3 - \eta_2}{\eta_3 + \eta_2}$$

$$= \frac{(51.22 < 6.82°) - (113.84 < 5.17°)}{(51.22 < 6.82°) + (113.84 < 5.17°)}$$

$$= \frac{(50.86 + j6.08) - (113.38 + j10.26)}{(50.86 + j6.08) + (113.38 + j10.26)}$$

$$= \frac{-62.52 - j4.18}{164.24 + j16.34}$$

$$= -0.38 + j0.01$$

$$\frac{1}{1 - \Gamma_{32}} = 0.72 + j0.01$$

Propagation constant of muscle is $\gamma_m = 0.0448 + j0.38$

Therefore, $\gamma_m h_m = (0.0448 + j0.38) \times 20 = 0.896 + j7.6.$

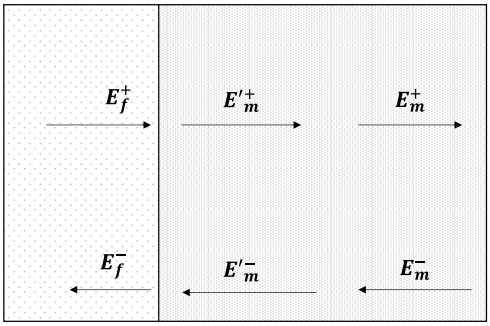

Fig. 5.7: Reflecting and transmitting electric fields from fat to muscle layer

So, $e^{\gamma_m h_m} = e^{0.896}.e^{j7.6} = 0.62 + j2.37$

and, $e^{-\gamma_m h_m} = e^{-0.896}.e^{-j7.6} = 0.1 - j0.40$

Amplitude transmission matrix for muscle layer,

$$[A]_{muscle} = \begin{bmatrix} 0.1 - j0.4 & 0 \\ 0 & 0.62 + j2.37 \end{bmatrix}$$

Discontinuity transfer matrix for the interface between fat and muscle layer is,

$$[D]_{muscle,fat} = \begin{bmatrix} 1 & 0.3 - j0.01 \\ 0.3 + j0.01 & 1 \end{bmatrix} \times (0.72 + j0.01)$$

Therefore, transfer matrix for air and skin will be,

$$[T]_{muscle,fat} = [A]_{muscle} \times [D]_{muscle,fat}$$

$$= \begin{bmatrix} 0.1 - j0.4 & 0 \\ 0 & 0.62 + j2.37 \end{bmatrix} \times \begin{bmatrix} 1 & 0.3 - j0.01 \\ 0.3 + j0.01 & 1 \end{bmatrix}$$

$$\times (0.72 + j0.01)$$

$$[T]_{muscle,fat} = \begin{bmatrix} 0.08 - j0.29 & 0.02 - j0.09 \\ 0.14 + j0.51 & 0.42 + j1.71 \end{bmatrix}$$

From Fig. 5.7, it can be written as,

$$\begin{bmatrix} E_m^+ \\ E_m^- \end{bmatrix} = \begin{bmatrix} 0.08 - j0.29 & 0.02 - j0.09 \\ 0.14 + j0.51 & 0.42 + j1.71 \end{bmatrix} \begin{bmatrix} E_f^+ \\ E_f^- \end{bmatrix}$$

where E_m^+, E_m^-, E_f^+ and E_f^- are respective peak values of transmitting electric field in muscle, reflecting electric field from muscle and superstrate interface, transmitting electric field in fat and the reflecting electric field from muscle and fat interface.

Therefore, total transfer matrix of the 3-layer human body model can be written as,

$$[T]_{muscle,air} = [T]_{muscle,fat} \times [T]_{fat,skin} \times [T]_{skin,air}$$

$$= \begin{bmatrix} 0.08 - j0.29 & 0.02 - j0.09 \\ 0.14 + j0.51 & 0.42 + j1.71 \end{bmatrix} \times \begin{bmatrix} 1.31 - j0.5 & -0.40 + j0.17 \\ -0.45 - j0.12 & 1.42 + j0.45 \end{bmatrix} \times \begin{bmatrix} -0.14 - j0.42 & -0.12 - j0.3 \\ -0.18 + j0.52 & -0.27 + j0.70 \end{bmatrix}$$

$$= \begin{bmatrix} -0.06 - j0.38 & 0.09 + j0.01 \\ 0.45 - j0.22 & -0.32 + j2.44 \end{bmatrix} \times \begin{bmatrix} -0.14 - j0.42 & -0.12 - j0.3 \\ -0.18 + j0.52 & -0.27 + j0.70 \end{bmatrix}$$

$$= \begin{bmatrix} -0.17 + j0.12 & -0.13 + j0.12 \\ -1.37 - j1.76 & -1.74 - j0.99 \end{bmatrix}$$

So, it can be written as,

$$\begin{bmatrix} E_m^+ \\ E_m^- \end{bmatrix} = \begin{bmatrix} -0.17 + j0.12 & -0.13 + j0.12 \\ -1.37 - j1.76 & -1.74 - j0.99 \end{bmatrix} \begin{bmatrix} E_0^+ \\ E_0^- \end{bmatrix}$$

5.5 CONCLUSION

From this chapter, reflection and transmission of electric field due to each layer of the human body such as skin, fat and muscle is calculated. Transfer matrices for different interfaces are also calculated here to estimate electric field at muscle layer if any electric field is incident on skin from air. From this calculation, electric fields at each interface can also be calculated by knowing the value of E_0^+.

REFERENCES

[1] H. Oraizi and M. Afsahi, "Analysis of planer dielectric multilayers as fss by Transmission Line Transfer Matrix Method (TLTMM)," *Progress in Electromagnetics Research (PIER)*, vol. 74, pp. 217-240, January 2007.

[2] G. R. Rani and G. S. N. Raju, "Transmission and Reflection Characteristics of Electromagnetic Energy in Biological Tissues," *International Journal of Electronics and Communication Engineering*, vol. 6, no, 1, pp. 119-129, 2013.

Chapter 6

Implantable antenna design within skin layer

Contents	
	6.1 Introduction
	6.2 Development of skin phantom
	6.3 Design parameters of the antenna
	6.4 Developmental steps of the final antenna
	6.5 Simulated results
	6.6 Conclusion

6.1 INTRODUCTION

There are two possibilities to implant an antenna within human body. Antenna can be implanted either in skin layer or in muscle layer. Sometimes antenna is implanted in subcutaneous fat layer to measure glucose level in blood. However, researchers show more interest to implant in skin and muscle layers.

Implant in muscle layer is quite challenging for building up communication with external devices as it is surrounded by high lossy environment due to wave propagation through three lossy layers. In case of implantation in skin layer, system can provide more efficient communication channel than the first case. Therefore, for testing purpose of antenna performance within human body, antenna engineers show interest to implant within skin layer.

From the point of view of in-vitro experiment, development of single layered equivalent phantom is comparatively easier than multi-layered phantom model. *Phantom* is a model which mimic the properties of environment (especially for biological tissue) of the device (in this case antenna) to investigate the performance of it. In case of skin implant, it is not required to consider fat and muscle layers as it is expected that the implanted antenna does not have back lobes and it is able to communicate in its broad-side direction. Therefore, development of phantom model is comparatively easy for investigating performance of skin implant. In this chapter, an implantable antenna is designed within skin equivalent phantom model at 2.45 GHz ISM band.

6.2 DEVELOPMENT OF SKIN PHANTOM

Here a cubical skin phantom has been designed. The dimensions of the skin phantom are 100 mm × 100 mm × 100 mm. The three-dimensional view of the skin phantom is illustrated in Fig. 6.1. Permittivity, conductivity and tissue density of this phantom are taken as 38, 1.46 S/m and 1000 kg/m^3 respectively in 2.45 GHz ISM band [1-4].

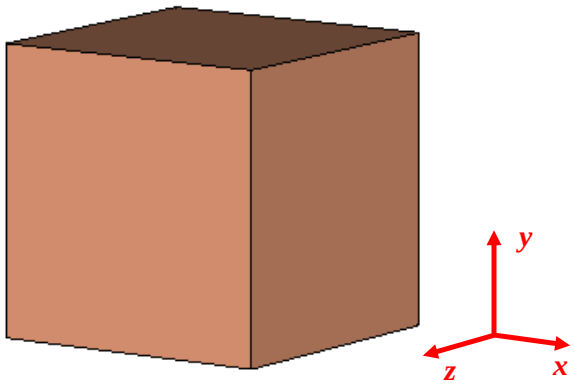

Fig. 6.1: Three-dimensional view of skin phantom

6.3 DESIGN PARAMETERS OF THE ANTENNA

Copper is used as the conducting material to design ground and patch of the antenna. Arlon AD 430 is used as the substrate and superstrate material – the same possesses dielectric constant (ϵ_r) of 4.3 and loss tangent (tan δ) of 0.003. Yellow coloured regions in Fig. 6.2 represent conductors (patch and ground) whereas the sky-blue coloured portions represent the substrate Arlon AD 430.

The superstrate has dimensions of 15 mm × 10 mm × 0.762 mm. Fig. 6.2 illustrates structure of the proposed antenna to be implanted in skin phantom. The thickness of superstrate and substrate is 0.762 mm while the thickness of ground and patch has been considered as 0.035 mm.

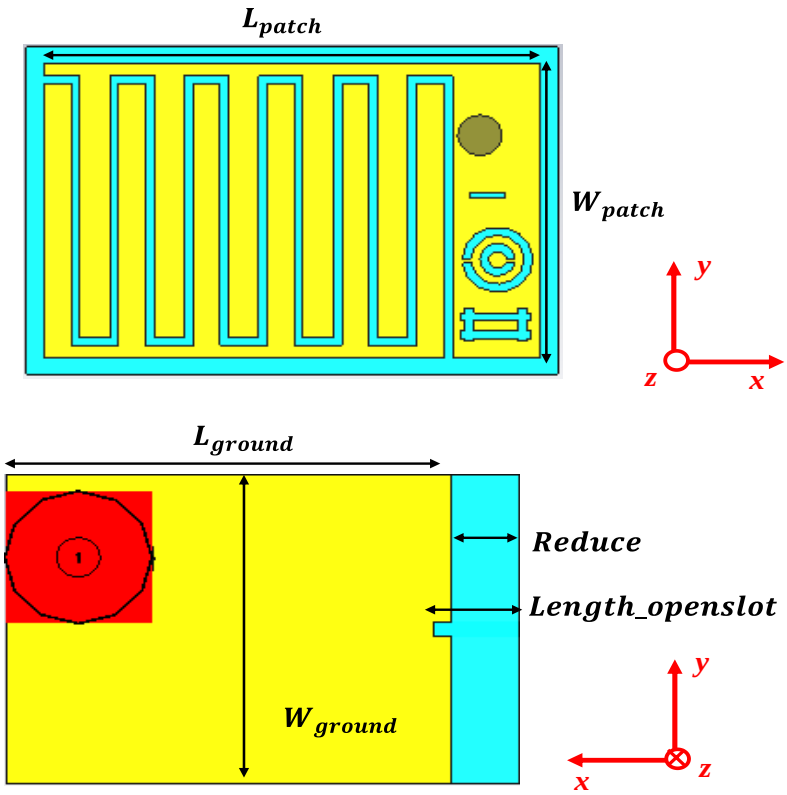

Fig. 6.2: Top view and bottom view of skin implanted antenna

The dimensions of the proposed antenna, shown in Fig. 6.2, are summarized in Table 6.1. Outer and inner conductor radii of the coaxial feed are 2.11 mm and 0.63 mm respectively to achieve 50 Ω impedance.

TABLE 6.1: Design parameters of skin-implant antenna

Parameters	Values (mm)	Parameters	Values (mm)
Length of Ground (L_{ground})	13	Width of Ground (W_{ground})	10
Length of Substrate ($L_{substrate}$)	15	Width of Substrate ($W_{substrate}$)	10
Length of Patch (L_{patch})	14	Width of Patch (W_{patch})	9
Thickness of Open slot	0.5	Reduce	2
Length of open slot (Length_openslot)	2.5	Thickness of Meander-Line slot	0.25
Outer radius of outer ring of SRR slot	1	Inner radius of outer ring of SRR slot	0.75
Outer radius of inner ring of SRR slot	0.5	Inner radius of inner ring of SRR slot	0.25
Thickness of thin slot	0.1875	Thickness of Hash slot	0.25

6.4 DEVELOPMENTAL STEPS OF THE FINAL ANTENNA

The final design has been achieved by optimizing some steps as illustrated in Figs. 6.3 and 6.4. According to the available literature [4-7], it is noted that the typical reported area for the implantable antennas is 160mm^2. Therefore, a simple rectangular patch antenna with dimensions of 14mm × 9mm has initially been

taken as shown in Fig. 6.3.1 – the area of the patch is 126 mm^2. However, the overall area of the antenna is 150 mm^2 due to 15 mm × 10 mm substrate.

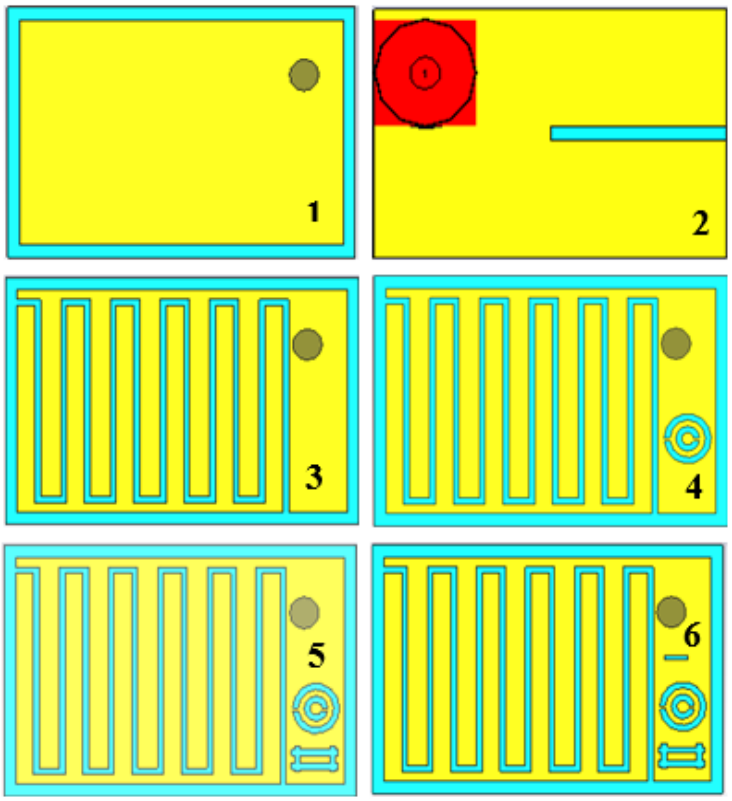

Fig. 6.3: Design evolution of patch of the skin implantable antenna

At initial stage, a simple ground of 15mm × 10mm without any slot has been incorporated. After simulating inside skin phantom, it is observed that this antenna is not tuned in 2.45 GHz ISM band. It's quite expected due to smaller dimensions of the simple rectangular patch antenna – thus, the resonant frequency is much above 2.45 GHz band.

In next step, an open slot has been cut on the ground plane without disturbing the patch structure (Fig. 6.3.2). Open slot on the ground plane can

enhance bandwidth and the same is also useful for miniaturization [8-9]. Therefore, an open slot having length of 7.5 mm has been introduced on the ground plane. However, no significant change in resonant frequency has been noted.

Next, keeping the ground structure same as in Fig 6.3.2, a meander-line slot with six meanders has been introduced on the patch as depicted in Fig 6.3.3. Capacitive and inductive loads increase in equivalent circuit of the antenna with a greater number of meanders on the patch structure [10]. Thus, increment in capacitance and inductance values can reduce the resonant frequency. After incorporating six meander slots, the resonant frequency has been reduced to 2.58 GHz with return loss of 17.32 dB.

In the following step, a Complementary Split Ring Resonator (CSRR) slot is further incorporated on the patch (as shown in Fig. 6.3.4) to increase reactance in the equivalent circuit. However, this slot has barely contributed to shift the resonant frequency near 2.58 GHz with 16.42 dB return loss.

Next, a new type of hash slot (#) has been introduced on the patch as illustrated in Fig 6.3.5. This hash slot has slightly reduced the resonant frequency at 2.57 GHz with 20.91 dB return loss.

At subsequent stage, a thin rectangular slot is incorporated on the patch structure as shown in Fig. 6.3.6. The thickness of the slot is acting as the distance (d) between two plates of equivalent capacitor-thus, with reduction in d, capacitance will increase.

Hence, this thin rectangular slot should contribute to reduce the frequency of operation. The observed resonant frequency is 2.53 GHz with a return loss of 39.60 dB. Finally, to further reduce the resonant frequency, a defected ground concept is utilized. The modification steps on ground plane are shown Fig 6.4.

With the half reduced ground structure illustated in Fig 6.4.1, the resonant frequency is 2.27 GHz with 21.54 dB return loss. As the 'Reduce' parameter is same as the length of open slot shown in Fig 6.4.2, practically no open slot is present here. It is expected that with the variation of the reduction amount 'Reduce', this antenna can be tuned at the desired range.

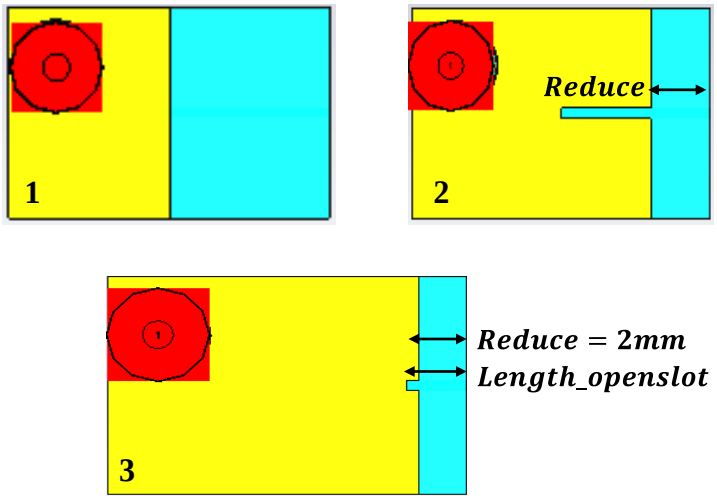

Fig. 6.4: Design evolution of ground of the skin implantable antenna

Next, the value of 'Reduce' has been varied as 1, 2, 3 and 4 mm keeping the open slot length 7.5 mm as shown in Fig 6.4.2. The corresponding results are tabulated in Table 6.2.

TABLE 6.2: Different values of 'Reduce'

Reduce (mm)	Resonant Freq. (GHz)	Return Loss (dB)
1	2.52	48.13
2	2.48	36.43
3	2.56	22.82
4	2.65	14.69

As reported in Table 6.2, it is observed that the modifed antenna is tuned in 2.45 GHz ISM band for 'Reduce'= 2mm. To improve the return loss, length of the open slot has been tuned further by keeping 'Reduce' = 2mm. Thus, a variable 'Length_openslot' has been taken to represent length of the open slot. The obtained results for different values of 'Length_openslot' are tabulate in Table 6.3.

TABLE 6.3: Different values of 'Length_openslot'

Length_openslot (mm)	Resonant Freq. (GHz)	Return Loss (dB)
2.5	2.49	43.17
3.75	2.61	30.82
5	2.52	23.23
6.25	2.49	28.70
7.5	2.48	38.01

It can be concluded that the proposed antenna has now been tuned to 2.45 GHz band with better return loss response (43.17 dB) for 'Length_openslot' = 2.5mm.

6.5 SIMULATED RESULTS

Computer Simulation Technology Microwave Studio 2017 (CST MWS 2017). Those structures have been positioned inside the skin phantom at the depth of 4 mm from the top surface. Return loss curves for all the evolution steps have been illustrated in Fig. 6.5 with names 6.3.1, 6.3.2, 6.3.3 and so on to label curves corresponding to respective figure numbers.

Curve 6.4.2 in Fig. 6.5 shows return loss for the design shown in Fig 6.4.2 with 'Reduce' = 2 mm and curve 6.4.3 is for 'Length_openslot' = 2.5 mm. Cross-polar discrimination plot for the final antenna structure within phantom is shown in

Fig. 6.6 and it confirms that the designed antenna is linearly polarized in spite of presence of meander-line slots and defected ground.

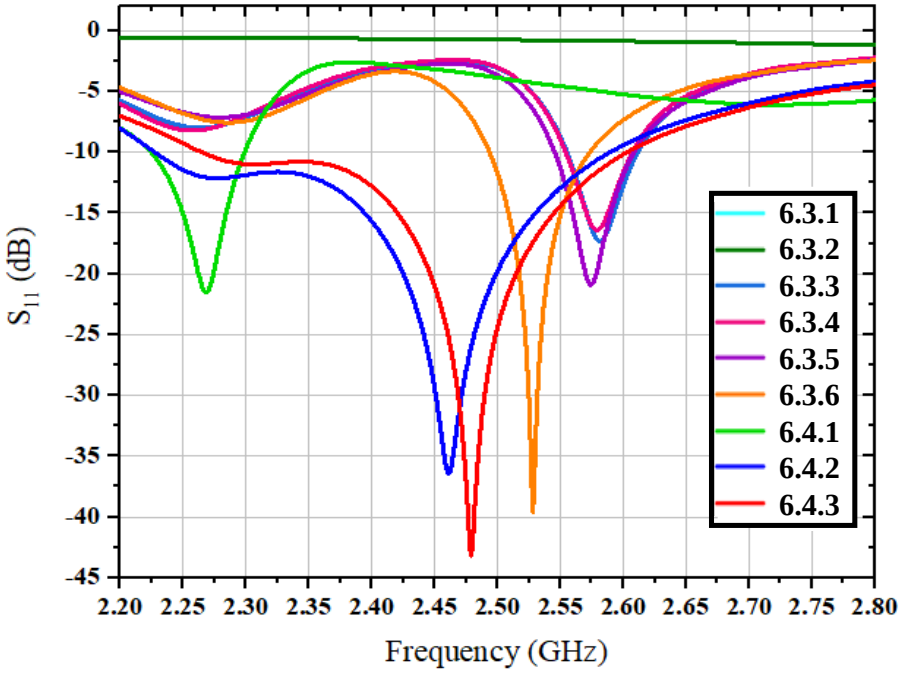

Fig. 6.5: Reflection coefficient curves for different variations of Figs. 6.3 and 6.4

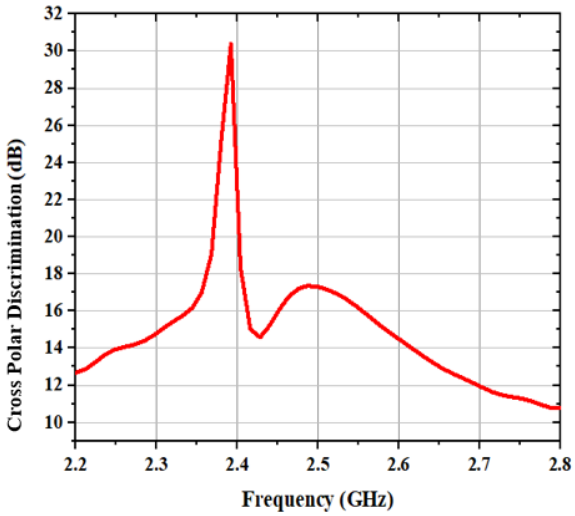

Fig. 6.6: Cross polar discrimination vs frequency for final antenna

Return loss of the proposed antenna in skin phantom is 43.17 dB at 2.49 GHz (refer to Fig. 6.7.1). This antenna has -10 dB bandwidth of 200 MHz i.e., from 2.36 GHz to 2.56 GHz. At 2.49 GHz, the proposed antenna has gain of -16.4 dBi with around 0.51% radiation efficiency (refer to Fig. 6.7.2) – the achieved responses are better than the reported design in literature [11].

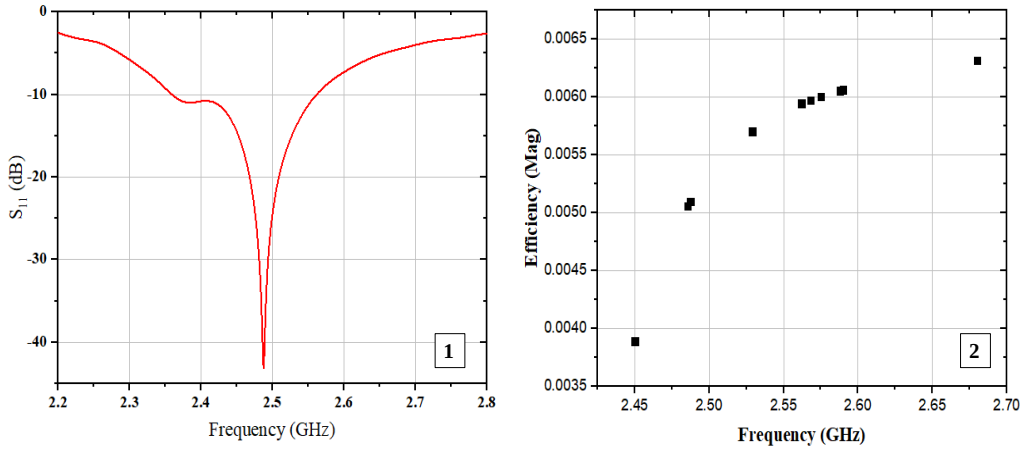

Fig. 6.7: (1) S_{11} vs frequency, (2) Efficiency vs frequency of final skin implantable antenna

This antenna is placed on xy-plane and coaxial feed is along z axis. So, E plane is represented by $\varphi = 90°$ and H plane is represented by $\varphi = 0°$. The H plane and E plane radiation patterns of the final antenna are shown in Figs. 6.8.1 and 6.8.2 respectively.

To ensure safe electromagnetic exposure, the SAR values should be less than 1.6 W/Kg averaged over 1g of contiguous tissue and 2 W/Kg averaged over 10g of contiguous tissue – as prescribed in global standards [12-13]. Respective peak SAR values, for 1 W average input power, are 274.1 W/Kg and 64.71 W/Kg while averaged over 1g and 10g contiguous tissue. To restrict SAR values within prescribed limits, maximum average input powers should be 5.8 mW and 30 mW while averaging over 1g and 10g contiguous tissue respectively.

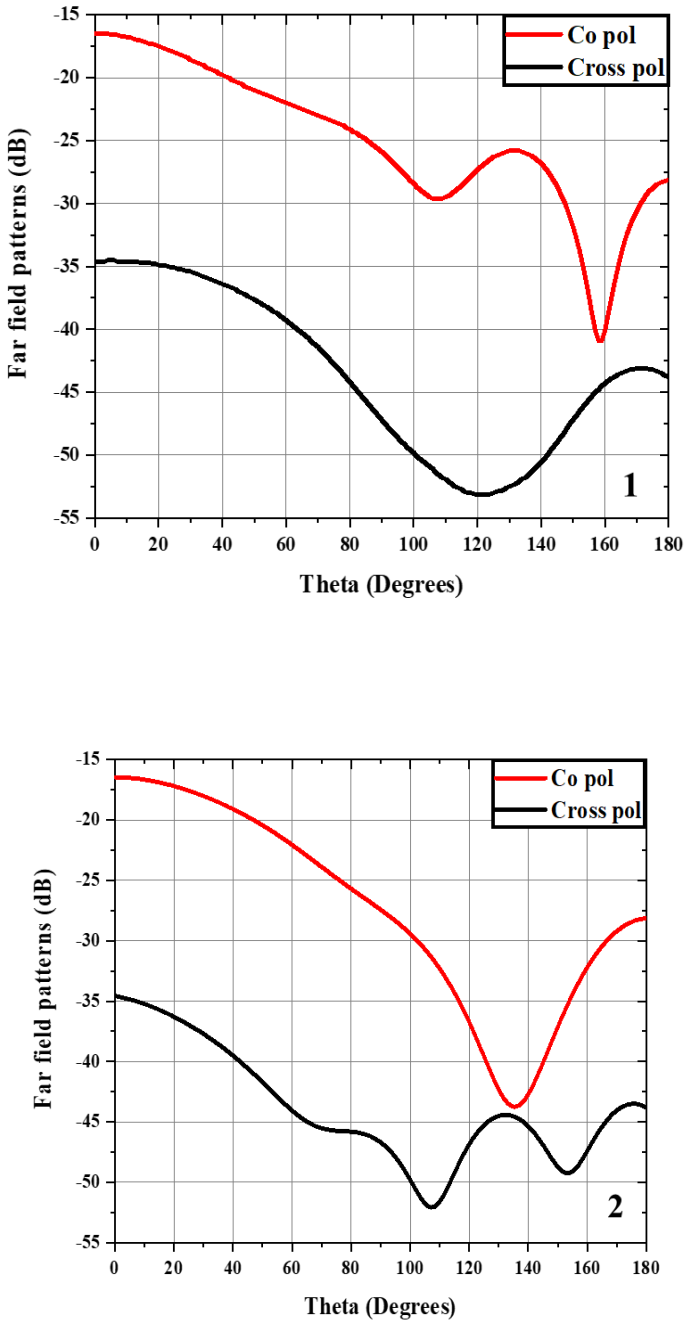

Fig. 6.8: Far field patterns in (1) $\varphi = 0^0$ and (2) $\varphi = 90^0$ plane at 2.49 GHz

Comparison of the final skin implantable antenna with some previous antenna performances is tabulated in Table 6.4.

TABLE 6.4: Comparison of final antenna with existing skin implantable antenna

Ref.	Gain (dBi)	Peak SAR (1W) (W/Kg) (1g)	Peak SAR (1W) (W/Kg)(10g)
[14]	-38	900	-
[15]	-22.8	807.34	102.04
[16]	-22.37	759.72	87.24
[17]	-21.0	769	-
This design	-16.4	274.1	64.71

6.6 CONCLUSION

In this chapter, an implantable antenna consisting of different slots on the patch along with a defected ground has been designed in 2.45 GHz ISM band. This antenna is positioned at 4 mm depth from top surface of the skin phantom (100 mm × 100 mm × 100 mm). A superstrate (15mm × 10mm × 0.762mm) is placed on the designed patch when this antenna is positioned inside the phantom. Overall volume of the designed antenna is 239.1mm^3. The antenna provides -16.4 dBi gain and 0.51% radiation efficiency at 2.49 GHz with 200 MHz bandwidth (2.36 GHz to 2.56 GHz). The respective peak SAR values are 274.1 W/Kg and 64.71 W/Kg while averaged over 1g and 10g contiguous tissue with 1 W average input power. However, to meet prescribed SAR limits, the respective maximum average input power should be 5.8 mW and 30 mW while averaged over 1g and 10g skin tissue.

REFERENCES

[1] http://niremf.ifac.cnr.it/tissprop/htmlclie/htmlclie.php.

[2] https://itis.swiss/virtual-population/tissueproperties/database/dielectric properties

[3] F. Gozasht and A. S. Mohan, "Miniaturized Slot PIFA Antenna for Triple band Implantable Biomedical Applications," *2013 IEEE MTT-S International Microwave Workshop Series on RF and Wireless Technologies for Biomedical and Healthcare Applications (IMWS-BIO), March* 2014.

[4] V. Kaim, B. K. Kanaujia, S. Kumar, H. C. Choi, K. W. Kim, and K. Rambabu, "Ultra-Miniature Circularly Polarized CPW-Fed Implantable Antenna Design and its Validation for Biotelemetry Applications," *Scientific Reports,* April 2020.

[5] T. Shaw and D. Mitra, "Wireless Power Transfer System Design for Biomedical Implants at 2.45 GHz", *2019 IEEE Asia-Pacific Microwave Conference (APMC),* March 2020.

[6] B. Mondal, L. Joseph, J. Ebrahimizadeh, M. D. Perez, D. Mitra, R. Augustine, "Low Profile Implantable Antenna for Fat Intra- Body Communication," *2020 14th European Conference on Antennas and Propagation (EuCAP),* July 2020.

[7] S. Das and D. Mitra, "A Compact Wideband Flexible Implantable Slot Antenna Design with Enhanced Gain", *IEEE Transactions on Antennas and Propagation,* vol. 66, no. 8, pp. 4309-4314, May 2018

[8] M. Zada, H. Yoo, "A Miniaturized Triple-Band Implantable Antenna System for Bio-Telemetry Applications", *IEEE Transactions on Antennas and Propagation*, vol. 66, no. 12, pp. 7378-7382, October 2018.

[9] F. Faisal and H. Yoo, "A Miniaturized Novel- shape Dual-Band Antenna for Implantable Applications", *IEEE Transactions on Antennas and Propagation*, vol 67, no. 2, pp. 774-783, February 2019.

[10] S. Ghosh, S. Das, D. Samantaray and S. Bhattacharyya, "Meander Line based Defected Ground Microstrip Antenna slotted with split- ring resonator for Terahertz range," *2020 Engineering Reports, Wiley*, vol. 2, no. 1, Article No. e12088, January 2020.

[11] Y. El-Saboni, M. K. Magill, G. Conway, W. Scanlon, "Assessing the RF Performance of Medical Implant Antennas", *Automated RF and Microwave Measurement Society conference (ARMMS)*, 2016.

[12] ICNIRP, "Guidelines for limiting exposure to electromagnetic fields (100 KHz to 300 GHz)," *Health Phys.*, vol. 118, no. 5, pp. 483-524, March 2020.

[13] R. F. Cleveland, Jr., D. M. Sylvar, and J. L. Ulcek, "Evaluating compliance with FCC guidelines for human exposure to radiofrequency electromagnetic fields," *FCC OET Bulletin*, vol. 65, Edition 97-01, Washington D.C., November 1997.

[14] W. C. Liu, S. H. Chen and C. M. Wu, "Bandwidth enhancement and size reduction of an Implantable PIFA Antenna for biotelemetry devices",

Microwave and Optical Technology Letters, vol. 51, no. 3, pp. 755-757, March 2009.

[15] S. A. A. Shah and H. Yoo, "Scalp-implantable antenna systems for intracranial pressure monitoring," *IEEE Transactions of Antennas Propagations.* vol. 66, no. 4, pp. 2170-2173 (2018).

[16] I. Gani and H. Yoo, "Multi-Band Antenna System for Skin Implant," *IEEE Microwave and Wireless Components Letters*, vol. 26, no. 4, April 2016.

[17] H. Zhang, L. Li, C. Liu, Y. X. Guo and S. Wu, "Miniaturized implantable antenna integrated with split ring resonate rings for wireless power transfer and data telemetry," *Microwave and Optical Technology Letters*, vol. 59, no. 3, pp. 710-714, March 2017.

Chapter 7

Human body equivalent homogeneous phantom liquid

Contents	
	7.1 Introduction
	7.2 Properties of homogeneous body phantom
	7.3 Materials used for phantom liquid
	7.4 Dielectric properties measurement of liquid
	7.5 Steps to achieve final body phantom liquid
	7.6 Conclusion

7.1 INTRODUCTION

In this work, our objective is to implant antenna within human muscle layer. As discussed in previous chapter, development of multi-layered phantom liquid design is a very challenging task. If multi-layered body model is estimated by a homogeneous single layered phantom model, it will be very easy for in-vitro testing of the designed antenna.

7.2 PROPERTIES OF HOMOGENEOUS BODY PHANTOM

The electrical properties of the phantom should be maintained properly for characterizing fields within body mimicking phantom based on prescribed guidelines. To investigate antenna performance within human body, a homogeneous

body equivalent phantom model has been developed. Table 7.1 shows the values of the electrical properties based on some standard guidelines [1-4].

TABLE 7.1: Electrical properties of body phantom at 2.45 GHz

Relative Permittivity (ϵ_r)	Conductivity (σ) (S/m)	Tissue density (ρ) (Kg/m^3)
52.7	1.95	1000

Loss tangent ($\tan\delta$) can be easily obtained from conductivity by using the following equation

$$tan\delta = \frac{\sigma}{\omega\epsilon} = \frac{\sigma}{\omega\epsilon_0\epsilon_r}$$

where relative permittivity for vacuum (ϵ_0) = 8.854×10^{-12} F/m.

Putting the values of conductivity, relative permittivity and operating frequency from Table 1 into the above expression, value of the loss tangent of the body phantom will be 0.27.

7.3 MATERIALS USED FOR PHANTOM LIQUID

In this work, mainly three chemical components have been used to achieve the prescribed values of permittivity and loss tangent for mimicking a liquid as human body equivalent. They are - low impedance (3 MΩ) Deionized Water (DI), Diethylene Glycol Monobutyl Ether 98% (DGME) and Sodium Chloride (NaCl). The recipe of body mimicking phantom liquid for 2.45 GHz ISM band has been shown in Table 7.2.

TABLE 7.2: Materials used for phantom liquid development

Sl. No.	Components	Quantity
1	Deionized Water	273 mL
2	DGME	127 mL
3	NaCl	794 mg

7.4 DIELECTRIC PROPERTIES MEASUREMENT OF LIQUID

Dielectric constant and loss tangent value of the mixture is measured by using Agilent 85070E dielectric probe kit for the frequency range 1000 MHz to 8000 MHz as shown in Fig. 7.1. Using probe kit, this phantom liquid has permittivity value of 52.72 and loss tangent of 0.275 at 2.45 GHz. Therefore, it is undoubtably concluded based on the above-mentioned prescribed values that this developed phantom liquid can be used to investigate antenna performance within human body.

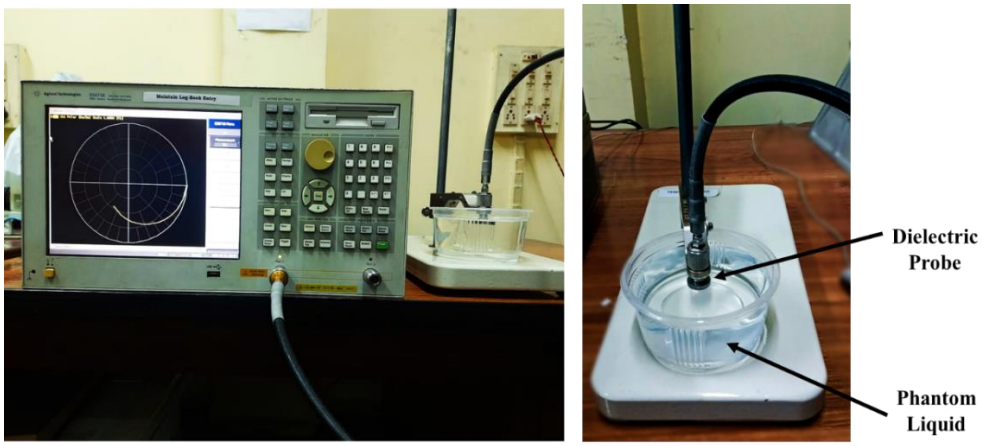

Fig. 7.1: Measurement of dielectric properties of phantom liquid using dielectric probe and network analyser

7.5 STEPS TO ACHIEVE FINAL BODY PHANTOM LIQUID

Several steps are performed to achieve human body equivalent phantom liquid with the permittivity and loss tangent prescribed by FCC.

Step 1: At first, dielectric properties of 100 mL deionized water are measured by using dielectric probe. Its relative permittivity and loss tangent for the frequency range from 1000 MHz to 8000 MHz are measured and plotted in Fig. 7.2. At 2.45 GHz, 100 mL DI water shows relative permittivity and loss tangent values as 77.24 and 0.12 respectively.

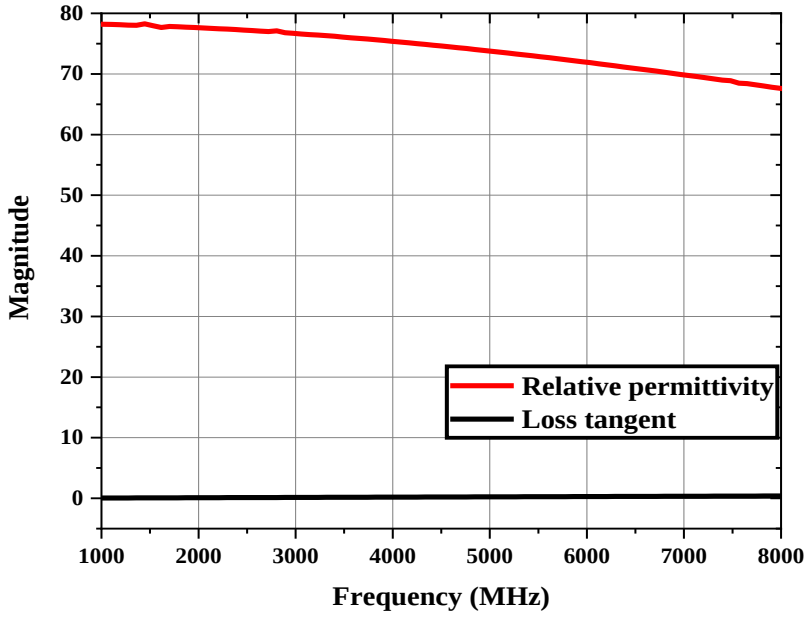

Fig. 7.2: Relative permittivity and loss tangent vs frequency for 100 mL DI

Step 2: 25 mL DGME is mixed with 77 mL deionized water in next step to reduce permittivity. Its relative permittivity and loss tangent for the frequency range from 1000 MHz to 8000 MHz are measured and plotted in Fig. 7.3. At 2.45 GHz, the

mixture shows relative permittivity and loss tangent values as 56.84 and 0.20 respectively. The permittivity value is reached within 10% tolerance but loss tangent value should be increase more.

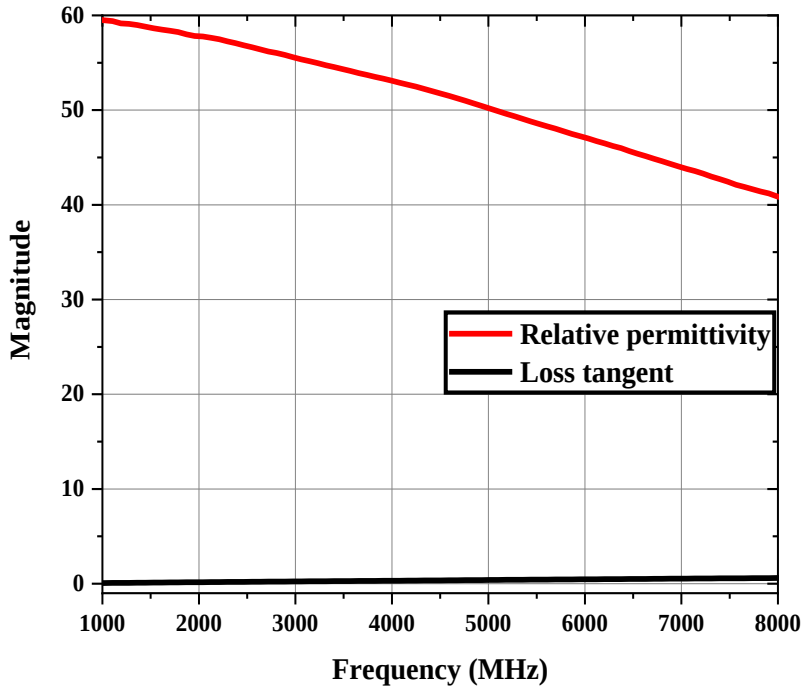

Fig. 7.3: Relative permittivity and loss tangent vs frequency for mixture of 77 mL DI and 25 mL DGME

Step 3: Next, 86 mL DI and 40 mL DGME are mixed thoroughly and its dielectric properties are measured by dielectric probe. Permittivity and loss tangent of the chemical plotted against frequency is illustrated in Fig. 7.4. This mixture has dielectric constant of 52.67 and 0.243. The relative permittivity value is almost same with the goal. However, loss tangent needs to be tuned slightly in spite of reaching 10 % tolerance to achieve better characteristics.

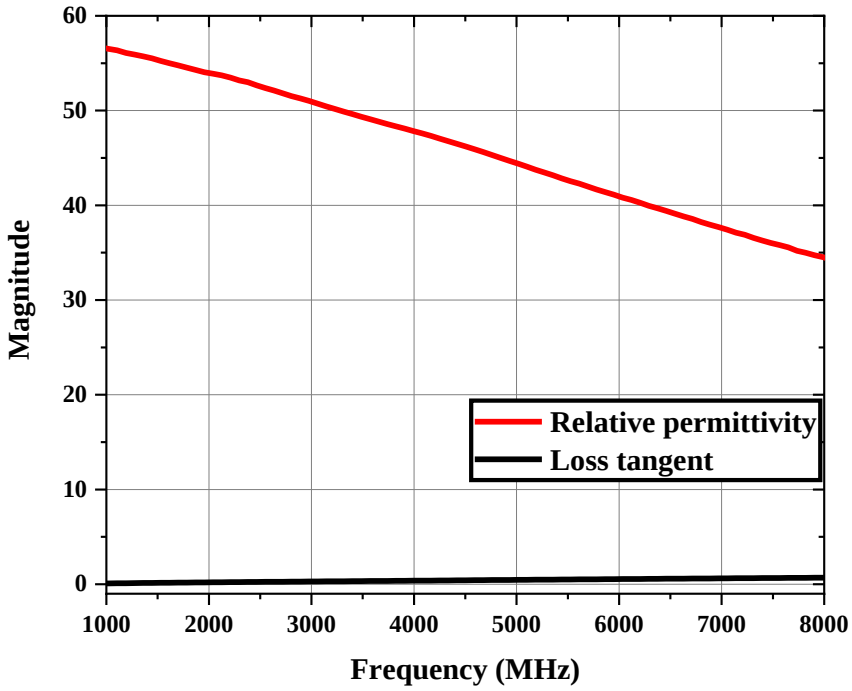

Fig. 7.4: Relative permittivity and loss tangent vs frequency for mixture of 86 mL DI and 40 mL DGME

Step 4: 250 mg sodium chloride (NaCl) is added with the mixture developed in Step 3. The dielectric characteristics of the liquid over frequency range of 1000 MHz to 8000 MHz are shown in Fig. 7.5. At 2.45 GHz, this liquid shows the relative permittivity of 52.72 and loss tangent of 0.277. Therefore, this liquid is finalized as body equivalent phantom model for this thesis work.

Keeping ratio of deionized water, DGME and NaCl same, phantom liquid is developed for volume of 400 mL. Therefore, 273 mL DI, 127 mL DGME and 794 mg NaCl are used for final phantom design.

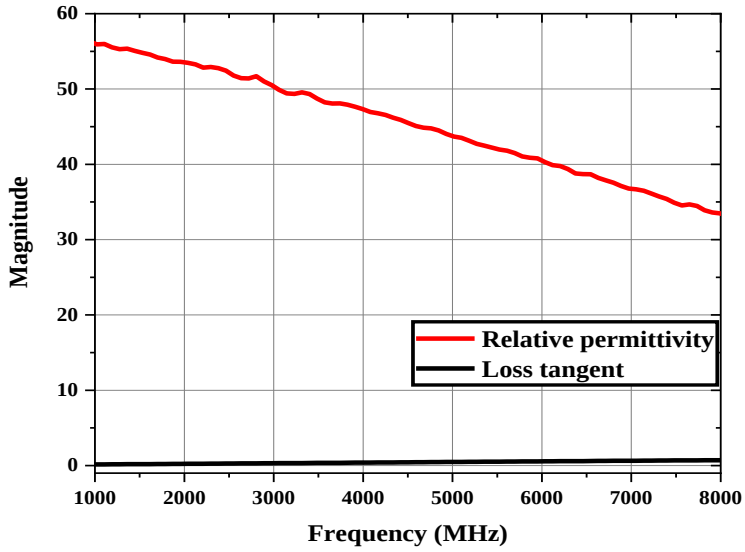

Fig. 7.5: Relative permittivity and loss tangent vs frequency for final phantom

7.6 CONCLUSION

Dielectric constant and loss tangent value of the mixture is measured by using Agilent 85070E dielectric probe kit for the frequency range 1000 MHz to 8000 MHz. All the evolution steps to achieve phantom liquid (relative permittivity of 52.72 and loss tangent of 0.277) are discussed in this chapter. Comparing the liquid properties with prescribed dielectric properties of the body phantom by FCC, it is concluded that this recipe can be followed for developing human body phantom.

REFERENCES

[1] http://niremf.ifac.cnr.it/tissprop/htmlclie/htmlclie.php.

[2] https://itis.swiss/virtual-population/tissueproperties/database/dielectric properties

[3] F. Gozasht and A. S. Mohan, "Miniaturized Slot PIFA Antenna for Triple band Implantable Biomedical Applications," *2013 IEEE MTT-S International Microwave Workshop Series on RF and Wireless Technologies for Biomedical and Healthcare Applications (IMWS-BIO), March* 2014.

[4] V. Kaim, B. K. Kanaujia, S. Kumar, H. C. Choi, K. W. Kim, and K. Rambabu, "Ultra-Miniature Circularly Polarized CPW-Fed Implantable Antenna Design and its Validation for Biotelemetry Applications," *Scientific Reports*, April 2020.

Chapter 8

Meander line slotted body implantable antenna design

Contents	
	8.1 Introduction
	8.2 Design of body phantom
	8.3 Design parameters of the antenna
	8.4 Developmental steps of the final antenna
	8.5 Results for the final antenna
	8.6 Conclusion

8.1 INTRODUCTION

Skin equivalent phantom model was majorly proposed in many reported articles to design implantable antennas. However, due to extremely small thickness (about 2 mm) of human skin layer, implantation of the antenna within skin layer is extremely challenging in practical applications. But it is easier to place an implantable antenna under the skin layer of human body. Thus, human body phantom has been utilized in this work so that implantation challenges can be minimized as well as simulated responses of the designed antenna can be synchronized with the practical antenna measurement data inside body equivalent phantom.

High lossy nature of human tissues, size of antenna, impedance matching, low power constraint, Specific Absorption Rate (SAR) limit etc. are the critical factors which make design of an implantable antenna quite challenging [1-2]. To design an implantable antenna in the allotted frequency bands, physical dimensions of the conventional antenna come out to be significantly large. However, to implant an antenna within human torso, antenna size should be as miniaturized as possible. Thus, different standard antenna miniaturization techniques can be adopted to design and develop an implantable antenna. Meandering, spiralling, waffling or incorporating slots on antenna patch can help to reduce frequency of operation by increasing current-flow path length and maintaining compact dimensions of the implantable antenna [3].

Superstrate can be placed on the top of patch because superstrate layer behaves as lower permittivity isolator from the human tissues [4-5]. In this chapter, an implantable antenna has been proposed and designed in the 2.45 GHz ISM band. Some meander-line slots have been introduced on patch and an open slot has been etched on the ground plane. The whole antenna structure has been implanted into human body mimicking phantom.

8.2 DESIGN OF BODY PHANTOM

A human body equivalent cubic phantom having dimensions of 100 mm × 100 mm × 100 mm has been designed in this work – Fig. 8.1 illustrates that three-dimensional body phantom. Propagation, reflection, and attenuation of electromagnetic waves in body equivalent phantom are dependent on the electrical properties of human tissue such as relative permittivity (ε_r), and conductivity (σ) along with frequency of operation [6].

To characterize fields inside human body mimicking phantom models, it is important to maintain the electrical properties of those phantom models according to prescribed guidelines. Relative permittivity (ε_r), conductivity (σ), and tissue density of this phantom are taken as 52.7, 1.95 S/m, and 1000 kg/m^3 respectively in 2.45 GHz ISM band [7-10].

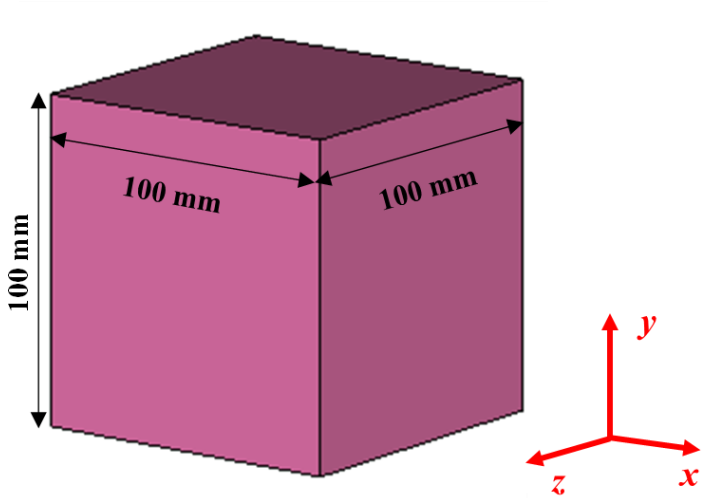

Fig. 8.1: Three-dimensional view of body phantom

8.3 DESIGN PARAMETERS OF THE ANTENNA

Fig. 8.2 illustrates the geometry of the proposed antenna which is designed at 2.45 GHz ISM Band. In this work, copper is used as the material for ground and patch – whereas, Arlon AD 430 is used to develop superstrate and substrate layers of the proposed antenna. To sustain the gain of implantable antenna inside high lossy human tissue layer, Arlon AD 430 is chosen as substrate due to low loss and availability for practical fabrication.

Yellow-coloured regions in Fig. 8.2 represent copper layer and sky-blue coloured parts represent Arlon AD 430. The relative permittivity and loss tangent of Arlon AD 430 are 4.3 and 0.003 respectively in 2.45 GHz band. The thickness of both superstrate and substrate layers are taken as 0.762 mm whereas the thickness of ground and patch of this antenna are taken as 0.035 mm. Overall area and volume of this antenna including superstrate are 130 mm^2 and 207.22 mm^3 respectively. Thus, it is clear that the antenna size is fairly small and it is easy to implant the same inside human body.

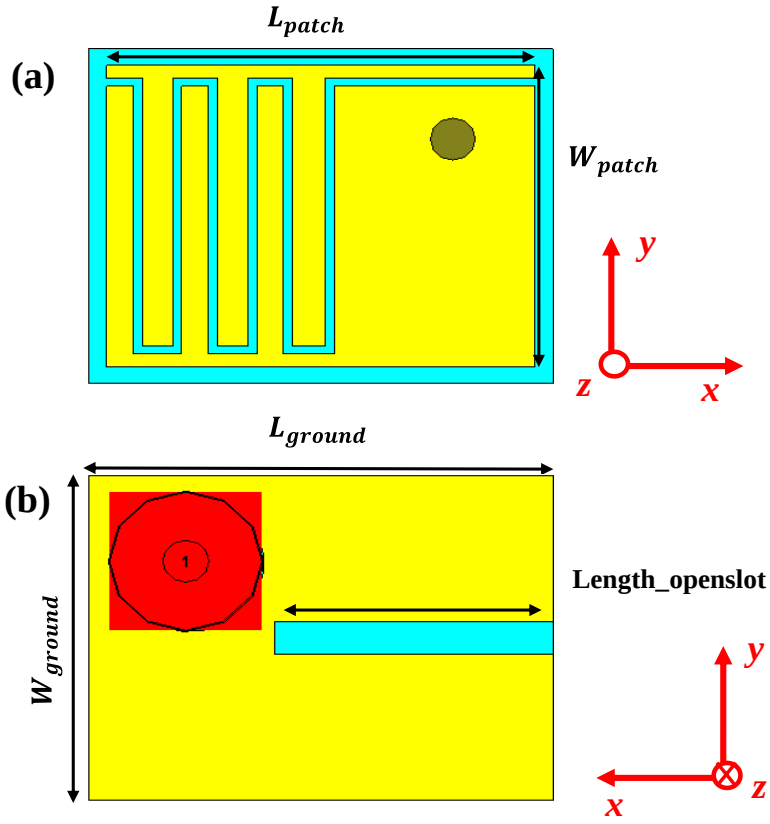

Fig. 8.2: Top view and bottom view of skin implanted antenna

The dimensions of the proposed antenna, shown in Fig. 8.2, are summarized in Table 8.1. Outer and inner conductor radii of the coaxial feed are 2.11 mm and 0.63 mm respectively to achieve 50 Ω impedance.

TABLE 8.1: Design parameters of muscle-implant antenna

Parameter	Value (mm)	Parameter	Value (mm)
Length of Ground (L_g)	13	Width of Ground (W_g)	10
Length of Substrate (L_s)	13	Width of Substrate (W_s)	10
Length of Patch (L_p)	12	Width of Patch (W_p)	9
Length of open slot (Length_openslot)	7.6	Thickness of the Meander-line slot	0.25

8.4 DEVELOPMENTAL STEPS OF THE FINAL ANTENNA

The final design of the proposed antenna has been achieved by optimizing several steps. All the intermediate stage antennas have been analysed inside body phantom at a depth of 4 mm from the top of phantom surface as illustrated in Fig. 8.3.

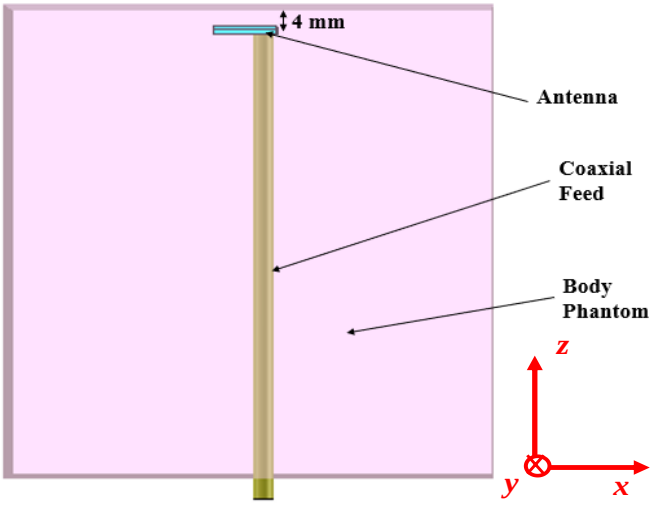

Fig. 8.3: Implantable antenna within body phantom

8.4.1. *Evolution of Patch Geometry*

According to relevant literature [11-15], typical area of the implantable antennas is reported to be around 160 mm^2. Therefore, in this work, a simple patch antenna has been taken where dimensions of the patch are 12 mm × 9 mm.

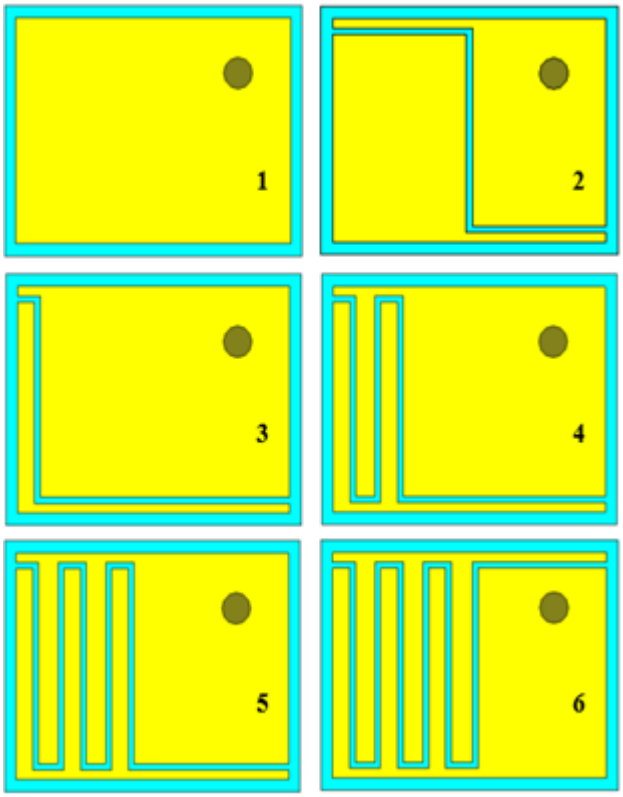

Fig. 8.4: Design evolution of patch of the body implantable antenna

At the preliminary stage, it is observed that simple rectangular patch antenna shown in Fig. 8.4.1 is not amenable to be tuned in 2.45 GHz ISM band – as illustrated in Fig. 8.5.1. To increase effective current path length and effective wavelength (keeping size of antenna fixed), multiple slots need to be introduced on the patch [16-17].

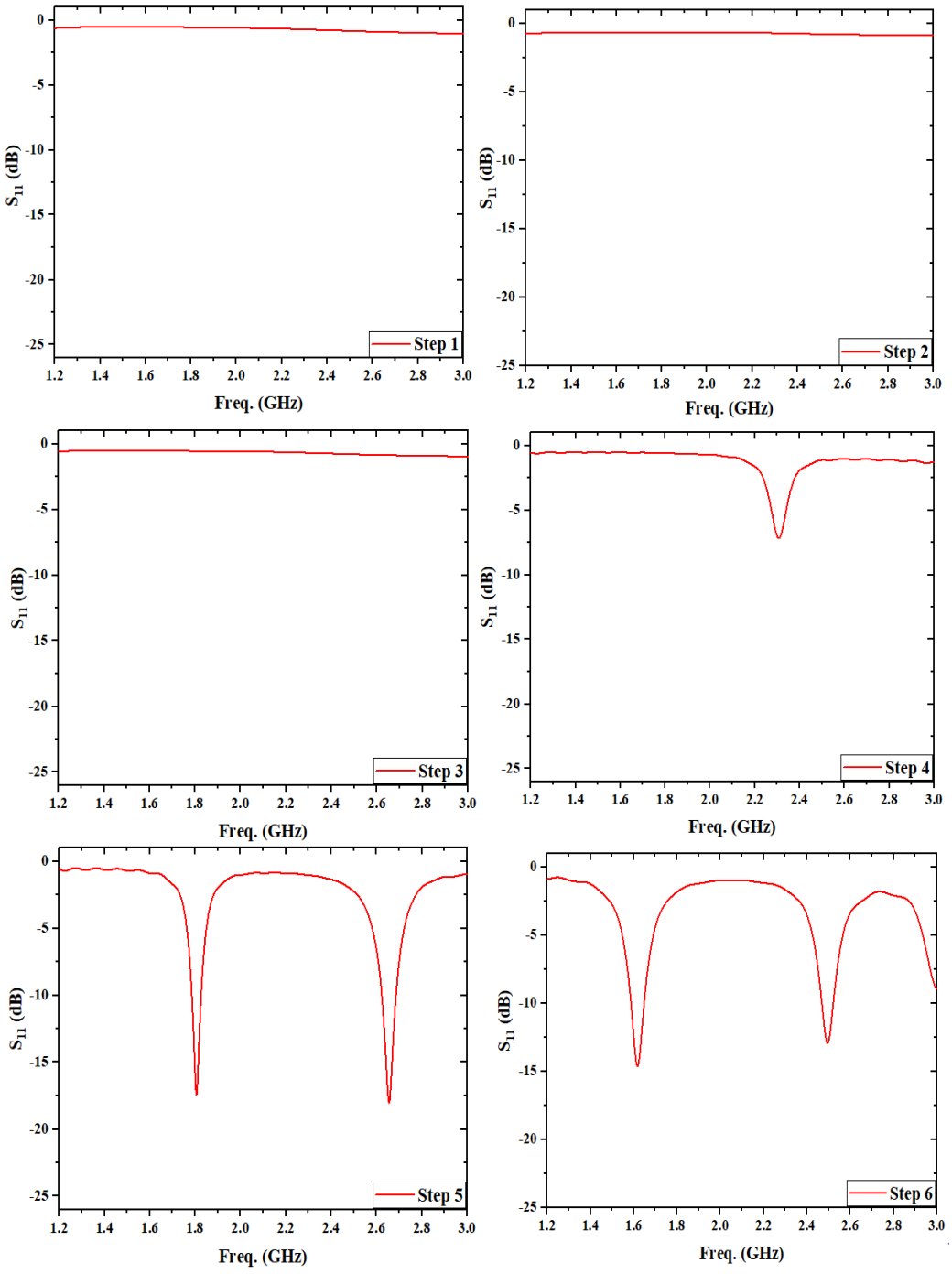

Fig. 8.5: S_{11} vs frequency plots of all steps shown in Fig. 8.4

Introducing meander-line slots on the patch leads to antenna geometry miniaturization – as reported in literature [17]. Therefore, in the next few steps as shown in Fig. 8.4, number of meander-line slots has been progressively increased on the patch so that the final antenna inside body equivalent phantom can be tuned in desired frequency band. Incorporating single meander-slot with two different shapes, as shown in Figs. 8.4.2 and 8.4.3, cannot tune the resonant frequency within desired band – as illustrated in Figs. 8.5.2 and 8.5.3 respectively.

In Fig. 8.5.4, slight response is observed in reflection coefficient curve after introducing two meander-line slots (refer to Fig. 8.4.4) instead of a single meander-line slot. However, a proper matching in S_{11} curve below –10 dB has not been achieved yet.

Next, after incorporating three meander slots (as illustrated in Fig. 8.4.5), matching in S_{11} curve below –10 dB has been observed at around two frequencies i.e., 1.81 GHz and 2.66 GHz. The second resonant frequency is quite close to the 2.45 GHz ISM band. Therefore, another half meander-line slot has further been added on the patch as depicted in Fig. 8.4.6. This additional half meander-line slot is able to further tune the resonant frequencies at 1.62 GHz and 2.5 GHz respectively – as illustrated in Fig. 8.5.6. The return loss values at 1.62 GHz and 2.5 GHz are 14.63 dB and 12.94 dB respectively.

8.4.2. *Evolution of Ground plane Geometry*

In Fig. 8.5.6, it is evident that the second resonant frequency at 2.5 GHz is within 2.45 GHz ISM band – however, 1.62 GHz frequency is not utilized for medical applications in general. As reported in relevant literature [18-19], the electrical length (L/λ) of open slot on small ground plane of antenna can be tuned to

control impedance matching at the desired frequency – where, L is the physical length of open slot and λ is the free space wavelength.

To this end, an open slot has further been introduced on the ground plane. The length of the open slot should be chosen properly to attain proper matching in S_{11} curve below –10 dB at 2.5 GHz. Next, an open slot is placed on the ground plane of this antenna and the length of this open slot is denoted as 'Length_openslot' (refer to Fig. 8.6). Obtained return loss values at the two resonant frequencies for different 'Length_openslot' values have been tabulated in Table 8.2.

According to [18], the –10 dB reflection coefficient bandwidth can be improved by increasing the open slot width. In this work, width of the open slot is taken as 1 mm and the same is way wider than the other slots incorporated in this antenna.

TABLE 8.2: Return loss values for different 'Length_openslot' values

Length_openslot (mm)	Return Loss in dB at First Resonance	Return Loss in dB at Second Resonance
4	14.17	23.96
5	8.37	19.69
6	7.33	16.93
7	7.30	25.94
7.2	7.38	33.63
7.4	7.74	42.57
7.6	8.14	44.94
7.8	8.43	37.79
8	9.17	32.21

A small shift in resonant frequency has been observed due to increased capacitance in the equivalent circuit of the antenna for introducing the open slot. The

two resonant frequencies i.e., 1.62 GHz and 2.5 GHz have now been shifted by a narrow margin to 1.54 GHz and 2.43 GHz respectively. Thereafter, the 'Length_openslot' parameter has gradually been increased by 1 mm step from 4 mm to 7 mm. A proper impedance matching has been achieved at 2.43 GHz for 'Length_openslot' = 7 mm and at the same time, the resonance at 1.54 GHz has been eliminated.

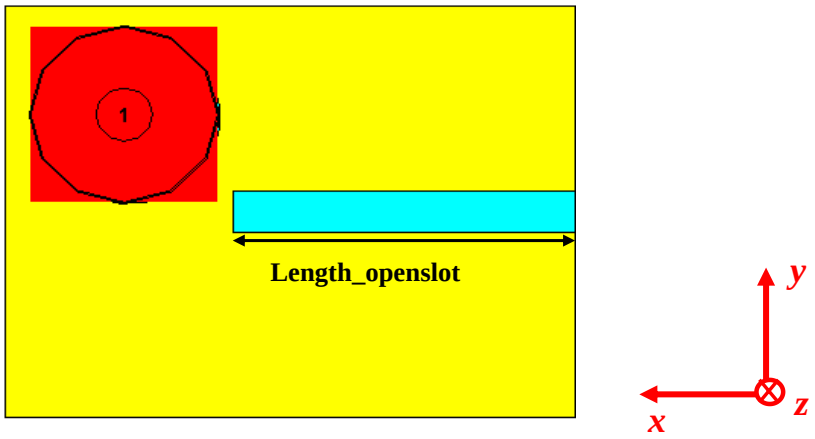

Fig. 8.6: Length_openslot variation

Then, the 'Length_openslot' parameter has further been increased with 0.2 mm step size. A better return loss value at 2.43 GHz has been observed for 'Length_openslot' = 7.6 mm. However further increasing the Length_openslot value beyond 7.6 mm results in deteriorated matching at 2.43 GHz.

Therefore, value of Length_openslot has been set at 7.6 mm. Thus finally, a 7.6 mm long open slot has been incorporated on ground plane as illustrated in Fig. 7. Introducing this open slot on the ground plane, near about 50 Ω impedance matching has been attained at 2.43 GHz – as observed in Fig. 8.7.

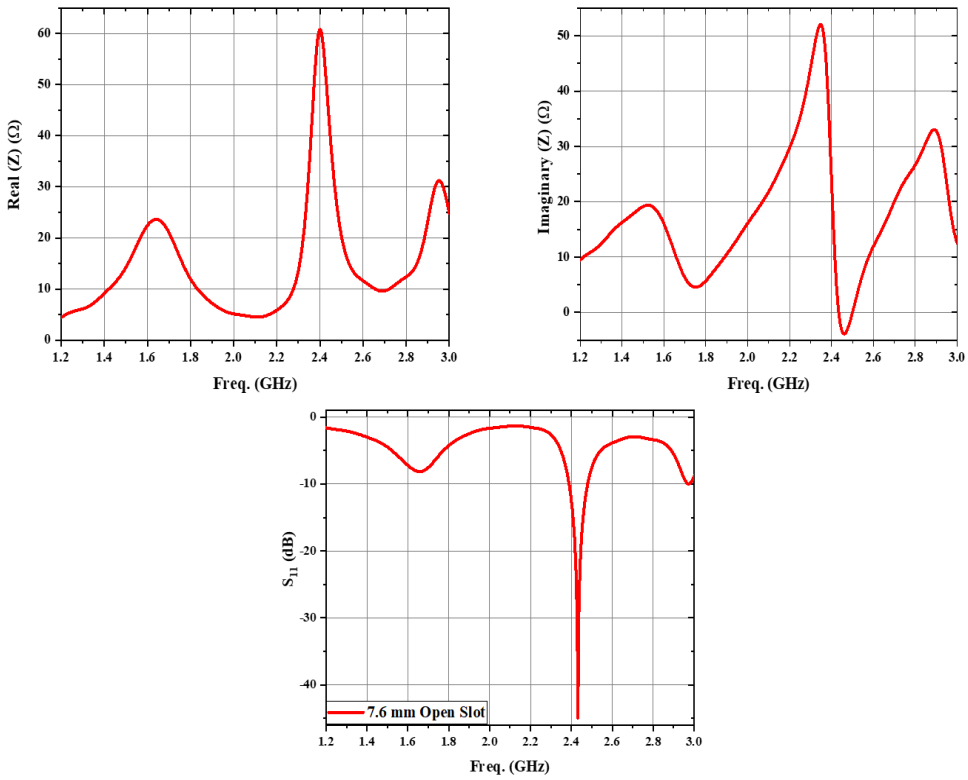

Fig. 8.7: Impedance and reflection coefficient curves for 7.6 mm open slot

8.5 RESULTS FOR THE FINAL ANTENNA

All the antenna structures shown in above figures have been simulated using the transient solver available in Computer Simulation Technology Microwave Studio (CST MWS) 2017. The final antenna is also fabricated and placed within body phantom liquid. The fabricated antenna is shown in Fig. 8.8.

Simulated and measured return loss values of the proposed antenna inside body equivalent phantom model is 44.94 dB at 2.43 GHz – as observed in Fig. 8.9. This antenna possesses –10 dB reflection coefficient bandwidth of 90 MHz (2.39 GHz to

2.48 GHz) at around 2.43 GHz. The proposed antenna provides a realized gain of –20.6 dBi at above mentioned resonant frequency inside body equivalent phantom.

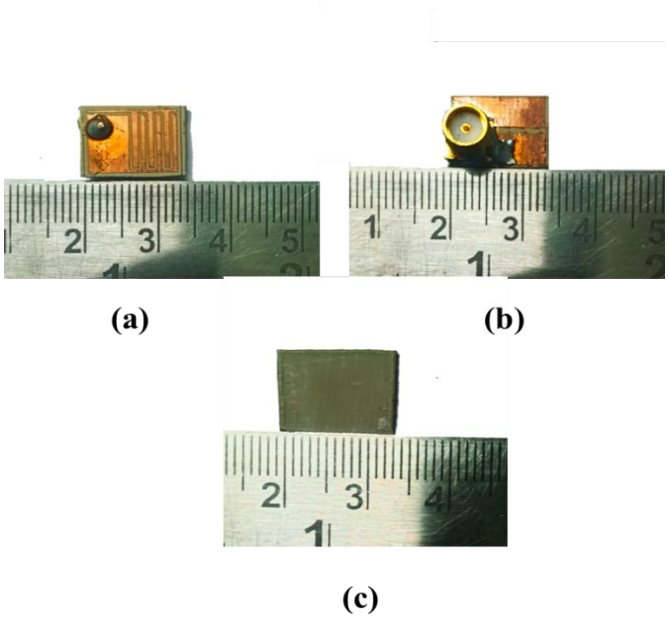

Fig. 8.8: (a) Top view (b) Bottom view of fabricated antenna (c) Top view of superstrate

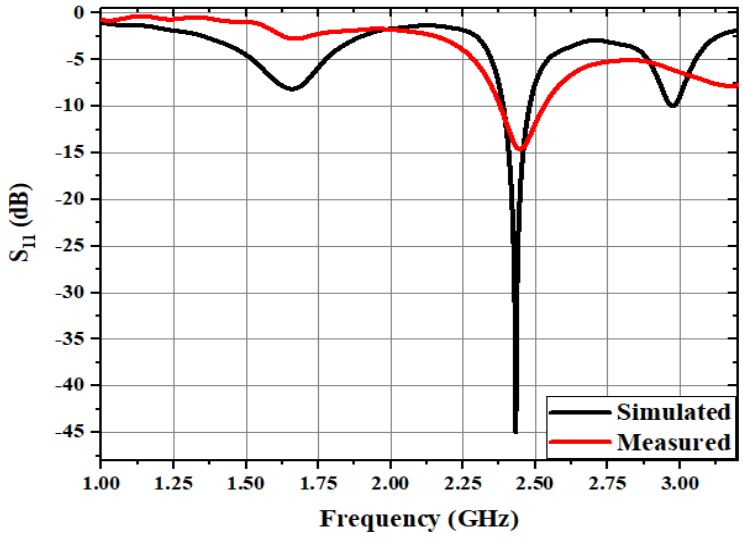

Fig. 8.9: S_{11} vs frequency plot for final antenna within body phantom

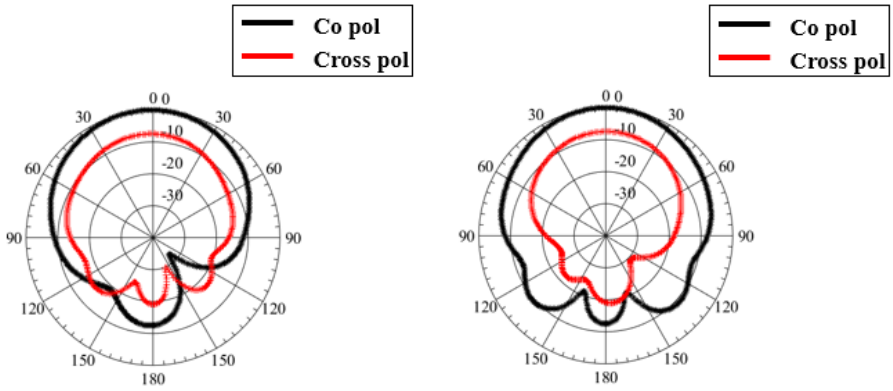

Fig. 8.10 Simulated co-polarized and cross-polarized radiation patterns of the proposed antenna at 2.43 GHz (a) E-plane and (b) H-plane

E-plane and H-plane of the designed antenna is represented by $\varphi = 90^{\circ}$ and $\varphi = 0^{\circ}$ respectively, because this antenna has been designed on the x-y plane and the coaxial feed is along z axis. The E-plane and-H plane radiation patterns (co-polarization and cross-polarization) of the proposed antenna inside phantom model are illustrated in Figs. 8.10 (a) and 8.10 (b) respectively.

To ensure safe electromagnetic exposure, the SAR values should be less than 1.6 W/Kg averaged over 1g of contiguous tissue and 2 W/Kg averaged over 10g of contiguous tissue – as prescribed in global standards [20-21].

For 1 W average input power, the final antenna contributes 352.2 W/Kg and 64.78 W/Kg peak SAR values respectively averaged over 1g and 10g contiguous tissue. To maintain the prescribed specific absorption rate limits, the maximum average input powers should be 4.5 mW and 25 mW while averaged over 1g and 10g of contiguous tissue respectively.

Comparison of the final body implantable antenna with some previous antenna performances is tabulated in Table 8.3.

TABLE 8.3: Comparison of final antenna with existing implantable antennas

Ref.	Phantom Type	Gain (dBi)	Peak SAR (1W) (W/Kg)(1g)	Peak SAR (1W) (W/Kg)(10g)
[22]	Skin	-22.8	807.34	102.04
[23]	Skin	-22.7	733.5	-
[24]	Skin	-22.37	759.72	87.24
This design	Body	-20.6	352.2	64.78

8.6 CONCLUSION

In this work, an implantable antenna consisting of 0.25 mm thick meander-line slots on the patch along with a 7.6 mm long open slot on the ground plane has been designed in 2.45 GHz ISM band. This antenna is implanted inside a body equivalent phantom (100mm × 100mm × 100mm). A superstrate (13 mm × 10mm × 0.762mm) made of Arlon AD 430 is placed on the patch. Overall volume of the designed antenna is 207.22 mm^3 and the total area including superstrate is 130 mm^2. Due to current unavailability of biocompatible material, Arlon AD 430 is used here as superstrate in simulation as well as to perform practical verification in near future. The antenna provides –20.6 dBi realized gain at 2.43 GHz along with a –10 dB reflection coefficient bandwidth of 90 MHz. The designed antenna can radiate over 2.39 GHz to 2.48 GHz. For 1 W average input power, the respective peak SAR values are 352.2 W/Kg and 64.78 W/Kg while averaged over 1g and 10g contiguous tissue respectively. The respective maximum average input power should be 4.5 mW and 25 mW while averaged over 1g and 10g of body equivalent phantom to check SAR value against the prescribed limits.

REFERENCES

[1] T. Karacolak, A. Z. Hood and E. Topsakal, "Design of a Dual – Band Implantable Antenna and Development of Skin Mimicking Gels for Continuous Glucose Monitoring," *IEEE Transactions on Microwave theory and Techniques*, vol. 56, no. 4, April 2008.

[2] T. Yilmaz, T. Karacolak and E. Topsakal, "Characterization and Testing of a Skin Mimicking Material for Implantable Antennas Operating at ISM Band (2.4 GHz – 2.48 GHz)," *IEEE Antennas and Wireless Propagation Letters*, vol. 7, pp. 418 – 420, June 2008.

[3] A. Kiourti and K. S. Nikita, "A Review of Implantable Patch Antennas for Biomedical Telemetry: Challenges and Solutions [Wireless Corner]," *IEEE Antennas and Propagation Magazine*, vol. 54, no. 3, pp. 210 – 228, June 2012

[4] M. Zada and H. Yoo, "A Miniaturized Triple – Band Implantable Antenna System for Bio -Telemetry Applications," *IEEE Transactions on Antennas and Propagation*, vol. 66, no. 12, pp. 7378 – 7382, October 2018.

[5] Y. Rahmat–Samii and E. Topsakal, "Antenna and Sensor Technologies in Modern Medical Applications," *Wiley – IEEE Press*, 2021.

[6] J. R. Nagel, C. M. Furse, D. A. Christensen and C. A. Durney, "Basic Introduction to Bioelectromagnnetics," *CRC Press, Taylor & Francis Group*, 2019.

[7] http://niremf.ifac.cnr.it/tissprop/htmlclie/htmlclie.php.

[8] https://itis.swiss/virtual-population/tissueproperties/database/dielectric properties

[9] F. Gozasht and A. S. Mohan, "Miniaturized Slot PIFA Antenna for Triple band Implantable Biomedical Applications," *2013 IEEE MTT-S International Microwave Workshop Series on RF and Wireless Technologies for Biomedical and Healthcare Applications (IMWS-BIO), March* 2014.

[10] V. Kaim, B. K. Kanaujia, S. Kumar, H. C. Choi, K. W. Kim, and K. Rambabu, "Ultra-Miniature Circularly Polarized CPW-Fed Implantable Antenna Design and its Validation for Biotelemetry Applications," *Scientific Reports*, April 2020.

[11] F-J. Huang, C-M. Lee, C-L. Chang, L-K. Chen, T-C. Yo and C-H. Luo, "Rectenna Application of Miniaturized Implantable Antenna Design for Triple-Band Biotelemetry Communication," *IEEE Transactions on Antennas and Propagation*, vol. 59, no. 7, pp. 2646 – 2653, July 2011.

[12] C. Liu, Y-X. Guo and S. Xiao, "A Hybrid Patch/Slot Implantable Antenna for Biotelemetry Devices," *IEEE Antennas and Wireless Propagation Letters*, vol. 11, pp. 1646 – 1649, 2012.

[13] L-J. Xu, Y-X. Guo and W. Wu, "Miniaturised slot antenna for biomedical applications," *Electronics Letters*, vol. 49, no. 17, pp. 1060 – 1061, August 2013.

[14] S. Das and D. Mitra, "A Compact Wideband Flexible Implantable Slot Antenna Design with Enhanced Gain," *IEEE Transactions an Antennas and Propagation,* vol. 66, no. 8, pp. 4309 – 4314, August 2018.

[15] C. Liu, Y-X. Guo and S. Xiao, "Circularly Polarized Helical Antenna for ISM Band Ingestible Capsule Endoscope Systems," *IEEE Transactions an Antennas and Propagation,* vol. 62, no. 12, pp. 6027 – 6039, December 2014.

[16] N. Behdad and K. Sarabandi, "Bandwidth enhancement and further size reduction of a class of miniaturized slot antennas," *IEEE Transactions an Antennas and Propagation,* vol. 52, pp. 1928– 1935, Aug. 2004.

[17] D. Mitra, D. Das and S. R. B. Chaudhuri, "Miniaturization of Meander line Slot Antenna," *2015 IEEE – APS Topical Conference on Antennas and Propagation in Wireless Communications (APWC),* October 2015.

[18] J. X. Yun and R. G. Vaughan, "Open Slot Antenna in a Small Groundplane at the Second Resonance," *2010 IEEE Antennas and Propagation International Symposium*, September 2010.

[19] M. Kahrizi, T. K. Sarkar and Z. A. Maricevic, "Analysis of a wide radiating slot in the ground plane of a microstrip line," *IEEE Transactions on Microwave Theory and Techniques,* vol. 41, no. 1, pp. 29 – 37, January 1993.

[20] ICNIRP, "Guidelines for limiting exposure to electromagnetic fields (100 KHz to 300 GHz)," *Health Phys.,* vol. 118, no. 5, pp. 483-524, March 2020.

[21] R. F. Cleveland, Jr., D. M. Sylvar, and J. L. Ulcek, "Evaluating compliance with FCC guidelines for human exposure to radiofrequency electromagnetic

fields," *FCC OET Bulletin*, vol. 65, Edition 97-01, Washington D.C., November 1997.

[22] S. A. A. Shah and H. Yoo, "Scalp-implantable antenna systems for intracranial pressure monitoring," *IEEE Transactions of Antennas Propagations.* vol. 66, no. 4, pp. 2170-2173 (2018).

[23] R. Li, Y-X. Guo, B. Zhang and G. Du, "A Miniaturized Circularly Polarized Implantable Annular – Ring Antenna," IEEE Antennas and Wireless Propagation Letters, vol. 16, pp. 2566 – 2569, July 2017.

[24] I. Gani and H. Yoo, "Multi-Band Antenna System for Skin Implant," *IEEE Microwave and Wireless Components Letters*, vol. 26, no. 4, April 2016.

Chapter 9

Meander-line based body implantable antenna design

Contents	
	9.1 Introduction
	9.2 Design of body phantom
	9.3 Design parameters of the antenna
	9.4 Developmental steps of the final antenna
	9.5 Results for the final antenna
	9.6 SAR and Link budget analysis
	9.7 Conclusion

9.1 INTRODUCTION

In the previous chapter, meander-line type slot was implemented on a patch antenna and its effect on antenna performance was investigated. In this chapter, the meandering concept has been implemented for miniaturization purpose. The antenna is tuned at 2.45 GHz ISM band while it is implanted inside body phantom. Here an implantable antenna having serpentine shaped patch has been designed, fabricated and measured. A liquid human body mimicking phantom has been developed to place the antenna and measure its responses within it. A link budget is also performed in this chapter to verify that the designed antenna can communicate with external environment through its lossy environment.

9.2 DESIGN OF BODY PHANTOM

A conical shaped plastic container (as shown in Fig. 9.1(a)) having top diameter of 110 mm, bottom diameter of 94 mm and height of 50 mm has been taken to keep the phantom liquid for measurement purpose. To match the simulated results with measured ones, a conical shaped body equivalent phantom model having same dimensions as the plastic container has been designed in CST Microwave Studio 2017 software as shown in Fig. 9.1(b) providing the relative permittivity and loss tangent values as 52.72 and 0.277 respectively.

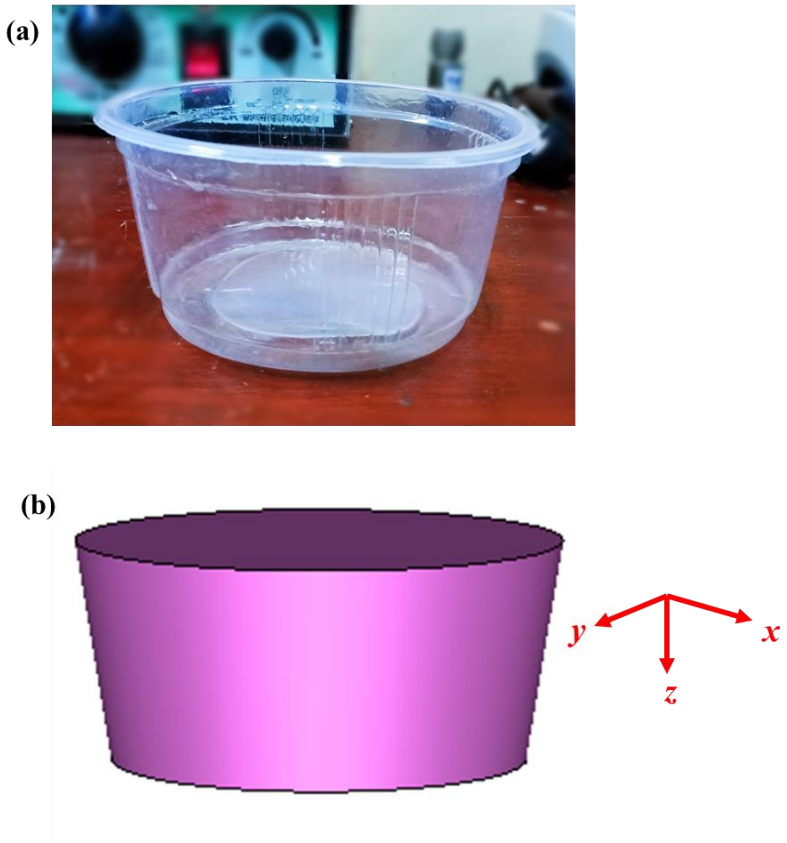

Fig. 9.1: (a) Phantom container, (b) Conical body phantom designed in CST Microwave Studio 2017, (c) Permittivity and loss tangent vs frequency of body equivalent phantom liquid from CST Microwave Studio 2017

9.3 DESIGN PARAMETERS OF THE ANTENNA

Fig. 9.2 illustrates the geometry of the proposed implantable antenna which is tuned at 2.45 GHz ISM band after implanting it within body equivalent phantom. Here also, copper is utilized as the material for ground and radiator part - whereas, Arlon AD 430 is used as the material for superstrate and substrate layers of the antenna.

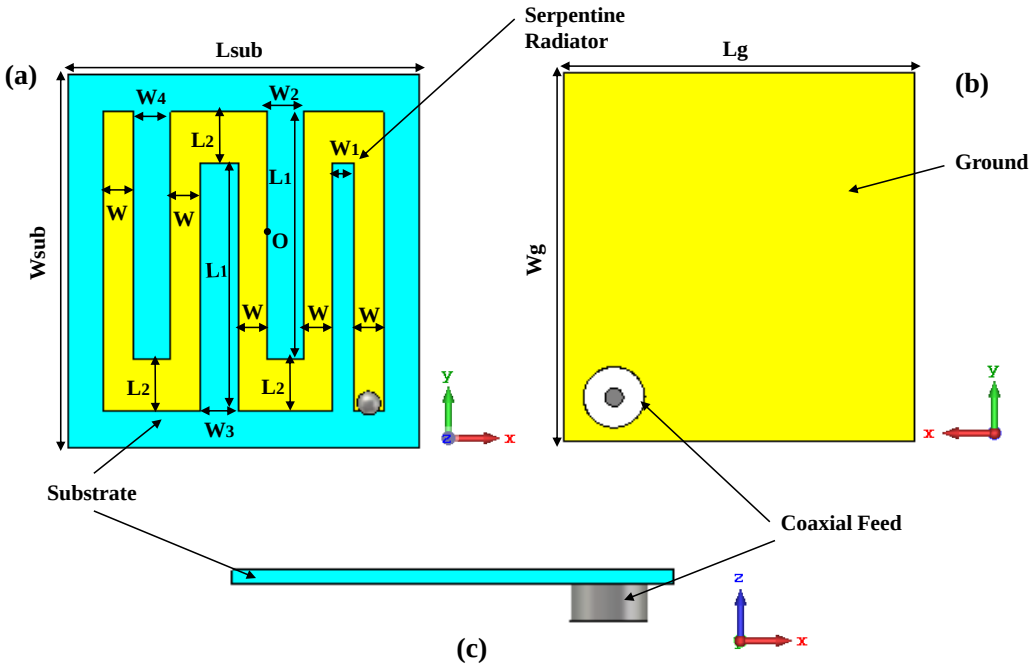

Fig. 9.2: (a) Top view, (b) bottom view and (c) side view of the antenna

Due to its low loss and availability for fabrication, Arlon AD 430 has been selected as substrate material for maintaining sufficient gain of the implantable antenna inside highly absorbing tissue layer so that it can communicate with external devices. Yellow-coloured regions and sky-blue coloured parts in Fig. 9.2 represent copper layer and Arlon AD 430 respectively.

The values of relative permittivity and loss tangent of Arlon AD 430 at 2.45 GHz band are 4.3 and 0.003 respectively. The thickness of Arlon AD 430 is 0.762 mm i.e., 30 mil whereas the thickness of copper plates of this antenna is 0.001 mm. The design parameters of the proposed implantable antenna are enlisted in Table 9.1.

A superstrate having same dimensions as the substrate is placed on the radiator of this antenna. A coaxial feed is connected to excite the radiator and the feedpoint is set properly to achieve proper matching. In order to attain 50 Ω impedance match, the outer and inner conductor diameters of the feed are 4.22 mm and 1.26 mm respectively correspondind to a standard 50 Ω SMA connecter.

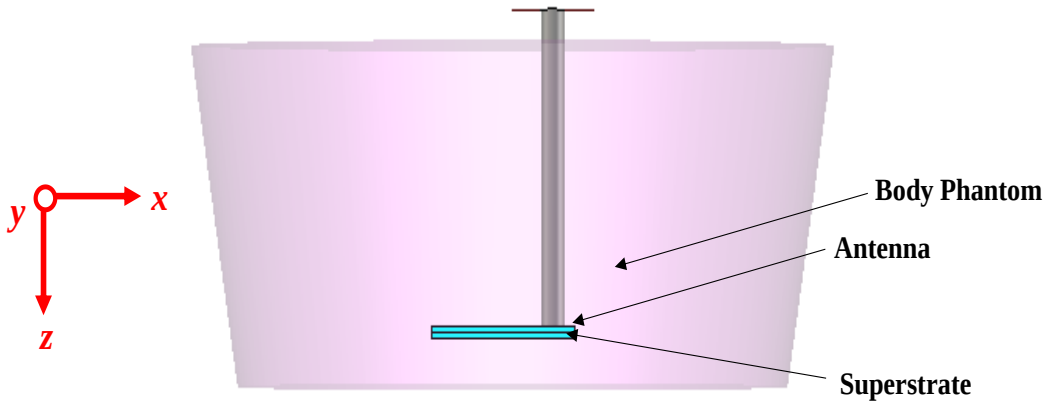

Fig. 9.3: Side view of antenna inside body phantom

The antenna performance is investigated by implanting the antenna shown in Fig. 9.2 inside the body phantom as shown in Fig. 9.3. The final design of the proposed antenna is achieved by optimizing different variables mentioned in Fig. 9.2.

TABLE 9.1: Design parameters of meander-line antenna

Antenna Dimension	Value (mm)	Antenna Dimension	Value (mm)
Length of substrate (Lsub)	24.21	Width of substrate (Wsub)	25.55
Length of ground (Lg)	24.21	Width of ground (Wg)	25.55
L_1	17	L_2	3.55
W	2	W_1	1.5
W_2	2.49	W_3	2.61
W_4	2.61	Feed location (x, y) with respect to origin O	(6.99, -11.5)

9.4 DEVELOPMENTAL STEPS OF THE FINAL ANTENNA

9.4.1. *Initial step of antenna design*

At the initial stage of this work, the four meandered line-based antenna structure shown in Fig. 9.4 (a) had been designed for observation. The values of the parameters L_1, L_2, W, W_1, W_2, W_3 and W_4 are 17 mm, 3 mm, 2 mm, 2.7 mm, 2.7 mm, 2.7 mm and 2.7 mm respectively.

Placing this antenna within the body phantom, reflection coefficient curve illustrated in Fig. 9.4 (b) is obtained. From this plot, it is clear that this antenna is not operating at the desired range of frequency. Return loss value of this design is 11.42 dB at 3.117 GHz.

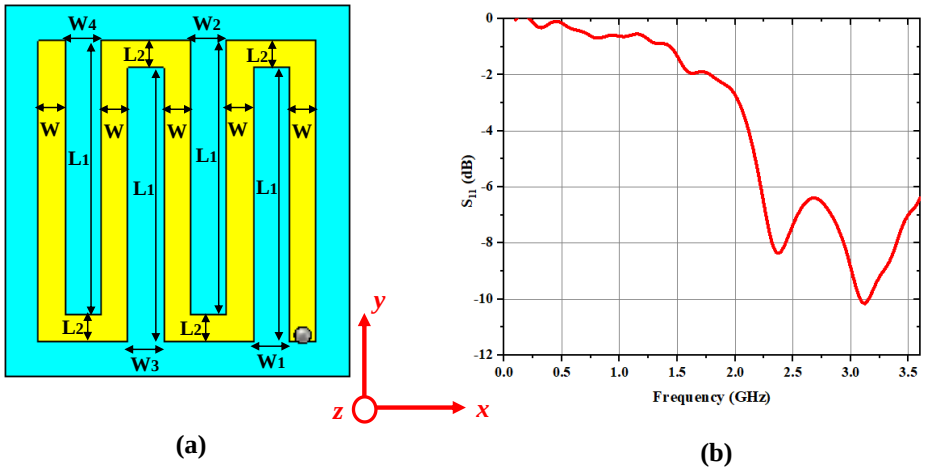

Fig. 9.4: (a) Initial antenna geometry, (b) S_{11} vs frequency

9.4.2. *Optimization of antenna parameters to the final antenna*

The main objective is to shift the resonant frequency of the implanted antenna from 3.117 GHz to around 2.45 GHz i.e., within desired frequency range. The antenna structure shown in Fig. 9.4 (a) has been decomposed into 17 sections (shown in Fig. 9.5) and the lumped circuit element values have been calculated according to the process mentioned in Das et. al. [1].

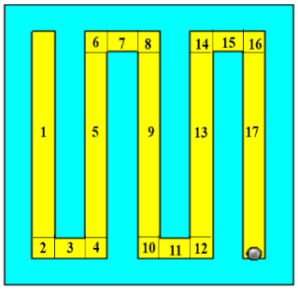

Fig. 9.5: Decomposition of meander line structure into 17 sections

The equivalent circuit of the above antenna in free space has been designed using Advanced Design System (ADS) based on the calculated lumped element values tabulated in Table 9.2.

TABLE 9.2: Lumped parameter values of initial antenna geometry

Length of line (mm)	**Width of line (mm)**	**Section Numbers**	**Components**	**Component numbers**	**Component values (Using Formula)**
$L_1 = 17$	W = 2	1, 17	Left Inductors	L11, L117	2.16 nH
			Right Inductors	L21, L217	2.16 nH
			Capacitors	C1, C17	2.49 pF
W_i = 2.7 (i = 1, 2, 3 and 4)	$L_2 = 3$	3, 7, 11, 15	Left Inductors	L13, L15, L111, L115	0.53 nH
			Right Inductors	L23, L25, L211, L215	0.53 nH
			Capacitors	C3, C5, C11, C15	0.53 pF
($L_1 – L_2$) = 14	W = 2	5, 9, 13	Left Inductors	L15, L19, L113	1.78 nH
			Right Inductors	L25, L29, L213	1.78 nH
			Capacitors	C5, C9, C13	2.05 pF
W = 2	$L_2 = 3$	Right angle sections (2, 4, 6, 8, 10, 12, 14, 16)	Left Inductors	Lb12, Lb14, Lb16, Lb18, Lb110, Lb112, Lb114, Lb116	0.28 nH
			Right Inductors	Lb22, Lb24, Lb26, Lb28, Lb210, Lb212, Lb214, Lb216	0.28 nH
			Capacitors	Cb2, Cb4, Cb6, Cb8, Cb10, Cb12, Cb14, Cb16	0.59pF

The capacitance tuned at the open end of the meander-line structure is C_{open} = 0.90 pF. A resistance is connected in series with C_{open} to represent the ohmic loss. Next, this antenna with superstrate is dipped within phantom model. A CL network is placed in cascaded form to represent the additional effect of phantom and superstrate. The complete equivalent lumped circuit model of the system has been illustrated in Fig. 9.6.

The values of C18 and L218 are tuned to match the S_{11} (dB) curve of the lumped circuit with S_{11} (dB) curve of original system simulated in CST. Keeping the values of C18 and L218 same to retain system effect unchanged, some lumped element values corresponding to antenna parameters are optimized to tune the antenna in desired band. The optimized values of these parameters are tabulated in Table 9.3.

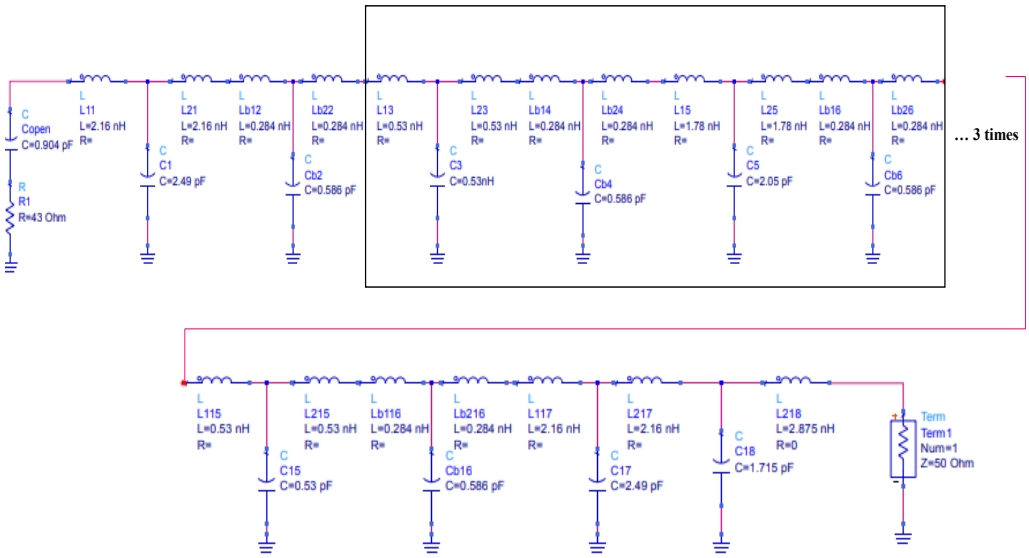

Fig. 9.6: Equivalent lumped Circuit model of initial antenna within phantom designed in ADS

TABLE 9.3: Optimization of lumped element values to tune at 2.45 GHz

Lumped parameters	Tuning Range	Optimized value	Lumped parameters	Tuning Range	Optimized value
R1	20.79 – 100 Ω	89.7 Ω	L111, L211	0.12 – 0.36 nH	0.22 nH
L13, L23	0.13 – 0.38 nH	0.17 nH	C11	0.25 – 0.74 pF	0.63 pF
C3	0.27 – 0.79 pF	0.66 pF	L115, L215	0.072 – 0.4 nH	0.13 nH
L17, L27	0.13 – 0.38 nH	0.22 nH	C15	0.01 – 0.45 pF	0.29 pF
C7	0.27 – 0.79 pF	0.42 pH	-	-	-

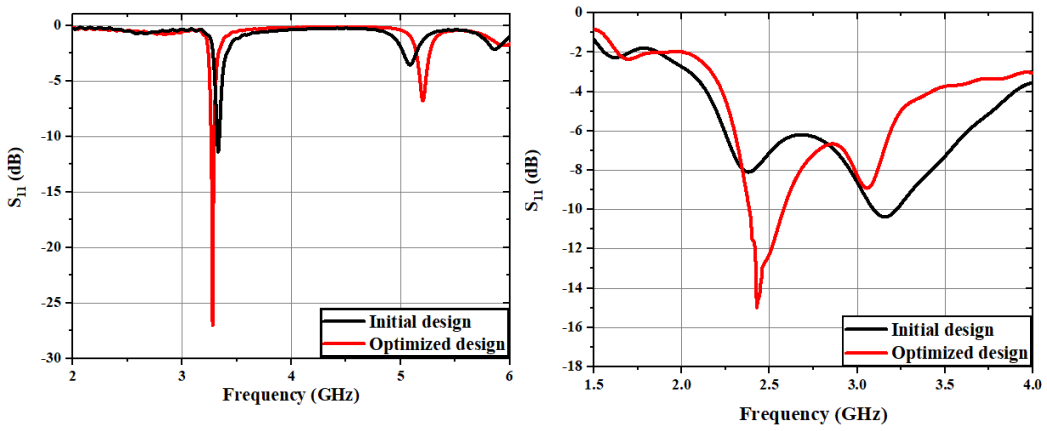

(a) **(b)**

Fig. 9.7: S_{11} (dB) curves of initial and optimized antenna (a) in air and (b) inside phantom

Using transmission line model concept from [1], the final antenna design parameters are obtained using optimized lumped parameter values mentioned in Table 9.3. The optimized antenna shown in Fig. 9.2 is tuned to 2.45 GHz ISM band while placing it inside body phantom. The S_{11} (dB) curves for the initial antenna and the optimized antenna in free space and within phantom model are depicted in Fig. 9.7 (a) and (b) respectively.

9.5 RESULTS FOR THE FINAL ANTENNA

The proposed antenna has been fabricated and its reflection coefficient curve has been measured by using Vector Network Analyser (VNA). Top and bottom views of fabricated antenna are shown in Fig 9.8. At first, S_{11} (dB) curve for the antenna in free space has been shown observed and the plot is compared with its simulated response as shown in Fig. 9.9 (a).

According to the plot of Fig. 9.9(a), the fabricated antenna has return loss value of 15.11 dB at resonant frequency of 3.29 GHz whereas simulation result shows the corresponding value of the antenna is 27 dB at 3.28 GHz.

Fig. 9.8: (a) Top view (b) Bottom view of fabricated antenna

The resonant frequency of the antenna has been shifted due to placement of superstrate on it as shown in Fig. 9.9 (b). The simulated return loss value of the antenna along with superstrate is 20.13 dB at 3.22 GHz whereas the fabricated antenna with superstrate shows a return loss value of 22.52 dB at 3.19 GHz. Owing to a small air gap between radiator and superstrate in the time of measurement, a frequency shift is observed from the simulated result.

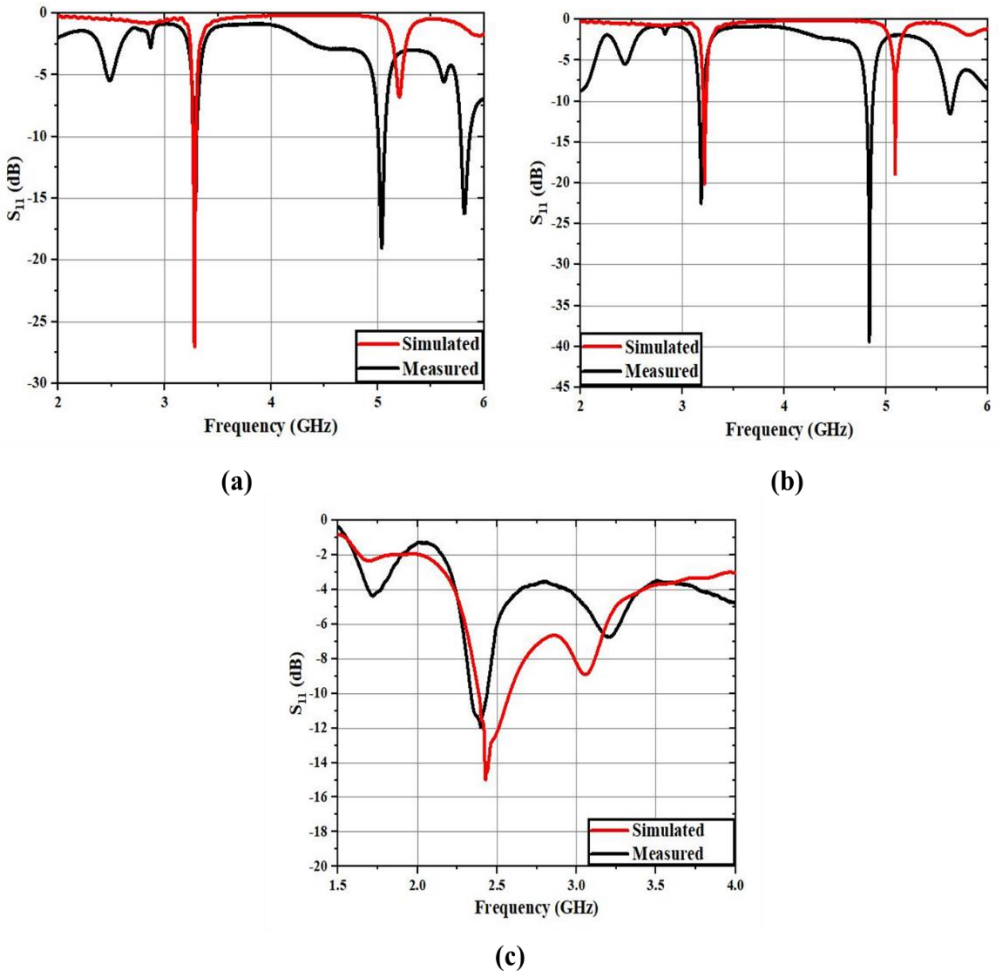

Fig. 9.9: Simulated and measured S_{11} (dB) curve of (a) final antenna in air (b) antenna along with superstrate (c) Antenna along with superstrate within phantom

After implanting the final antenna within body phantom, resonant frequencies are shifted to 2.43 GHz and 2.41 GHz with return loss values of 14.98 dB and 11.95 dB observed in simulation and measurement respectively as shown in Fig. 9.9 (c). This antenna possesses 10 dB return loss bandwidths 210 MHz and 110 MHz respectively within body equivalent phantom around resonant frequencies as observed from simulation and measurement.

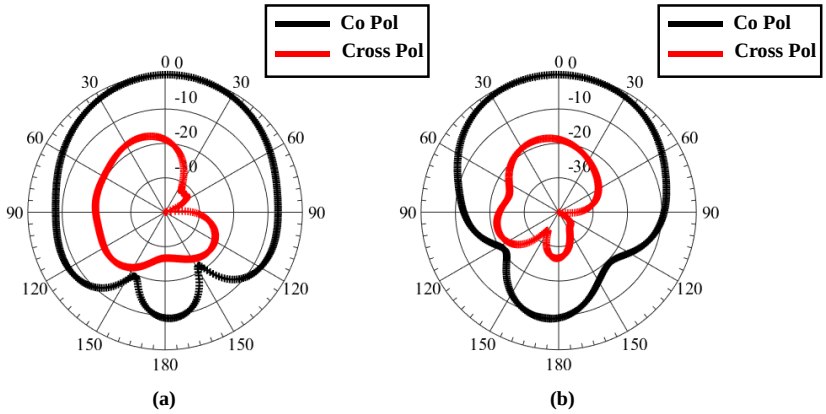

Fig. 9.10 Simulated co-polarized and cross-polarized radiation patterns of the antenna at 2.43 GHz (a) E-plane and (b) H-plane

The proposed antenna offers a realized gain of –19 dBi inside body equivalent phantom. Fig. 9.10 (a) and (b) show E plane and H plane radiation patterns (co-polar and cross-polar) of the proposed implantable antenna inside body phantom model respectively at 2.43 GHz.

9.5 SAR AND LINK BUDGET ANALYSIS

According to some international electromagnetic regulatory guidelines [2-3], average Specific Absorption Rate (SAR) values to ensure safety of human body should be less than 1.6 W/Kg and 2 W/Kg over 1g and 10g of contiguous tissue

respectively. The proposed antenna contributes 189.7 W/Kg and 49.74 W/Kg peak SAR values for 1W input power respectively averaged over 1g and 10g contiguous human tissue. SAR distributions for 1g and 10g tissue model are shown in Fig. 9.11. To maintain the prescribed SAR limits in IEEE C95.1-2005, the maximum input powers should be 8 mW and 35 mW for 1g and 10g tissue respectively.

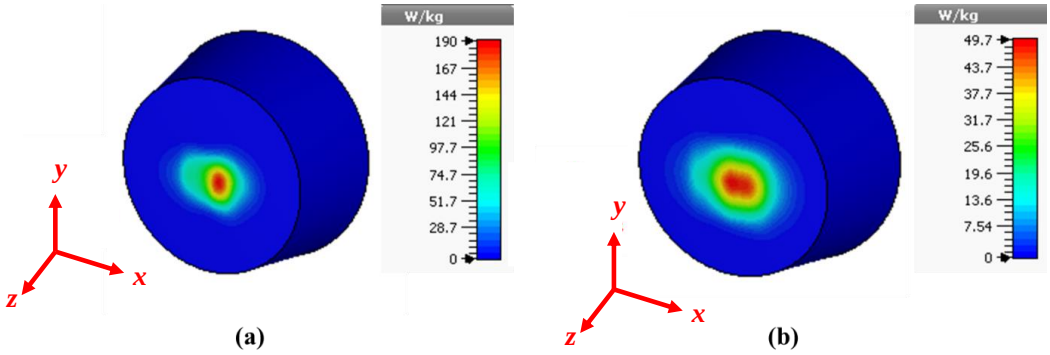

Fig. 9.11 Specific Absorption Rate (SAR) distribution for 1 W input power averaged over (a) 1g and (b) 10 g contiguous tissue model

Link budget analysis is an essential part of performance analysis of implantable antenna to establish proper communication link between antenna implanted inside body and external device. For link budget, S_{21} measurement in different distances is performed by connecting proposed antenna with port1 of VNA and a horn antenna placed in line of sight of the transmitting antenna with port 2.

This measurement is performed in two different environments: (a) keeping the proposed antenna in free space and (b) implanting this antenna inside the phantom liquid at 10 mm depth from the upper surface of the phantom. These two S_{21} responses are plotted in Fig. 9.12.

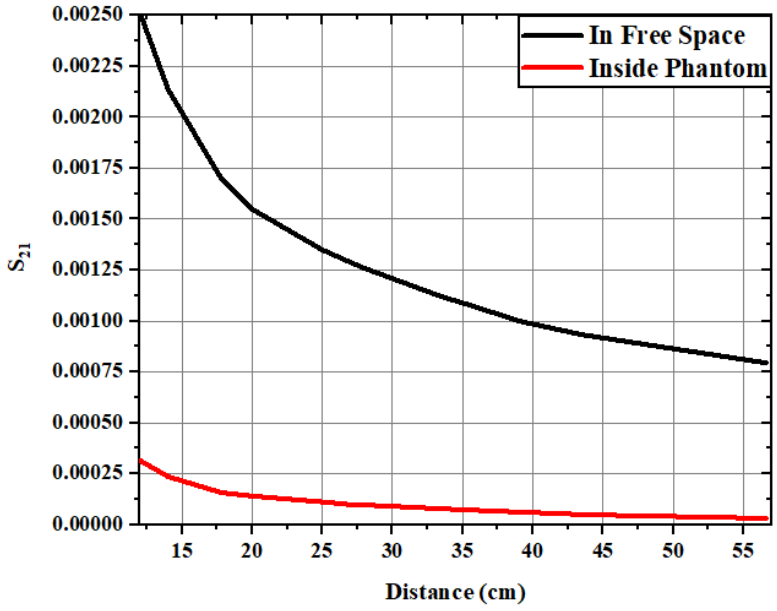

Fig. 9.12: S_{21} plots with respect to distance (d) of the proposed antenna

Based on SAR distribution, input power applied to the implanted antenna is 7 mW which can satisfy prescribed limit of SAR for both 1g and 10g human tissue. Therefore, transmitted power (P_T) will be – 16.64 dBm. Gain of the transmitting antenna in free space considering superstrate place on it, G_T, is 2.98 dB and gain of the receiving antenna, G_R, is 10 dB. For far-field communication, the link budget can be expresses as [4],

$$[P_R]_{dBm} = [P_T]_{dBm} + [G_T]_{dB} + [G_R]_{dB} - (loss)_{dBm}$$

Let us suppose, receiver horn antenna is placed at a distance of d = 27 cm from the transmitting antenna. In the first case, antenna with superstrate is kept in free space. From the Fig. 9.12, S_{21} value at that distance is 0.0013 (-28.9 dB). Therefore, power received by the horn antenna is $[P_R]_{dBm} = [S_{21}]_{dB} + [P_T]_{dBm} =$ -

28.9 + (-16.64) = -45.54 dBm. The loss due to air medium from equation 2 is 41.88 dBm or 15.42 W.

When the transmitting antenna is submerged into phantom keeping receiver antenna in same place, S_{21} value is reduced to 0.0001 (-40 dB). Received power will be $[P_R]_{dBm}$ = -56.64 dBm. The combined loss due to air and phantom from equation (2) is 52.98 dBm or 198.61 W. That means, loss due to phantom is 52.64 dBm or 183.19 W.

Keeping the transmitting antenna within phantom, let us consider that instead of horn antenna with 10 dB gain, another antenna having 5 dB gain is placed at the same position. Therefore, path loss will be the same as in previous setup. Then amount of power received by this receiver is calculated from the equation as -61.64 dBm.

The path loss factor can be written as, $[loss]_{dB} = (\frac{4\pi d}{\lambda})^2$ where λ is operating wavelength. Let us consider that the threshold value of received power is -100 dBm. In this step, the maximum range or distance of receiver with 5 dB gain from an implantable antenna to receive -100dBm power is calculated. Path loss value obtained from above equation for this setup is 75.38 dBm. Therefore, from the expression of path loss factor the maximum distance can be obtained as d = 3.56 m.

The performance of the proposed antenna in comparison with several recently reported (2016 onwards) implantable antenna is demonstrated in Table 9.4. According to this table, proposed antenna provides better gain than other existing implantable antennas mentioned in the table. When 1 W average input power has been delivered to implantable antennas, proposed antenna affects human contiguous tissue less than other antennas due to their high SAR values for both 1 g and 10 g tissue models with respect to this work.

TABLE 9.4: Comparison of final antenna with existing implantable antennas

Ref.	Phantom type	Gain (dBi)	Peak SAR (1 W) (W/Kg)	
			1 g	10 g
[5]	Skin	-22.99	591.40	82.71
[6]	Skin	-22.93	347.08	66.55
[7]	Skin	-22.8	802.34	102.04
[8]	Skin	-22.7	733.5	-
[9]	Skin	-22.37	759.72	87.24
[10]	Skin	-21.2	491.9	59
[11]	Skin	-14.6	595	79.87
Proposed design	Body	-19	189.7	49.74

9.7 CONCLUSION

An implantable antenna having serpentine radiator operating in 2.45 GHz ISM band is proposed in this manuscript. This antenna is submerged inside a conical shaped body phantom liquid. A superstrate made of Arlon AD 430 has been kept on the upper surface of the antenna. For simulation as well as for practical measurement purpose, Arlon AD 430 is utilized as superstrate for current unavailability of biocompatible material such as alumina, Teflon etc. in laboratory. The antenna provides –19 dBi realized gain at 2.43 GHz. The designed antenna can radiate over 110 MHz and 210 MHz -10 dB return loss bandwidth around 2.41 GHz and 2.43 GHz observed in measurement and simulation respectively. The respective peak

SAR values for 1 W average input power are 189.7 W/Kg and 49.74 W/Kg for 1g and 10g contiguous human tissue. The maximum average input power should be 8 mW and 25 mW for over 1g and 10g of body phantom respectively for keeping SAR value within the standard prescribed limits. Link budget analysis has also been performed to determine loss due to the lossy environment as well as to characterize corresponding communication link properly.

REFERENCES

[1] A. Das, S. Dhar and B. Gupta, "Lumped circuit model analysis of meander line antennas," *2011 11th Mediterranean Microwave Symposium (MMS)*, November 2011.

[2] ICNIRP, "Guidelines for limiting exposure to electromagnetic fields (100 KHz to 300 GHz)," *Health Phys.*, vol. 118, no. 5, pp. 483-524, March 2020.

[3] R. F. Cleveland, Jr., D. M. Sylvar, and J. L. Ulcek, "Evaluating compliance with FCC guidelines for human exposure to radiofrequency electromagnetic fields," *FCC OET Bulletin*, vol. 65, Edition 97-01, Washington D.C., November 1997.

[4] A. Kiourti and S. Nikita, "Miniature Scalp-Implantable Antennas for Telemetry in the MICS and ISM Bands: Design, Safety Considerations and Link Budget Analysis," *IEEE Transactions on Antennas and Propagation*, vol. 60, no. 8, August 2012.

[5] F. Faisal, M. Zada, A. Ejaz, Y. Amin, S. Ullah and H. Yoo, "A Miniaturized Dual-band Implantable Antenna System for Medical Applications," *IEEE Transactions on Antennas and Propagation*, vol. 68, no. 2, pp. 1161-1165, February 2020.

[6] M. S. Singh, J. Ghosh, S. Ghosh and A. Sarkhel, "Miniaturized Dual-Antenna System for Implantable Biotelemetry Application," *IEEE Antennas and Wireless Propagation Letters*, vol. 20, no. 8, pp. 1394-1398, August 2021.

[7] S. A. A. Shah and H. Yoo, "Scalp-implantable antenna systems for intracranial pressure monitoring," *IEEE Transactions of Antennas Propagations.* vol. 66, no. 4, pp. 2170-2173, 2018.

[8] R. Li, Y-X. Guo, B. Zhang and G. Du, "A Miniaturized Circularly Polarized Implantable Annular – Ring Antenna," *IEEE Antennas and Wireless Propagation Letters*, vol. 16, pp. 2566 – 2569, July 2017.

[9] I. Gani and H. Yoo, "Multi-Band Antenna System for Skin Implant," *IEEE Microwave and Wireless Components Letters*, vol. 26, no. 4, April 2016.

[10] H. Yoo and Y. Cho, "Miniaturized Dual-Band Implantable Antenna for Wireless Biotelemetry," *Electronics Letters*, vol. 52, no. 12, pp. 1005-1007, April 2016.

[11] G. Samanta and D. Mitra, "Miniaturised and radiation efficient implantable antenna using reactive impedance surface for biotelemetry," *IET Microwaves, Antennas & Propagation*, vol. 14, no. 2, pp. 177-184. November 2019.

Chapter 10

Madelung's disease detection

Contents	
	10.1 Introduction
	10.2 Problem statement
	10.3 Receiving antenna design
	10.4 Performance of antenna with fat thickness variation
	10.5 Madelung's disease detection
	10.6 Conclusion

10.1 INTRODUCTION

Madelung's disease occurs due to deposition of fat in subcutaneous layer in torso, neck, mammary, abdominal areas and in the upper and lower limbs. Therefore, for detection of Madelung's disease it is required to observe how the performance of implantable antenna is influenced by gradual growth of the subcutaneous fat layer.

10.2 PROBLEM STATEMENT

Let us suppose a doctor performed operation on a patient who had been suffering from Madelung's disease. After the operation, accumulated fat was removed from his body. To check whether further growth in fat layer in the same place has occurred due to Madelung's disease or not, doctor can implant the antenna

inside muscle layer of the patient at this place of body of the patient. In this chapter, probable detection process of Madelung's disease in post-operative case at same place of the body using implantable antenna is discussed.

10.3 RECEIVING ANTENNA DESIGN

To record the response of transmitting antenna implanted within muscle layer, a receiving antenna is designed at 2.43 GHz to tune it properly with transmitting antenna designed in Chapter 9. Fig. 10.1 illustrates the geometry of the receiving antenna which is tuned at 2.45 GHz ISM Band. Here, copper is utilized as the material for ground and radiator part - whereas, Arlon AD 430 is used as the material for substrate of the antenna.

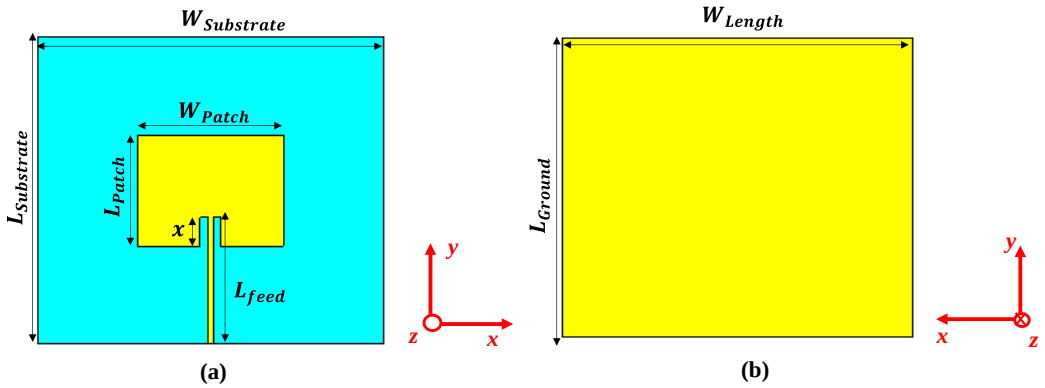

Fig. 10.1: (a) Top view, (b) bottom view of simulated receiving antenna

The values of relative permittivity and loss tangent of Arlon AD 430 at 2.45 GHz band are 4.3 and 0.003 respectively. The thickness of Arlon AD 430 is 0.762 mm i.e., 30 mil whereas the thickness of copper plates of this antenna is 0.001 mm. The design parameters of the receiving antenna are enlisted in Table 10.1.

TABLE 10.1: Design parameters of receiving antenna

Antenna Dimension	Value (mm)	Antenna Dimension	Value (mm)
Length of substrate ($L_{substrate}$)	80	Width of substrate ($W_{substrate}$)	90
Length of ground (L_{Ground})	80	Width of ground (W_{Ground})	90
Length of patch (L_{Patch})	29	Width of patch (W_{Patch})	38
Length of feed (L_{feed})	33	x	7.5

The top view and bottom view of the fabricated receiving antenna are shown in Fig. 10.2. A standard 50 Ω SMA connecter is connected with the microstrip feed line.

(a) **(b)**

Fig. 10.2: (a) Top view, (b) bottom view of fabricated receiving antenna

The simulated and measured S_{11} vs frequency plots for this antenna are shown in Fig. 10.3. The simulated return loss value of this antenna is 30.02 dB at 2.46 GHz whereas the fabricated antenna shows a return loss value of 26.42 dB at 2.47 GHz. The receiving antenna provides 4.96 dB realized gain at 2.46 GHz. The normalized radiation patterns for E plane ($\varphi = 0^0$) and H plane ($\varphi = 90^0$) are shown in Fig. 10.4.1 and 10.4.2 respectively.

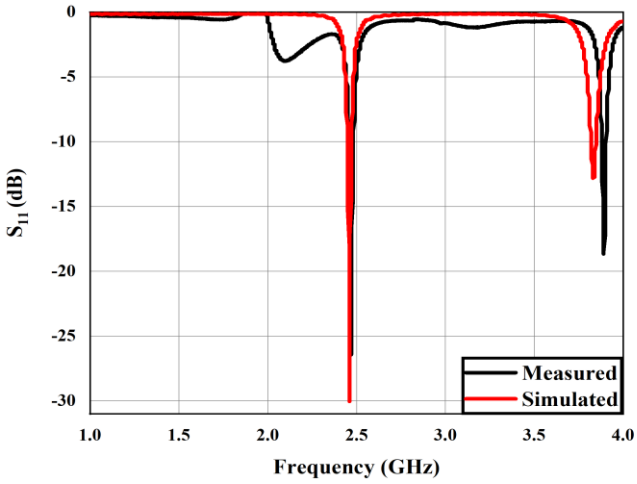

Fig. 10.3: S_{11} vs frequency for receiving antenna

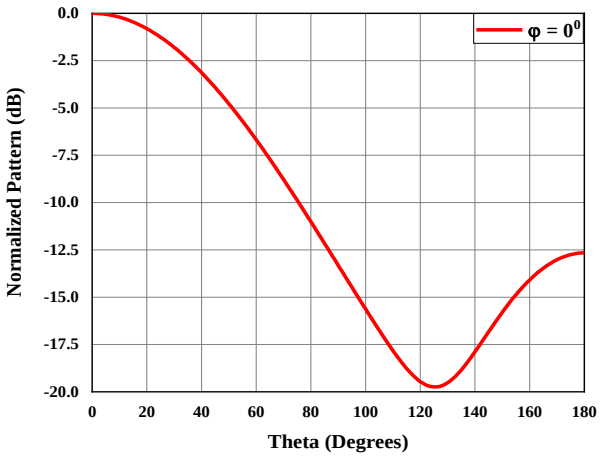

(a)

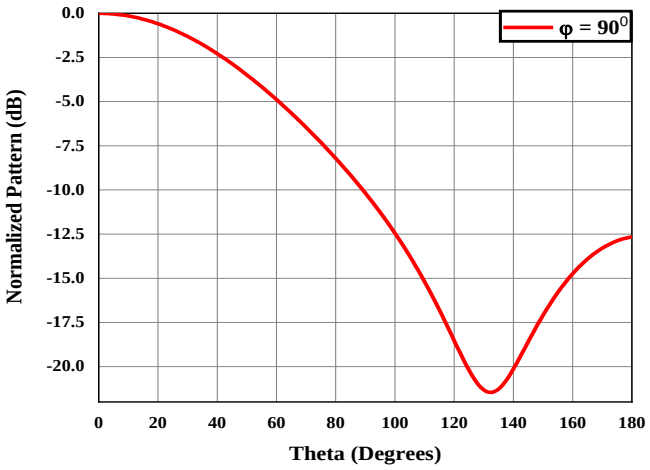

(b)

Fig. 10.4: Normalized pattern vs theta plots for (a) E plane (b) H plane for receiving antenna at 2.46 GHz

10.4 PERFORMANCE OF ANTENNA WITH FAT THICKNESS VARIATION

From literature survey on Madelung's disease, it was observed that Madelung's disease develops due to irregular fat metabolism and storage of fat in subcutaneous layer of skin (fat layer) at a high rate. It is very important to observe the performance of implantable antenna while the fat layer grows.

The meander-line based antenna designed in Chapter 9 is placed at muscle layer of the three-layer system (refer to Chapter 5) as shown in Fig. 10.5. The receiving antenna shown in Fig. 10.1 is placed at a distance of d = 30 mm from the top surface of the skin layer. Fat thickness in Fig. 10.5 is taken as 2 mm which is representing the fat thickness after performing operation. The S_{11} and S_{21} response of this system are shown in Fig. 10.6.

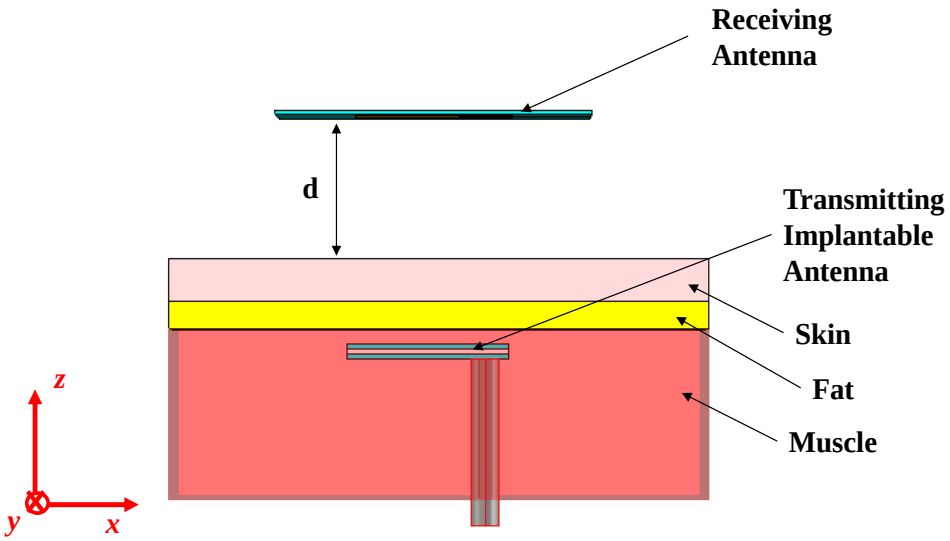

Fig. 10.5: Implantable antenna within 3-layer body model and receiving antenna placed at distance d = 30 mm

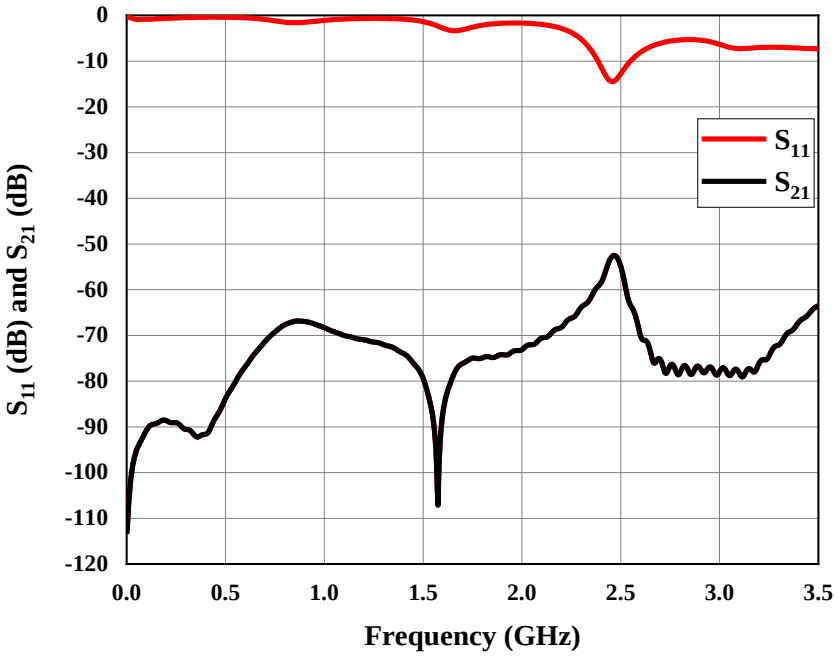

Fig. 10.6: S_{11} and S_{21} vs frequency of system shown in Fig. 10.5

From Fig. 10.6, the values of S_{11} and S_{21} are -14.51 dB and -52.69 dB at the resonant frequency of 2.457 GHz. In next step, we are going to investigate values of S_{11} and S_{21} at the same frequency for fat thickness values ranging from 2 mm to 25 mm with step size 1 mm and tabulated in Table 10.2. The S_{11} and S_{21} values obtained for fat variation are plotted against fat layer thickness in Fig. 10.7 and 10.8 respectively.

TABLE 10.2: S_{11} and S_{21} values for different fat thickness

Thickness of Fat (mm)	**S_{11} (dB)**	**S_{21} (dB)**
2	-14.51	-52.69
3	-14.09	-53.78
4	-13.78	-54.88
5	-13.58	-55.55
6	-13.45	-55.96
7	-13.38	-56.16
8	-13.36	-56.12
9	-13.38	-56.18
10	-13.42	-55.83
11	-13.52	-55.36
12	-13.61	-54.69
13	-13.71	-54.14

Thickness of Fat (mm)	S_{11} (dB)	S_{21} (dB)
14	-13.82	-53.17
15	-13.91	-52.51
16	-13.99	-51.94
17	-14.06	-51.57
18	-14.05	-51.76
19	-14.01	-51.9
20	-13.95	-52.25
21	-13.89	-52.72
22	-13.85	-53.22
23	-13.8	-53.69
24	-13.76	-54.12
25	-13.72	-54.46

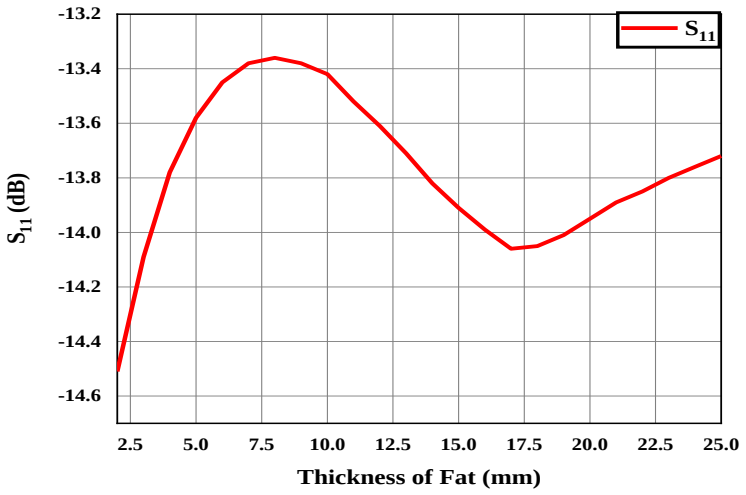

Fig. 10.7: S_{11} vs Thickness of fat plot

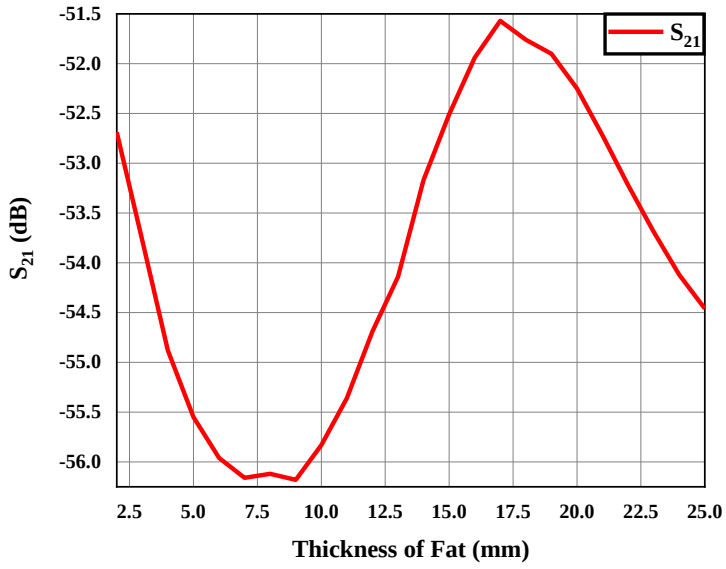

Fig. 10.8: S_{21} vs Thickness of fat plot

With the increment of fat layer thickness, more loss is added in the environment of the implantable antenna. Therefore, it is obvious that S_{21} values are reduced with the increment of fat layer thickness.

However, there is an increment of S_{21} value for the thickness values from 8 mm to 17 mm. For this range of thickness values, abnormal behaviour of S_{21} curve is observed due to internal reflection of electromagnetic waves between skin and muscle layers as their conductivities are very high. For this range contribution of this internal reflection is dominant over loss due to fat layer.

When the fat layer thickness is increased to more than 17 mm, the loss contributed by fat layer dominates over internal reflection between them due to large separation between skin and muscle layer. Therefore, after 17 mm fat layer thickness, the S_{21} value decreases with increment of fat thickness.

10.5 MADELUNG'S DISEASE DETECTION

As fat accumulation rate is high for Madelung's disease, the patient should check every day. Let us suppose, an implantable antenna is implanted at the red circled area of a patient as shown in Fig. 10.9. A receiving antenna is placed at the wall. A rod is connected with wall in such a way that distance between skin and receiving antenna will be 30mm.

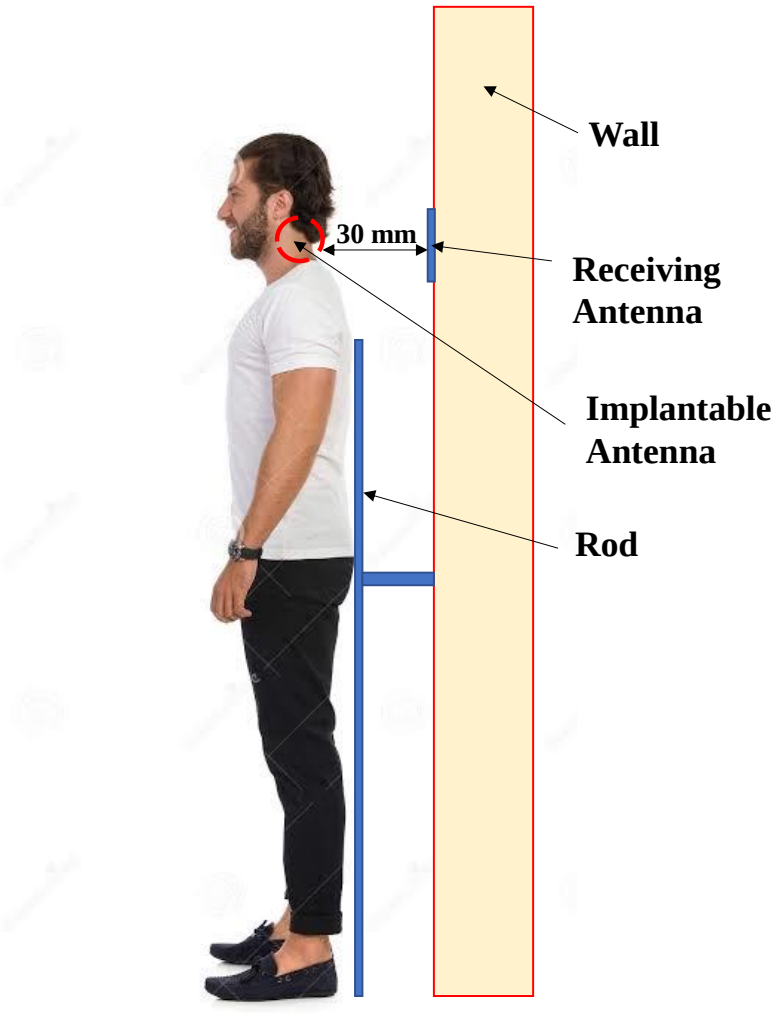

Fig. 10.9: Madelung's disease detection process

If the variation of S_{21} follows the nature of Fig. 10.8 and the change of S_{21} value changes in each day or couple of days without changing resonant frequency, it can be concluded that the patient is suffering from Madelung's disease.

However, another confusion may occurs about a lump in early stage whether it is due to fat deposition or due to development of any tumour in skin as shown in Fig. 10.10.

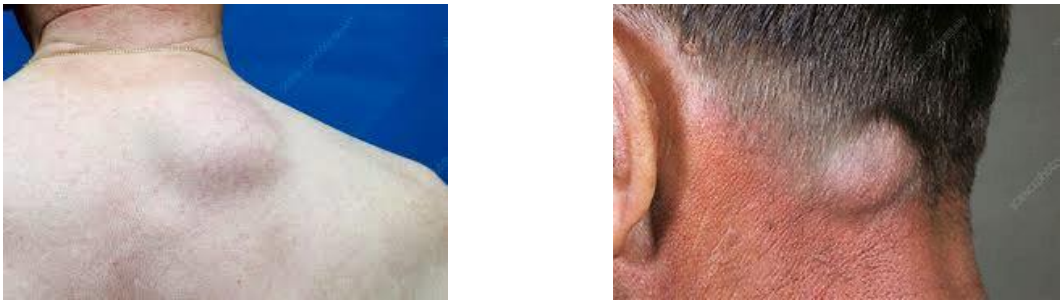

(a) **(b)**

Fig. 10.10: (a) Early stage of Madelung's disease, (b) tumour

From different literature, it is observed that permittivity and conductivity for a skin tumour is higher than skin. The resonant frequency will be shifted and maximum power will be received in a frequency other than 2.45 GHz due to tumour development.

Therefore, lump due to tumour and lump due to early stage of Madelung's disease can be distinguished by observing the change in frequency at which maximum power is received. The stage of Madelung's disease can be identified by observing S_{21} or received power level. In this way, Madelung's disease can be detected by using implantable antenna.

10.6 CONCLUSION

In this chapter, a meander-line based antenna is implanted at muscle layer of 3-layer human body model as implantable antenna is operating at 2.45 GHz ISM band. A receiving antenna is designed at 2.45 GHz in tune with the implanted antenna. This receiving antenna is placed at a wall to monitor the fat layer thickness variation due to Madelung's disease. By observing S_{21} or received power level at the receiver end, the stage of the Madelung's disease can be detected.

Chapter 11

Conclusion and Future Scope

Contents	
	11.1 Overall summary of the thesis 11.2 Principal contribution 11.3 Future scope

11.1 OVERALL SUMMARY OF THE THESIS

The aim of this thesis is to present Madelung's disease detection using implantable antenna. Implantable antenna is an antenna which can be located inside the human body by surgery to perform in-vivo communication. Design of implantable antennas is a challenging task due to implanting it inside highly lossy human torso. Study of the implantable antennas have been performed for different therapeutical applications like pacemakers, deep brain stimulators, cardioverter defibrillators, internal temperature sensors, implantable hormone therapy pumps, functional electrical stimulators etc. However, there is a considerable knowledge gap in studying performance of implantable antenna in subcutaneous fat layer related disease.

Keeping this thing in mind, we performed this work to analyse changes in radiation characteristics of an implanted antenna with the change in its environment due to accumulation in the fat layer due to Madelung's disease.

MICS (Medical Implant Communication System) band and 2.45 GHz ISM (Industrial, Scientific and Medical) bands have been mostly used to design implantable antennas. WMTS (Wireless Medical Telemetry Service) and MedRadio (Medical Device Radiocommunication Service) bands are also focussed for the same purposes. In Chapter 3, the reason of choosing 2.45 GHz ISM band for designing of implantable antenna for this work is discussed.

Chapters 4 and 5 are presenting the behaviour of electromagnetic waves propagating through different lossy human body layers (skin, fat and muscle). The values of different properties (such as permittivity, permeability, conductivity, attenuation constant, phase constant, intrinsic impedance) for each body layer are also estimated at our desired frequency. Based of electric field expressions, transfer matrices for skin, fat and muscle layers are calculated in Chapter 5.

There are two possible ways for implanting an antenna within human body. Antenna can be implanted either in skin layer or in muscle layer. Sometimes antenna is implanted in subcutaneous fat layer to measure glucose level in blood. Implant in muscle layer is quite challenging for building up communication with external devices as it is surrounded by high lossy environment resulting in wave propagation through three lossy layers.

In case of implantation in skin layer, the system can provide more efficient communication channel than the first case. Therefore, for testing purpose of antenna performance within human body, antenna engineers show interest to implant within skin layer. Chapter 6 represents a skin implantable antenna design at 2.45 GHz ISM band in CST Microwave Studio 2017. Its radiation and matching performances with a cubical shaped skin phantom model are also investigated. Novelty of this design is observed by comparing its performances with some existing skin implantable antennas.

In this work, our objective is to implant antenna within human muscle layer. As discussed in previous chapters, development of multi-layered phantom liquid design is a very challenging task also. If multi-layered body model is estimated by a homogeneous single layered phantom model, it will be very easy for in-vitro testing of the designed antenna. In Chapter 7, an equivalent homogeneous body model is designed by using FCC guidelines at 2.45 GHz. A meander-line slotted antenna and a meander-line based antenna are designed to operate in that body equivalent model in Chapter 8 and 9 and their performances are studied by simulating them in CST as well as by fabricating and measuring.

The meander-line antenna is utilised for detecting Madelung's disease in Chapter 10. A receiver is also designed in this chapter for observing received power level as well as resonant frequency. Based on these values, prediction of the growth stages of Madelung's disease is presented in Chapter 10.

11.2 PRINCIPAL CONTRIBUTION

- Development of miniaturized antenna using meander-lining technique having better radiation properties inside contiguous tissue model than reported implantable antennas.
- Analysis and observation of performance of implantable antenna with the variation of subcutaneous fat layer.
- Detection of Madelung's disease using implantable antenna and receiver at 2.45 GHz ISM band.
- Development of implantable antenna having higher gain compared to other reported antennas in spite of placing inside human skin and body equivalent phantoms to establish a proper communication link.

11.3 FUTURE SCOPE

Several different open and potential areas have come up during the course of this work. These are outlined below:

- In this work, we are basically focused on development of lump due to Madelung's disease at the broadside direction of the implanted antenna. If the lump is not developed at the broadside direction of it, how the performances of antenna will change and how this disease will be detected by using implantable antenna are not studied in this work.

- There are other diseases related to fat deposition in subcutaneous layer other than Madelung's disease. Those diseases are not studied here.

Appendix

Electromagnetic behaviour within Human body

Contents

A.1 INTRODUCTION

The behaviour of static and time-varying electric field and magnetic field are governed by Maxwell - Heaviside or colloquially Maxwell's equations. James Clerk Maxwell simply summarized the mathematical equations for electric and magnetic field formulated by Faraday, Ampere, Gauss and others and established as a self-consistent set through removing the inconsistencies. In this chapter, application of the Maxwell's equations in bioelectromagnetics has been discussed. Along with it, behaviour of the electromagnetic waves for different size of objects has been explained.

A.2 MAXWELL'S EQUATIONS

A.2.1 *Equations of electric field:*

The fundamental sources of electric fields are electric charges at rest. Maxwell's equations are able to describe the process of generation of electric fields from static electric charges. According to Maxwell's equations, there are two sources of electric fields. One of them is time varying magnetic field ($\vec{B}$) and other is charge density (ρ).

According to Faraday's law,

$$\vec{\nabla} \times \vec{E} = -\frac{\partial \vec{B}}{\partial t} \qquad (A.2.1)$$

Equation A.2.1 states that the time derivative of a time varying magnetic displacement through any surface bounded by a path can generate a time varying electromotive force that curls around the path [1].

Gauss's law states that the total electric flux coming out from a closed surface bounded by a volume is equal to the total charge enclosed by that volume. That means, charge density (ρ_v) can induce electric field. Mathematical expression of Gauss's law can be written as,

$$\vec{\nabla} \cdot \vec{D} = \rho_v \qquad (A.2.2)$$

where, $\vec{D}$ is electric displacement density. Equation A.2.1, A.2.2 are belonging to the set of Maxwell's equations.

A.2.2 *Equations of magnetic field:*

Electric charges in motion can produce magnetic field. According to Ampere's law, the magnetomotive force ($\vec{H}$) around a closed loop is equal to the

sum of conduction current density ($\vec{J}$) and time derivative of electric displacement density ($\vec{D}$).

$$\vec{\nabla} \times \vec{H} = \vec{J} + \frac{\partial \vec{D}}{\partial t} \qquad (A.2.3)$$

Gauss' law of magnetism states that the net magnetic flux ($\vec{B}$) emerging through any closed surface is zero. Therefore,

$$\vec{\nabla} \cdot \vec{B} = 0 \qquad (A.2.4)$$

Equation A.2.3 and A.2.4 are also considered as Maxwell's equations.

A.2.3 *Constitutive relations:*

There are three constitutive relations that concern the characteristics of any medium. The relations are,

$$\vec{D} = \epsilon \vec{E} \qquad (A.2.5)$$

$$\vec{B} = \mu \vec{H} \qquad (A.2.6)$$

$$\vec{J} = \sigma \vec{E} \qquad (A.2.7)$$

where ϵ, μ and σ are the permittivity, permeability and conductivity of the medium in which the fields exist. Therefore, equations A.2.1, A.2.2, A.2.3 and A.2.4 can be rewritten using the constitutive equations as,

$$\vec{\nabla} \times \vec{E} = -\mu \frac{\partial \vec{H}}{\partial t} \qquad (A.2.8)$$

$$\vec{\nabla} \cdot \vec{E} = \frac{\rho_v}{\epsilon} \qquad (A.2.9)$$

$$\vec{\nabla} \times \vec{H} = \sigma\vec{E} + \epsilon\frac{\partial\vec{E}}{\partial t} \qquad (A.2.10)$$

$$\vec{\nabla} \cdot \vec{H} = 0 \qquad (A.2.11)$$

A.2.4 *Phasor form:*

A time varying electric field may be expressed in terms of phasor as,

$$\tilde{\vec{E}}(\vec{r},t) = Re\{\vec{E}(\vec{r},t)e^{j\omega t}\}$$

In the same way, magnetic field ($\tilde{\vec{H}}$) can also be considered as,

$$\tilde{\vec{H}}(\vec{r},t) = Re\{\vec{H}(\vec{r},t)e^{j\omega t}\}$$

Therefore, equation A.2.10 can be written as,

$$\vec{\nabla} \times \tilde{\vec{H}}(\vec{r},t) = \sigma\tilde{\vec{E}}(\vec{r},t) + \epsilon\frac{\partial\tilde{\vec{E}}(\vec{r},t)}{\partial t}$$

$$\vec{\nabla} \times Re\{\vec{H}(\vec{r},t)e^{j\omega t}\} = \sigma Re\{\vec{E}(\vec{r},t)e^{j\omega t}\} + \epsilon\frac{\partial Re\{\vec{E}(\vec{r},t)e^{j\omega t}\}}{\partial t}$$

$$Re\left\{\left(\vec{\nabla} \times \vec{H} - \sigma\vec{E} - j\omega\epsilon\vec{E}\right)e^{j\omega t}\right\} = 0$$

$$\vec{\nabla} \times \vec{H} = \sigma\vec{E} + j\omega\epsilon\vec{E}$$

From equation A.2.12, it is clear that phasor form of Maxwell's equations for time varying fields can be obtained by replacing time derivatives of equations A.2.8, A.2.9, A.2.10 and A.2.11 with the term $j\omega$ [1]. Therefore, the phasor form of Maxwell's equations will be,

$$\vec{\nabla} \times \vec{E} = -j\omega\mu\vec{H} \qquad (A.2.13)$$

$$\vec{\nabla} \cdot \vec{E} = \frac{\rho_v}{\epsilon} \qquad (A.2.14)$$

$$\vec{\nabla} \times \vec{H} = \sigma\vec{E} + j\omega\epsilon\vec{E} \qquad (A.2.15)$$

$$\vec{\nabla} \cdot \vec{H} = 0 \qquad (A.2.16)$$

A.3 ELECTRIC AND MAGNETIC FIELD INTERACTIONS WITH MATERIALS

One of the important aspects of bioelectromagnetism is how electric and magnetic fields interact with human body and how human body affects those fields. Electric and magnetic fields apply forces on the charges of the materials. The *applied fields* are produced by external sources of the material. The *internal fields* of the human body are the combination of fields produced by both internal and external sources of the body [2].

The electrical dipole can be considered as two positive and negative charges having same magnitude (Q) and separated by a finite distance (r) as shown in Fig. A.3.1.

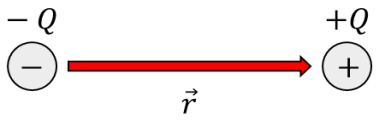

Fig. A.3.1. Dipole Moment [3]

Let $\vec{r}$ be a vector from the negative to positive charge. The dipole moment can be written as,

$$\vec{p} = Q\vec{r} \qquad (A.3.1)$$

As the region contains same amount of positive and negative charge, the net charge is zero for this region. The center of the negative charge of electrons and center of positive nucleus are coincident with each other within an atom. Therefore, the net charge of an atom is zero and no dipole moment is present within it [2,3].

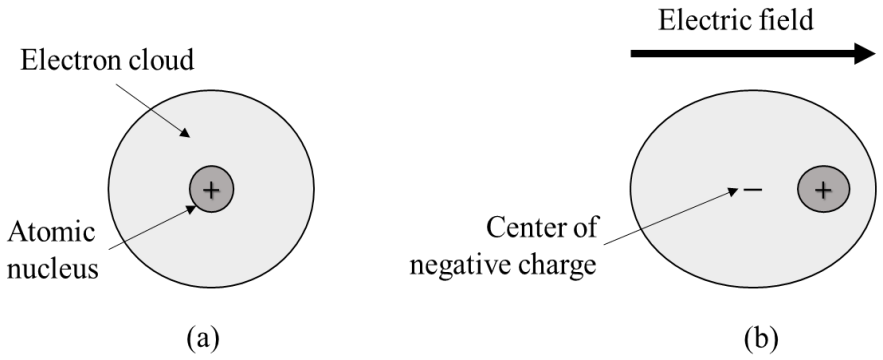

Fig. A.3.2. (a) An atom in equilibrium (no electric field) [3]
(b) Dipole moment in electric field [3]

Due to presence of external electric field, a dipole moment will develop. The electrons are lighter than nucleus. So, the electrons become easily displaced and center of negative charges will shift from its equilibrium position as shown in Fig. A.3.2. This separation of negative and positive charge center and resulting dipole moment are termed as *polarization* [3].

The relation between induced polarization and applied electric field can be written as,

$$\vec{p} = \alpha\, \vec{E} \qquad (A.3.2)$$

where, α is a coefficient called *polarizability* [3].

In hydrogen-based biological materials, electric dipoles already exist in spite of absence of electric field. These dipoles are randomly oriented to maintain net field they produce as zero. When an external electric field is applied on that kind of materials, the permanent dipoles partially align with the applied electric field as shown in Fig. A.3.3.

The permanent dipole will rotate slightly as the applied electric field exerts an electric force on positive and negative charges of the dipole in opposite directions to each other. Therefore, the dipole aligns partially with the external electric field as shown in Fig. A.3.3. As the charges are repositioned effectively inside the material by either induced polarization or alignment of permanent dipole due to rate of change of effective electric field, a *displacement current* will generate.

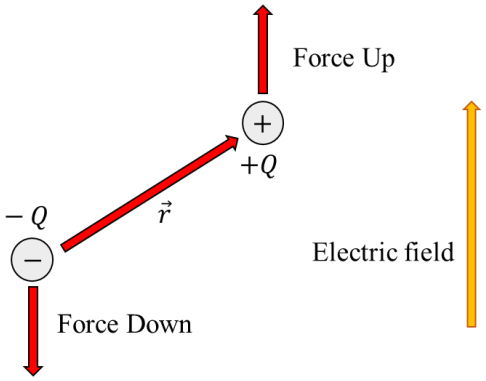

Fig. A.3.3. Partial alignment of a permanent dipole due to applied field [2]

Some charges such as electrons and ions present in human body, are in free state as they are loosely bound and are able to move between molecules in response to an electric field. These free charges can move a short distance and collide with other particles. Therefore, an average velocity will generate at the direction of applied electric field. The movement of free charges will develop *conduction current*. Tissues with high water content have more free charges than insulating

body materials such as bone and fat. This conduction currents also cause heating and power loss in a material. Besides electric field, magnetic field also can cause partial alignment of magnetic dipoles in materials. But this is not analogous to separation of electric charge as discussed above. The alignment of magnetic dipole is very important in magnetic resonance imaging (MRI) purposes.

As the interactions of electric and magnetic fields are very complex to keep track of in terms of individual charges, three parameters have been defined to account for interaction of the fields on a macroscopic scale – *permittivity* or *dielectric constant*, *conductivity* and *permeability*. With the application of electric field, amount of induced polarization and partial alignment of permanent electric dipole occur can be characterized by *permittivity* (ϵ) of the material. The amount of conduction current generated within material can be characterized by its conductivity (σ). With the application of magnetic field, amount of partial alignment of permanent magnetic dipole occur can be characterized by permeability (μ) of the material. The units of permittivity, conductivity and permeability are F/m, S/m and H/m respectively. For general cases, the human body is very weakly magnetic. Therefore, the relative permeability of human tissue is taken as μ_r = 1 [2].

A.4 CONCEPTS OF DIELECTRIC LOSS AND LOSS TANGENT

A.4.1 *Complex permittivity:*

The static dielectric constant is an effect of electrical polarization under the dc conditions. However, when a sinusoidal electric field is applied, the polarization of the material leads to an ac dielectric constant. The sinusoidally varying electric field tries to line up the permanent dipoles one way and then the opposite way with

its variation of magnitude and direction simultaneously. So, at any instant the induced dipole moment per molecule due to field variation can be expressed as,

$$\vec{p} = \alpha_d \vec{E} \qquad (A.4.1)$$

The polarizability α_d has its maximum value for dc conditions. If applied field varies rapidly, the dipoles cannot follow the variation and remain randomly oriented. Therefore, α_d will be zero at high frequencies as the field cannot induce a dipole moment. At low frequencies the dipole can follow the field variations and α_d can reach its maximum value.

Suppose an electric field shown in Fig. A.4.1 is applied on a dipole. The electric field has a sharp decay from its dc value E_o to E ($< E_o$) at t = 0. The dc dipole moment per molecule should be smaller and value of dipole moment at that condition is $\alpha_d(0)E$, where $\alpha_d(0)$ is polarizability at ω = 0, i.e., dc condition. So, the induced dipole moment per molecule decreases from $\alpha_d(0)E_o$ to $\alpha_d(0)E$.

The decrement or the relaxation process occurs by random collisions with each other. The average time between two collisions is called *relaxation time* and generally it is represented by τ.

If p is an instantaneous induced dipole moment, the excess dipole moment from Fig. A.4.1 will be $p - \alpha_d(0)E$. The rate of change of excess dipole moment can be expressed as [3],

$$\frac{dp}{dt} = -\frac{p - \alpha_d(0)E}{\tau} \qquad (A.4.2)$$

In place of dc electric field, let us consider that a complex exponential ac electric field having representation $E(t) = E_o e^{j\omega t}$ is applied.

Therefore equation A.4.2 can be written as,

$$\frac{dp}{dt} = -\frac{p - \alpha_d(0)E_o\, e^{j\omega t}}{\tau} \qquad (A.4.3)$$

After solving this equation, the induced dipole moment will get as [3],

$$p = \alpha_d(\omega)\; E_o\, e^{j\omega t}$$

where, $\alpha_d(\omega) = \frac{\alpha_d(0)}{1+j\omega\tau}$ = orientational polarizability under ac field.

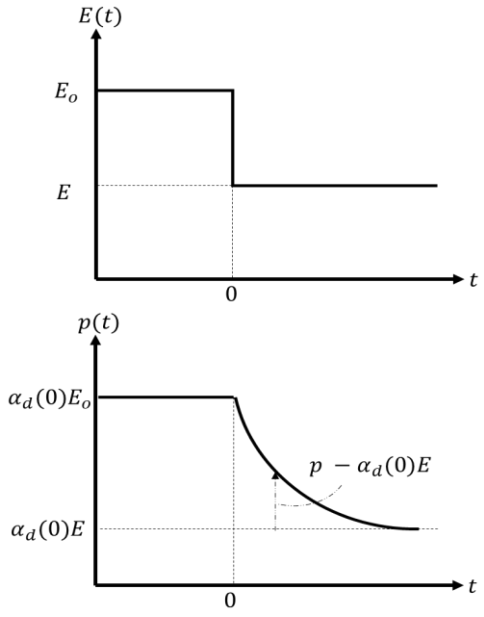

Fig. A.4.1. Dipole moment variation (bottom) with the application of external electric field (top) [3]

If N is representing the number of molecules per unit volume of the material, in terms of electronic polarization, the relation between relative permittivity (ϵ_r) and polarizability α_d will be,

$$\epsilon_r = 1 + \frac{N\,\alpha_d}{\epsilon_o}$$

The complex nature of $\alpha_d(\omega)$ leads to a complex number for ϵ_r. This is the concept of *complex permittivity* which can be represented as,

$$\epsilon_r = \epsilon_r' - j\epsilon_r'' \qquad (A.4.4)$$

where, ϵ_r' and ϵ_r'' are frequency dependent real and imaginary parts of the complex dielectric constant ϵ_r. The real part decreases from maximum value $\epsilon_r'(0)$ to 1 corresponding to low frequency to high frequency whereas imaginary part will be zero for both low and high frequencies and maximum when $\omega\tau = 1$. The plot of complex permittivity verses frequency is shown in Fig. A.4.2. The real part of permittivity ϵ_r' represents relative permittivity to calculate the capacitance value by using formula $C = \epsilon_o \epsilon_r' \frac{A}{d}$. The imaginary part ϵ_r'' represents energy loss in dielectric material [3].

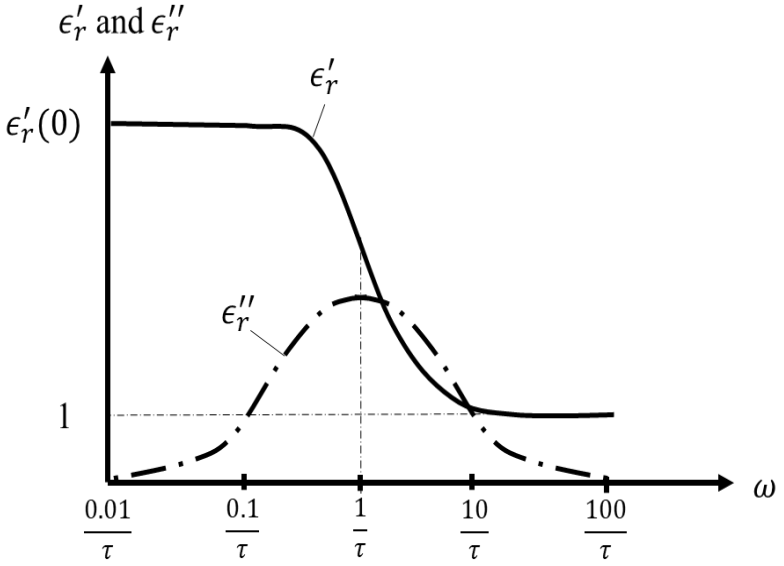

Fig. A.4.2. Plot of complex permittivity with frequency

A.4.2 *Loss tangent:*

Let us consider a sinusoidal voltage $v(t) = V_o \sin \omega t$ across a capacitor having complex dielectric material within two plates as shown in Fig. A.4.3.

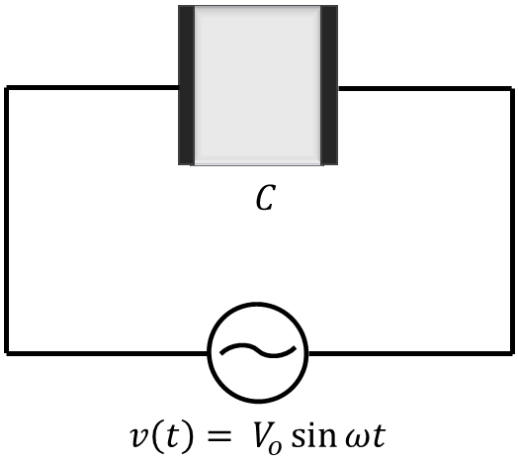

Fig. A.4.3. Capacitor having complex dielectric material between two plates

The admittance Y of capacitor with dielectric ϵ_r written as,

$$Y = \frac{j\omega A\epsilon_o \epsilon_r(\omega)}{d} = \frac{j\omega A\epsilon_o \epsilon_r{}'(\omega)}{d} + \frac{\omega A\epsilon_o \epsilon_r{}''(\omega)}{d}$$

which can be written as,

$$Y = j\omega C + G \qquad (A.4.5)$$

where, C = capacitance and G = conductance of capacitor

$$C = \frac{A\epsilon_o \epsilon_r{}'}{d}$$

$$G = \frac{\omega A \epsilon_o \epsilon_r''}{d}$$

According to equation A.4.5, the nature of admittance is identical to parallel combination of ideal or lossless capacitor having relative permittivity ϵ_r' and a resistor having resistance value $\frac{1}{G}$. The power dissipation occurs due to equivalent resistance of the dielectric material.

The input power using equation A.4.5 can be written as,

$$P_{in} = YV^2 = j\omega CV^2 + V^2 G$$

As the second term of input power is real, power dissipation in dielectric material has occurred due to the ϵ_r''. From Fig. A.4.2, the maximum power dissipation will happen when $\omega = \frac{1}{\tau}$. This phenomenon is called *dielectric resonance* [3].

Ideally the value of ϵ_r'' should be very less compared to ϵ_r'. The ratio of ϵ_r'' to ϵ_r' is termed as *loss tangent* or *loss factor* and denoted by $\tan\delta$ as,

$$\tan\delta = \frac{\epsilon_r''}{\epsilon_r'}$$

A.4.3 *Power dissipation in dielectric material:*

The power dissipated due to resistance can be written as,

$$P_{dissipated} = \frac{Power\ Loss}{Volume}$$

$$P_{dissipated} = \frac{V^2 G}{d\ A} = \frac{V^2}{d^2}\omega\epsilon_o\epsilon_r'' = \frac{V^2}{d^2}\omega\epsilon_o\epsilon_r' \tan\delta$$

From above expression of power dissipation, it is clear that the dielectric loss is influenced by frequency (ω), electric field (As electric field = $\frac{V}{d}$) through the material and loss tangent value ($\tan\delta$). Different tissues have different water, salt and oil contents as well as the cells have different shapes for example, bone cells are long, nerve cells are spindly etc. Both of these factors control electrical properties of the tissues. The human tissues are non-magnetic in nature. So, the relative permeability μ_r can be taken as 1 for all tissues. Blood is very weakly magnetic. Its relative permeability is very small as to be neglected. Using Gabriel's dispersion relationship [4-5], the relative permittivity and conductivity (S/m) values of different tissues for three different widely used medical bands (such as 402-405 MHz MICS, 1.4 GHz WMTS and 2.45 GHz ISM bands) are shown in Table A.4.1 [5-9]. Except the values given in Table A.4.1, there are several data available for other human body tissues. As those specific tissues will be used to keep on this work, those particular values are tabulated here.

Table A.4.1. Electrical properties of human tissues at different frequencies

Tissue	**403 MHz**		**1.4 GHz**		**2.45 GHz**	
	$\boldsymbol{\epsilon_r}$	$\boldsymbol{\sigma\ (S/m)}$	$\boldsymbol{\epsilon_r}$	$\boldsymbol{\sigma\ (S/m)}$	$\boldsymbol{\epsilon_r}$	$\boldsymbol{\sigma\ (S/m)}$
Skin	46.7	0.689	39.7	1.04	38	1.46
Fat	11.6	0.081	11.2	0.150	10.8	0.268
Muscle	57.1	0.797	54.1	1.14	52.7	1.74
Blood	64.1	1.35	60.1	1.79	58.3	2.54
Bone	13.1	0.182	12.1	0.211	11.4	0.394

A.5 MAXWELL'S EQUATIONS FOR DIFFERENT MEDIA

A.5.1 *Lossless medium:*

A medium having zero conductivity along with finite permittivity and permeability can be considered as lossless medium. Therefore, no attenuation of electric and magnetic fields is observed when electromagnetic waves propagate through lossless medium. Due to having zero conductivity (i.e., $\sigma = 0$), loss tangent of this medium is zero. So, lossless medium does not have complex permittivity ($\epsilon_r'' = 0, \epsilon_r = \epsilon_r'$). The medium is considered as *homogeneous* and *isotropic* in nature. Then, the Maxwell's equations for lossless medium will be,

$$\vec{\nabla} \times \vec{E} = -j\omega\mu_o\mu_r\vec{H} \qquad (A.5.1)$$

$$\vec{\nabla} \cdot \vec{E} = \frac{\rho_v}{\epsilon_o\epsilon_r} \qquad (A.5.2)$$

$$\vec{\nabla} \times \vec{H} = j\omega\epsilon_o\epsilon_r\vec{E} \qquad (A.5.3)$$

$$\vec{\nabla} \cdot \vec{H} = 0 \qquad (A.5.4)$$

A.5.2 *Free space:*

Free space is a perfect dielectric medium containing no conducting charges in it. That means, the conduction current ($\vec{J}$) will be zero for free space. The relative permittivity (ϵ_r) and permeability (μ_r) for this medium are 1. The Maxwell's equations for free space are,

$$\vec{\nabla} \times \vec{E} = -j\omega\mu_o\vec{H} \qquad (A.5.5)$$

$$\vec{\nabla} \cdot \vec{E} = \frac{\rho_v}{\epsilon_o} \qquad (A.5.6)$$

$$\vec{\nabla} \times \vec{H} = j\omega\epsilon_o \vec{E} \qquad (A.5.7)$$

$$\vec{\nabla} \cdot \vec{H} = 0 \qquad (A.5.8)$$

A.5.3 *Conducting medium:*

A medium having finite conductivity is called conducting medium. Let us consider, a homogeneous conducting medium having conductivity, permittivity and permeability of σ, ϵ_o and μ_o respectively. Maxwell's equations for this medium can be written as,

$$\vec{\nabla} \times \vec{E} = -j\omega\mu_o \vec{H} \qquad (A.5.9)$$

$$\vec{\nabla} \cdot \vec{E} = \frac{\rho_v}{\epsilon_o} \qquad (A.5.10)$$

$$\vec{\nabla} \times \vec{H} = \sigma\vec{E} + j\omega\epsilon_o \vec{E} \qquad (A.5.11)$$

$$\vec{\nabla} \cdot \vec{H} = 0 \qquad (A.5.12)$$

A.5.4 *Human tissue:*

Different tissues of human body have different conductivities as well as relative permittivity values as discuss in Section A.4.3. Therefore, a human body can be assumed as inhomogeneous medium. Let, conductivity of a volume conductor be considered as $\sigma(x, y, z)$. There are endogenous voltages and currents inside the body. Therefore, electric and magnetic fields exist within tissues. It is seen in ECG of heart, EMG of brain etc. Nerve impulses and muscle actions are electrical in nature.

The membranes can influence the electrical properties of an excitable cell by regulating ions from inner and outer portions of cells. A cell membrane consists of two types of charges. The outside of the membrane is positively charged and inner part of it, i.e., cytoplasm, is negatively charged. The cytoplasm is K^+ rich area whereas amount of Na^+ is comparatively high in outer region. When a cell is activated by some stimulus, Na^+ ions come inside and K^+ ions go to outside of the cell. For this reason, each active cell has conductivity. As some current is flowing through tissues, it is obvious to have nonconservative sources within tissues. It can easily be considered that electromotive forces (*emf*) present inside any active tissues [10]. Therefore, equation A.5.9 can be modified as,

$$\vec{\nabla} \times \vec{E} = -j\omega\mu\vec{H} + emf \qquad (A.5.13)$$

The presence of impressed current density ($\vec{J^i}$) within human tissues has been discussed. There is no charge density associated with impressed current due to having solenoidal nature. So, by adding $\vec{J^i}$ in equation A.5.11, we get [10],

$$\vec{\nabla} \times \vec{H} = (\sigma + j\omega\epsilon)\vec{E} + \vec{J^i} \qquad (A.5.14)$$

The volume charge density (ρ_v) cannot exist in conducting medium. Therefore, the expression of divergence of electric field (i.e., $\vec{\nabla} \cdot \vec{E}$) should be modified. Taking divergence in both sides of equation A.5.14 we get,

$$\vec{\nabla} \cdot (\vec{\nabla} \times \vec{H}) = (\sigma + j\omega\epsilon)\,(\vec{\nabla} \cdot \vec{E}) + (\,\vec{\nabla} \cdot \vec{J^i}\,)$$

As divergence of curl of a vector is zero, $\vec{\nabla} \cdot \left(\vec{\nabla} \times \vec{H}\right) = 0$.

$$(\sigma + j\omega\epsilon)\left(\vec{\nabla} \cdot \vec{E}\right) + \left(\vec{\nabla} \cdot \vec{J^i}\right) = 0$$

$$\left(\vec{\nabla} \cdot \vec{E}\right) = \frac{-\left(\vec{\nabla} \cdot \vec{J^i}\right)}{(\sigma + j\omega\epsilon)} \qquad (A.5.15)$$

A.6 WAVE PROPERTIES IN DIFFERENT MATERIALS

A.6.1 *Lossless materials:*

As discussed earlier, the conductivity of a lossless material is zero and no power loss of electromagnetic waves will happen due to zero loss tangent. These materials are also referred as *perfect dielectric* materials. They contain no free charges. Therefore, lossless materials make good insulators.

Let us consider a sinusoidal wave propagating in z direction with a phase velocity v_P and angular frequency ω ($= 2\pi f = \frac{2\pi}{T}$, where f and T are linear frequency and time period of the propagating wave).

The wavelength λ can be defined as the distance between two peaks of the wave and phase velocity v_P refers how fast the wave is propagating. If β (rad/m) is propagation constant of the wave, it can be written as,

$$\beta = \frac{\omega}{v_P} = \frac{2\pi}{\lambda}$$

where phase velocity v_P can be defined as,

$$v_P = \lambda f$$

A.6.2 *Lossy materials:*

Biological tissues are high lossy; The tissue with high water content, such as muscle, is more lossy than tissue with less water content, such as bone and fat. When electromagnetic waves interact with biological materials, the waves will be attenuated and some amount of power loss will be happened due to this absorbing nature of tissues and the material will heat up.

Propagating through a lossy medium, magnitude of the wave decreases exponentially which is expressed by,

$$E(z,t) = E_0 e^{-\alpha z} \sin(\omega t - \beta z - \phi)$$

This above expression is for electric field. The attenuation constant (α) represents how much the propagating wave attenuates. E_0 is the amplitude of electric field at the surface of the lossy material.

The attenuation constant can be expressed as,

$$\alpha = \omega \sqrt{\frac{\mu'\epsilon'}{2}\left[\sqrt{1+\left(\frac{\sigma_{eff}}{\omega\epsilon'}\right)^2}-1\right]} \qquad (A.6.1)$$

The propagation constant can be represented as,

$$\beta = \omega \sqrt{\frac{\mu'\epsilon'}{2}\left[\sqrt{1+\left(\frac{\sigma_{eff}}{\omega\epsilon'}\right)^2}+1\right]} \qquad (A.6.2)$$

The term β indicates amount of phase shift occurring due to propagation of fields through lossy material. An example has been taken here to understand the concepts discussed above.

Example: From Table A.4.1, the conductivity and relative permittivity of muscle are 1.74 S/m and 52.7 respectively at 2.45 GHz.

The angular frequency corresponding to 2.45 GHz is $\omega = 2\pi \times 2.45 \times 10^9 = 15.4 \times 10^9$ rad/sec. If $\frac{2}{3}$ muscle is used to represent human body, both relative permittivity and conductivity will be multiplied by $\frac{2}{3}$. So, the values of ϵ_r and σ for this muscle will be 35.13 and 1.16 S/m.

Using equations A.6.1 and A.6.2, we get $\alpha = 6.03$ Np/m and $\beta = 51.367$ rad/m. The phase velocity within this muscle will be $v_p = 2.99 \times 10^8$ m/s.

Let us consider that an electric field $E(z,t) = 2\sin(15.4 \times 10^9 t)$ is propagating through the above taken muscle. The field at z = 10 cm inside muscle will be $E_0 e^{-\alpha z} = 1.77$ V/m.

A.7 BOUNDARY CONDITION FOR DIFFERENT MATERIALS

A.7.1 *Lossless materials:*

Boundary conditions are the relationships between electromagnetic fields that should be satisfied at the interface between two media as required by Maxwell's equations.

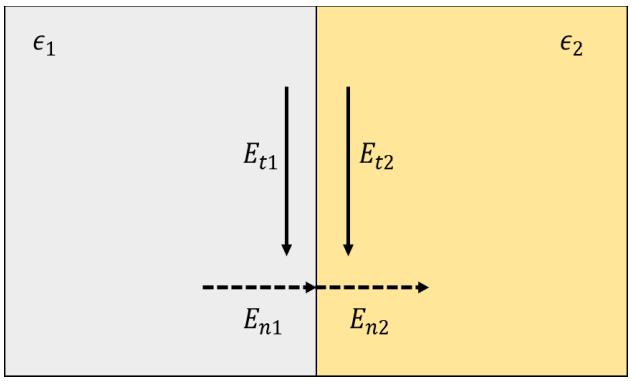

Fig. A.7.1. Conditions on electric fields at the interface of two media

As electric field is a vector, it can be decomposed into two components – tangential component parallel to boundary (E_t) and normal component perpendicular to the boundary (E_n).

Fig. A.7.1 shows electric field components at an interface between two dielectric media having relative permittivities ϵ_1 and ϵ_2. The boundary conditions for electric field components are that tangential components of electric fields in two media are continuous. If surface current density at the boundary is zero, then electric flux densities of two media will be equal. From Fig. A.7.1, it is written as,

(i) $E_{t1} = E_{t2}$ $(A.7.1)$

(ii) $\epsilon_1 E_{n1} = \epsilon_2 E_{n2}$ $(A.7.2)$

A.7.2 *Lossy materials:*

Biological materials are lossy in nature. The human tissue has complex permittivity as discussed in Section A.4. Therefore, equation A.7.1 and A.7.2should slightly be modified by replacing ϵ_1 and ϵ_2 with $\epsilon_{complex1}$ and $\epsilon_{complex2}$.

At the boundary, the equation A.7.1 and A.7.2 can be written as,

(i) $E_{t1} = E_{t2}$ $(A.7.3)$

(ii) $\epsilon_{complex1} E_{n1} = \epsilon_{complex2} E_{n2}$ $(A.7.4)$

A.8 ELECTROMAGNETIC BEHAVIOUR: FUNCTION OF SIZE AND WAVELENGTH

Maxwell's equations can be applied over broad frequency spectrum. The behaviour of EM system depends on size of the device compared to wavelength of the wave. Let, the wavelength of wave and maximum dimension of the device be λ and L respectively. Therefore, there are three possible categories: $\lambda \gg L$, $\lambda \approx L$ and $\lambda \ll L$.

A.8.1 *When wavelength is larger than size of device:*

The wavelength of 1 MHz in free space is 300 m. The wavelength of the wave having frequency below 1 MHz is comparatively larger than size of the people. Object having very small dimension with respect to wavelength is illustrated in Fig. A.8.1.

Lightning and other static charges are some natural electric and magnetic effects in low frequency range. The nervous system consists of some neurotransmitters and receptors. Electromyography (EMG), electrocardiogram (ECG), cardiac defibrillation or pacing etc. are some applications in low frequency range. In this range, mostly stimulation and reception of nerves and tissues are performed than imaging as low frequency fields cannot generate good image [2].

There are some approximations when the wavelength is large compared to material size. An important approximation for low frequency is circuit theory which consists of KCL, KVL and other related analysis and theorems. Circuit theory is nothing but an approximation of Maxwell's equations. Circuit theory deals with mainly voltage and current whereas electric and magnetic fields are principal

variables of electromagnetic theory. However, circuit theory is simpler than EM theory [2].

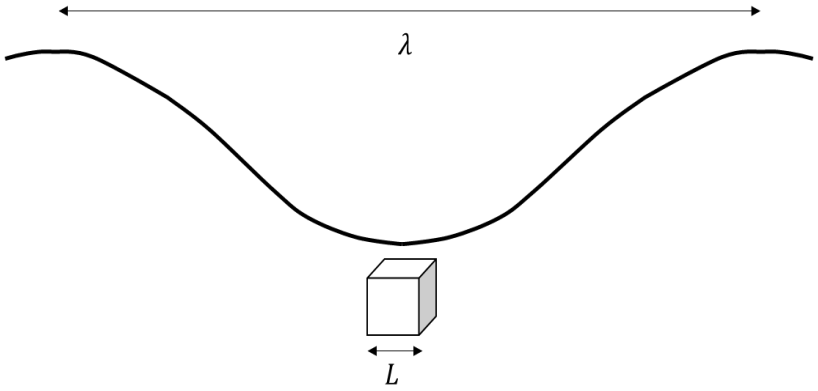

Fig. A.8.1. The wavelength is larger than the size of device

Other important low frequency approximation is *quasi-static EM field theory*. The spatial variations of $\vec{E}$ and $\vec{B}$ fields in this approximation are approximated as static. EM variations in static case is simpler than time varying condition. In quasi-static field theory, $\vec{E}$ and $\vec{B}$ fields can exist independently; they are said to be uncoupled. According to the Maxwell's equations, electric field $\vec{E}$ can be generated due to either a time varying magnetic fields or a distribution of charges or both. In static case, $\frac{\partial \vec{B}}{\partial t}$ is very small and neglected in comparison to the contribution of electric field due to charges. Therefore, a quasi-static electric field can be produced without influence of $\vec{B}$ field. In similar manner, $\vec{B}$ field can be produced independently without any influence of $\vec{E}$ field. Fig. A.8.2 shows the interaction of electric and magnetic fields separately with objects. The incident electric field (E_{inc}) and incident magnetic field (B_{inc}) are the fields produced by sources without the human body present. The internal electric field (E_{int}) and magnetic field (B_{int}) exist inside the body. The external scattered electric field (E_{sc})

and magnetic field (B_{sc}) are scattered from the body. The internal fields can be found by either E_{int} or B_{int} alone because electric and magnetic fields are uncoupled at low frequencies.

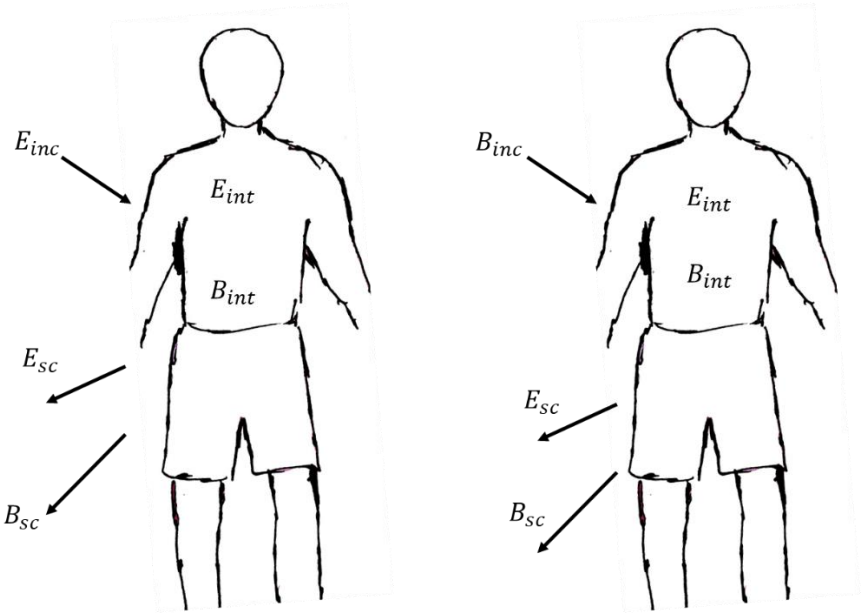

(a) (b)

Fig. A.8.2. The internal and scattered electric and magnetic fields due to (a) an incident electric field alone (b) an incident magnetic field alone

A.8.2 *When wavelength is comparable with size of device:*

When the dimension of device is of same order of wavelength, *electromagnetic theory* will be used. This case has been illustrated in Fig. A.8.3. Unique potential difference cannot be defined in this frequency range. Propagation effects have dominance in this range and electric and magnetic fields behave as propagating waves. These fields are strongly coupled – the presence of one of them generates other. Energy transmits through coaxial cables, waveguides and beamed through air. Maxwell's equations are used in this range [2].

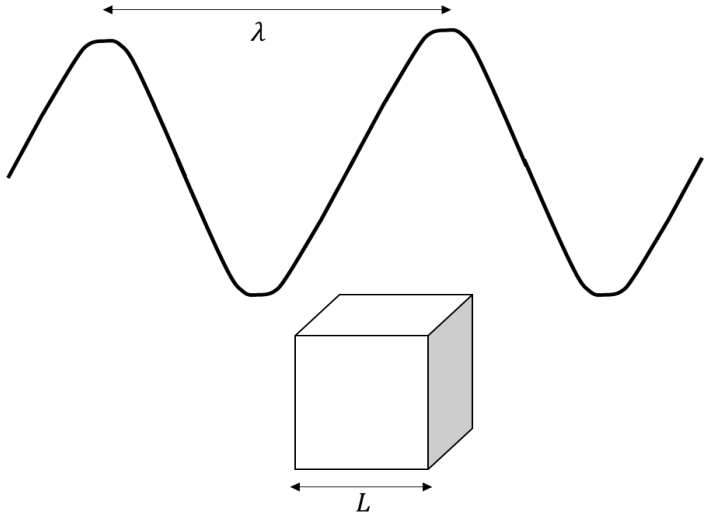

Fig. A.8.3. The wavelength is comparable with the size of device

The fields below this mid frequency region are treated as voltages and currents. The fields above this range are termed as rays. In this range, they act as waves. Resonance and oscillation effects are seen in this range. This band is used for communication, telemetry for implantable devices, external communication devices such as cellular telephone etc.

Resonance causes power absorption at specific frequencies. In high frequency regions attenuation plays dominant role for power absorption within human body whereas, resonance causes the human body to absorb large amounts of power within a small frequency band.

Electromagnetic absorption in human depends on some important parameters such as frequency, electrical properties of tissue, size and shape of the body etc. The resonant frequencies in human body and head are given in Table A.8.1 for undergrounded plane wave exposure conditions [2]. According to the table, it is clear that the absorption cross section is near about 3 times larger than human head which specifies that head can absorb about three times more power than the power predicted from physical cross section.

Table A.8.1. Resonance effects in human body and head [2]

Age	Body		Head	
	Resonant frequency (MHz)	**Absorption cross section/ Physical cross section**	**Resonant frequency (MHz)**	**Absorption cross section/ Physical cross section**
5 years	130	3.47	330	2.92
10 years	100	3.88	270	2.84
Adult	75	3.92	205	2.78

A.8.3 *When wavelength is smaller than size of device:*

When the dimension of device is of same order of wavelength, as shown in Fig. A.8.4, the electromagnetic fields can be described by *optical theory*, Propagation effects dominate in this consideration. Electric and magnetic fields are strongly coupled in this range. This high frequency range includes infrared, X -ray, visible light and ultraviolet light. The upper part of this frequency range is called *ionizing radiation range* and the range lies below ionizing range is called *non-ionizing radiation range*.

The tissues have different optical properties than typical dielectric materials used in optics. When a light beam propagates through biological materials, it should pass through numerous layers of the inhomogeneous tissue model. Therefore, multiple scattering has been occurred. Degree of the multiple scattering can be obtained from *scattering coefficient* μ'_s of the tissue. For soft tissue, the value of scattering coefficient is in the range of 0.5 to 4 mm^{-1}. A photon can travel only a distance of $1/\mu'_s$ before incident on next scattering object [2].

Besides the scattering, a part of light beam may also be absorbed by tissues. The amount of absorption can be dependent on the *absorption coefficient* μ_a. For soft tissue, the value of absorption coefficient is in the range of 0.01 to 1 mm^{-1}. A photon can travel only a distance of $1/\mu_a$ before losing an appreciable amount of energy. The value of absorption coefficient is smaller than that of scattering coefficient [2].

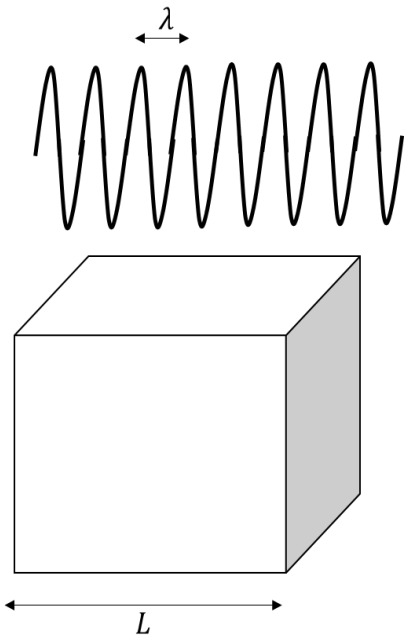

Fig. A.8.4. The wavelength is smaller than the size of device

Optical technology is very useful for *biometric applications*. A biometric system can be considered as a system which uses unique biological attributes of a person such as fingerprint, DNA (Deoxyribonucleic acid), iris scans etc to identify specific individuals. Optical technology is majorly used now a days for scanning iris, fingerprints etc. and storing then as biological passwords. The other way of using optical method is to scan the shape of fingers, hands, faces etc. in unlocking system. Infrared and X -rays have different applications in medical purposes and identification of biological characteristics.

A.9 CONCEPT OF SPECIFIC ABSORPTION RATE (SAR)

The electric field can transfer energy to the electrical charges whereas magnetic field does not transfer energy to charges within human tissues. However, magnetic field transfers energy through forces on magnetic dipoles. As biological tissues are non – magnetic, the effects of magnetic field cannot be dominant in electromagnetic interactions with biological materials [2].

The power density stored in electric and magnetic fields in a wave can be represented by *Poynting vector*. For sinusoidal plane waves, the magnitude of time averaged Poynting vector in terms of both electric field and magnetic field are represented as,

$$P = \frac{E_{rms}^2}{\sqrt{2}} \sqrt{\frac{\epsilon'}{\mu}} \sqrt{1 + \sqrt{1 + \left(\frac{\sigma_{eff}}{\omega \epsilon'}\right)^2}} \ (W/m^2)$$

$$or, P = \frac{H_{rms}^2}{\sqrt{2}} \sqrt{\frac{\mu}{\epsilon'}} \frac{\sqrt{1 + \sqrt{1 + \left(\frac{\sigma_{eff}}{\omega \epsilon'}\right)^2}}}{\sqrt{1 + \left(\frac{\sigma_{eff}}{\omega \epsilon'}\right)^2}} \ (W/m^2)$$

From the above equations, Poynting vector represents power per unit area of the material through which the wave is travelling. So, power absorbed by human body can be estimated by the concept of Poynting vector. The power transferred to the electrical charges belonging to an infinitesimal volume Δv of a material having effective conductivity σ_{eff} (S/m) can be defined as,

$$P = \sigma_{eff} E_{rms}^2 \Delta v \qquad (A.9.1)$$

where E_{rms} is root mean square value of electric field at a particular point. The term $\sigma_{eff}\ E_{rms}^2$ represents density of the absorbed power. Specific absorption rate (SAR) can be defined as transmitted power divided by mass of the material. The terms 'specific' and 'absorbed rate' refer to 'normalization of mass' and 'the rate of energy absorbed by the material' respectively. The time averaged SAR for sinusoidal steady-state electromagnetic fields is given by,

$$SAR = \frac{\sigma_{eff}\ E_{rms}^2}{\rho} \qquad (A.9.2)$$

where ρ is the mass density of the object in Kg/m^3. Generally, the value of ρ is taken as 1000 Kg/m^3 for most biological tissues except lung. Mass density for lung is about 0.347 Kg/m^3 [2]. The equation A.9.2 is the expression of SAR at a point. So, SAR calculated using equation A.9.2 at a point of biological tissues is called *local SAR*. To obtain SAR for whole body, local SAR at each point should be calculated and averaged over the whole body. The power absorbed is higher in high frequencies than low frequencies. Therefore, the high frequency signals are more attenuated when signals propagate through biological tissues than low frequency signals. The SAR distribution is a function of size of the body compared to wavelength of electromagnetic radiation. When body size is of same order of wavelength, the SAR distribution is non uniform within human body due to multiple reflections and refractions at the boundaries between materials having different electrical properties [2]. The effect of electromagnetic exposure within human body is generally measured by amount of increment of tissue temperature due to time of exposure. The heating effect within 1 g average contiguous tissues with heat capacity (C) for short duration of exposure (Δt) can be calculated as [11],

$$\Delta T = SAR\ \frac{\Delta t}{C} \qquad (A.9.3)$$

A.10 EFFECTS OF EM FIELDS ON BODY

An important aspect to study bioelectromagnetics is how electromagnetic fields affect human body. There are seven basic effects of EM fields on human tissues described below.

1. *Thermal effects:*

Thermal interaction within body is an effect of EM interactions. Thermal effects can be observed in some therapeutic processes such as heat therapy for muscle pain, hyperthermia for cancer treatment etc. The absorbed power in human tissues can cause heating [2]. As discussed earlier, power deposition within tissues is measured by specific absorption rate (SAR). To ensure safe electromagnetic exposure, the SAR value should be less than 1.6 W/Kg averaged over 1g of the contiguous tissue and 2 W/Kg averaged over 10g of the contiguous tissue - as prescribed in the international standards [12-13]. SAR value will be 1W/Kg for 1.1 hour - continuous exposure to achieve 1 ˚C increase in temperature [2].

2. *Audio effects:*

SAR value of the human head for high frequency EM field exposure can be more than 100 W/Kg. At 2.45 GHz, the adverse auditory effects require greater than 300 V/m in the human head. This effect can generate a thermoelastic wave in the skull and it can be sensed by auditory mechanism of the ear [2].

3. *Magnetohydrodynamic effects:*

A force can be induced on ions flowing through human blood by very high magnetic fields, i.e., ions are flowing in perpendicular to the magnetic field. The forces induced by magnetic fields can cause strange taste sensations and vertigo [2].

4. *Electroporation:*

Electric fields produce pores in a cell membrane of body is called *electroporation*. It occurs due to various magnetic and associated electric field across membrane. Electroporation is observed at field strengths as low as 50-300 V/cm. When membrane potential is about 800-1000 mV, the pores developed due to EM exposure will be enlarged and fluid will be allowed to pass [2].

5. *Peripheral nerve stimulation:*

Electromagnetic fields cause depolarization by about 15-20 mV (depends on strength of applied electric field) of neural membrane which causes nerve excitation. This activates the voltage-gated ion channels which produce propagating action potential and thus a sensation occurs [2].

6. *Visual phosphenes:*

Stimulation of flashing lights or phosphenes in eye is one of the most sensitive reactions to EM fields. This occurs due to a change of synaptic potentials in receptor neuron of retina. EM field can alter presynaptic resting potential of the cell. Generally, 20 MHz is most sensitive frequency for visual phosphenes [2].

7. *Direct muscle cell excitation:*

Muscle cell can be directly stimulated by electromagnetic fields. For skeletal muscle, about 6 V/m monophasic electric field must be present and a 12 V/m field is required to stimulate cardiac muscle [2].

REFERENCES

[1] E. C. Jordan and K. G. Balmain, "Electromagnetic Waves and Radiating Systems," *PHI Learning Private Limited*, India, 2nd Edition, 2013.

[2] J. R. Nagel, C. M. Furse, D. A. Christensen and C. H. Durney, "Basic Introduction to Bioelectromagnetics," *CRC Press, Taylor & Francis*, 3rd Edition.

[3] S. O. Kasap, "Principles of Electronic Materials and Devices," *Mc – Graw Hill*, 3rd edition.

[4] P. Soontornpipit, C. M. Furse and Y. C. Chung, "Design of implantable microstrip antenna for communication with medical implants," *IEEE Transactions on Microwave Theory and Techniques*, vol. 52, no. 8, pp. 1944 – 1951, August 2004.

[5] T. Karacolak, A. Z. Hood and E. Topsakal, "Design of a Dual – Band Implantable Antenna and Development of Skin mimicking Gels for continuous Glucose monitoring," *IEEE Transactions on Microwave Theory and Techniques*, vol. 56, no. 4, pp. 1001 – 1008, April 2008.

[6] T. Yilmaz, T. Karacolak and E. Topsakal, "Characterization and Testing of a Skin Mimicking Material for Implantable Antennas operating at ISM Band (2.4 GHz – 2.48 GHz)," *IEEE Antennas and Wireless Propagation Letters*, vol. 7, pp. 418 – 420, June 2008.

[7] C. Liu, Y -X Guo, S. Xiao, "Capacitively Loaded Circularly Polarized Implantable patch antenna for ISM band biomedical applications," *IEEE Transactions on Antenna and Propagations,* vol. 62, no. 5, pp. 2407 – 2417.

[8] https://itis.swiss/virtual-population/tissue-properties/database/dielectricproperties.

[9] http://niremf.ifac.cnr.it/tissprop/htmlclie/htmlclie.php.

[10] J. Malmivuo and R. Plonsey, "Bioelectromagnetism: Principles and Applications of Bioelectric and Biomagnetic Fields," *Oxford University Press*, New York, 1995.

[11] V. Karthik, "Performance analysis of Wearable antennas and Investigations on Electromagnetic interaction with Human body for Body – centric Wireless Communications," *PhD dissertation*, Department of Biomedical Engineering, SRM Institute of Science and Technology, December 2017.

[12] ICNIRP, "Guidelines for limiting exposure to electromagnetic fields (100 KHz to 300 GHz)," Health Phys., vol. 118, no. 5, pp. 483-524, 2020.

[13] R. F. Cleveland, Jr., D. M. Sylvar, and J. L. Ulcek, "Evaluating compliance with FCC guidelines for human exposure to radiofrequency electromagnetic fields," FCC OET Bulletin, vol. 65, Edition 97-01, Washington D.C., 1997.